Control and suppression of elastic waves using periodic metasurfaces and bridges

Peter Thomas Wootton

School of Computing and Mathematics

Keele University

A thesis submitted for the degree of

Doctor of Philosophy

June 2020

Declaration

I declare that the work contained within this thesis, submitted for the degree of Doctor of Philosophy at Keele University, has been solely composed by me, Peter Wootton, and has not been submitted, in part or as a whole, for any other degree. Except where otherwise stated by reference or acknowledgment the entirety of the work presented is entirely my own.

Signed: _____ Date: _____

(Peter Wootton)

Abstract

This thesis discusses how wave propagation in continuous linearly elastic media can be controlled or suppressed using periodic structures. This involves controlling 2D waves on a membrane, 3D longitudinal and transverse waves in a linearly elastic bulk, and waves across the surface of a linearly elastic half-space, termed 'Rayleigh waves'.

First, the concept of wave 'bridging' is introduced, using an array of periodic materials to carry waves across a void for two different continuous media. In a 2D membrane, the void is bridged by a periodic array of strings. Two arrays are considered; the first is a simple array of parallel strings, while the second is a square-based string lattice. For each, bridging is shown to be possible but with limitations. The lattice bridge is also shown to be capable of limited wave filtering.

A 3D linearly elastic bulk is then considered, with an array of membranes and thin, rigid sheets held in parallel, intended to bridge the out-of-plane and in-plane wave motion respectively. For bulk waves, 'perfect' wave bridging is shown to be possible for normally incident waves only, with any other incident angle causing wave conversion. For Rayleigh waves 'perfect' bridging is shown to be possible, but requires the bridge parameters to have dependence on depth, indicating that this bridge cannot bridge both Rayleigh waves and bulk waves. Furthermore, it is not possible to construct a broadband Rayleigh bridge.

Next, different metasurfaces are designed and treated, consisting of a periodic array

of vertical resonators attached to the surface of a half-space. These metasurfaces are intended to control and suppress Rayleigh waves. Earlier studies have considered the effect of compressional resonators. In this thesis, an asymptotic model is used to determine the approximate dispersion relation of the previously considered compressional metasurface, which is shown to be remarkably close to the full unimodal dispersion relation. The same asymptotic model is then used to consider a flexural metasurface, with resonators formed from Euler-Bernoulli beams. The dispersion relation is again compared with the full unimodal dispersion relation, again showing the same key behaviours. Special attention is given to the effect of different junction conditions, which are shown to significantly change the size and behaviour of any stop bands.

Finally, a second-order term is derived for the previously employed asymptotic model, verified by comparison to the Taylor expansion of the Rayleigh determinant. This new model is applied to three different systems; a point harmonic forcing, a moving load and a compressional metasurface. In each, the new model is shown to more closely represent the exact solution, at a cost of increased complexity.

Acknowledgments

I would like to hugely thank Professor Julius Kaplunov and Professor Graham Rogerson for their helpful supervision. This work would not have been possible without their guidance, both academically and personally.

I am also grateful to my collaborators, Dr Danila Prikazchikov, also at Keele University, Dr Daniel Colquitt, from the University of Liverpool, and Dr Nihal Ege and Dr Baris Erbas from Eskisehir Technical University for their many hours of fruitful discussions. Their contributions have helped to shape this work and together have resulted in several publications, as well as making the process of undertaking this work much more enjoyable.

I acknowledge Keele University for supporting my PhD. studies, in particular in providing me with ACORN funding. This allowed me to pursue my research without external worries, as well as giving me the opportunity to fully develop my personal and professional development through conferences and courses. I am exceptionally thankful to Jeff Neat and Martyn Parker for giving me their continuous support, advice and helpful direction.

Last, but by no means least, I would like to thank all of those who have supported me throughout my life, enabling me to undertake these studies. First, I am grateful to my family; to my parents who have supported me for many years, and to my brother Adam who has been a source of guidance and inspiration. I am especially thankful for

my girlfriend Izzi who has given constant, unwavering care and motivation. Finally, I am grateful to all of my friends, and to my friend and office mate Leyla who managed to endure sharing an office with me for three years.

Contents

Declaration i

Abstract iii

Acknowledgments v

List of Figures xi

List of Tables xvii

1 Introduction 1

1.1 Literature Review 1

1.1.1 Metamaterials 4

1.1.2 Seismic Metasurfaces 7

1.1.3 Wave Cloaking 8

1.1.4 Rayleigh Waves 11

1.2 Thesis Overview 13

2 Preliminaries 15

2.1 1D and 2D Material Descriptions 15

2.1.1 Infinitely Thin String 16

2.1.2 Stiff Elastic Rod 17

2.1.3 Flexural Beam 17

2.1.4 Infinitely Thin Membrane 19
2.1.5 Thin Stiff Sheet 20
2.2 Linear Elasticity Formulation 21
2.2.1 Elastic Bulk Waves 22
2.2.2 Rayleigh Waves 23
2.2.3 Asymptotic Rayleigh Wave Model 24
2.3 Homogenisation Procedure 26

3 Membrane Bridging **29**

3.1 Homogenised Boundary 30
3.1.1 Normal Incidence 31
3.1.2 Oblique Incidence 34
3.1.3 Oblique Boundary 36
3.1.4 Perfect transmission 38
3.2 Fourier Series method 47
3.2.1 Arbitrary Fourier Series 47
3.2.2 Fourier Series σ Analysis 51
3.2.3 Distributed Delta Function Boundary 54
3.3 Net Bridge 57
3.4 Membrane Bridge Conclusion 61

4 Linear Elasticity Bridging **65**

4.1 Elastic Bulk Wave Bridging 66
4.1.1 Single Material Bridges 67
4.1.2 Longitudinal and Transverse Bridging 78
4.1.3 Elastic Bulk Bridging Conclusion 92

4.2 Elastic Surface Wave Bridging 92
4.2.1 Rayleigh Bridge Formulation 93
4.2.2 Rayleigh Bridge Construction 97
4.2.3 Rayleigh Bridge Conclusion 100
4.3 Linear Elasticity Bridging Conclusion 102

5 Rod-Like Resonator Metasurface 103
5.1 Asymptotic Analysis 104
5.2 Fourier Series Solutions 108
5.2.1 Delta Function Fourier Series 108
5.3 Vertical Rod Metasurface Conclusion 114

6 Beam-Like Resonator Metasurface 117
6.1 Problem Statement 118
6.2 Simply Supported Beams 120
6.3 Beams on a Rail 125
6.4 Fully Matched Beams 128
6.5 Vertical Beam Metasurface Conclusions 137

7 Second Order Rayleigh Wave Asymptotics 139
7.1 Perturbed Governing Equations 140
7.2 Second Order Asymptotic Model 141
7.3 Example Problems 147
7.3.1 2D Harmonic Forcing 148
7.3.2 Plane Strain Steady-State Problem 150
7.3.3 Vertical Rod-like Resonators 153
7.4 Concluding Remarks 156

8 Conclusion **159**

8.1 Concluding Remarks 159

8.2 Future Work 163

Bibliography **167**

A Appendix **181**

A.1 Beam Boundary Conditions 181

A.2 Leading Order Asymptotic Model 184

List of Figures

3.1 An infinite elastic membrane with periodically inserted 1D strings bridging a void between $x = 0$ and $x = d$. 30

3.2 Ratio of amplitude of overall transmission to initial wave amplitude (3.1.45) against the parameter Γ. 39

3.3 Ratio of amplitude of overall transmission to initial wave amplitude (3.1.50) for different incident angles θ on a string bridge. The two plot lines show different choices of parameter tuning, with normal incidence tuning, $\Gamma = 1$ denoted in red, and maximum average transmission tuning $\Gamma = 0.612871...$ denoted in black. 41

3.4 Ratios of amplitudes of successive reflections (3.1.51) and transmissions (3.1.52) to initial wave amplitude against the parameter Γ. 42

3.5 Ratios of amplitudes of overall reflection (3.1.62) and transmission (3.1.63) to initial wave amplitude against the parameter Γ and the added phase difference φ. 44

3.6 Comparisons of the distributed delta function $\delta^{(h,l)}(x)$ for different values of the half-thickness h, where l is the separation between successive strings. 56

3.7 Schematic of an infinite elastic membrane with a square lattice of strings with separation l, bridging a void between $x = 0$ and $x = d$. 58

4.1 Cross-sectional view of an infinite linearly elastic bulk with periodically inserted 2D objects bridging a void between $x = 0$ and $x = d$. 66

4.2 Coefficients for longitudinal transmission (blue) and reflection (orange) from a longitudinal oriented bridge with $\gamma_R = 1$ for a longitudinal incident wave with incident angle θ_1. 73

4.3 Coefficients for shear transmission (blue) and reflection (orange) from a longitudinal oriented bridge with $\gamma_R = 1$ for a longitudinal incident wave with incident angle θ_1. 73

4.4 Coefficients for shear transmission (blue) and reflection (orange) from a transverse oriented bridge with $\gamma_M = 1$ for a shear incident wave with incident angle θ_2. 78

4.5 Coefficients for longitudinal transmission (blue) and reflection (orange) from a transverse oriented bridge with $\gamma_M = 1$ for a shear incident wave with incident angle θ_2. 78

4.6 Coefficients for longitudinal transmission (blue) and reflection (orange) from a mixed mode bridge with $\gamma_R, \gamma_M = 1$ for a longitudinal incident wave with incident angle θ_1. 89

4.7 Coefficients for shear transmission (blue) and reflection (orange) from a mixed mode bridge with $\gamma_R, \gamma_M = 1$ for a longitudinal incident wave with incident angle θ_1. 89

4.8 Coefficients for shear transmission (blue) and reflection (orange) from a mixed mode bridge with $\gamma_R, \gamma_M = 1$ for a shear incident wave with incident angle θ_2. 89

4.9 Coefficients for longitudinal transmission (blue) and reflection (orange) from a mixed mode bridge with $\gamma_R, \gamma_M = 1$ for a shear incident wave with incident angle θ_2. 89

4.10 Coefficients for longitudinal transmission (blue) and reflection (orange) from a mixed mode bridge with $\gamma_R, \gamma_M = 1$ for infinite longitudinal incident waves with incident angle θ_1. 91

4.11 Coefficients for shear transmission (blue) and reflection (orange) from a mixed mode bridge with $\gamma_R, \gamma_M = 1$ for infinite longitudinal incident waves with incident angle θ_1. 91

4.12 Coefficients for shear transmission (blue) and reflection (orange) from a mixed mode bridge with $\gamma_R, \gamma_M = 1$ for infinite shear incident waves with incident angle θ_2. 91

4.13 Coefficients for longitudinal transmission (blue) and reflection (orange) from a mixed mode bridge with $\gamma_R, \gamma_M = 1$ for infinite shear incident waves with incident angle θ_2. 91

4.14 Required values of γ_M and γ_S for bridging a Rayleigh wave of wavenumber k at a depth of z for a bulk material with Poisson Ratio $\nu = 0.4$ and bridging parameter $\gamma_R = 1$. 98

4.15 The smallest possible values of l/λ from (4.2.39) possible for a bridge for Rayleigh waves with $\gamma_R = 1$ in a bulk material with Poisson ratio ν 100

5.1 An array of rod-like resonators of length L and diameter h_r periodically attached with spacing l to the surface of a semi-infinite linearly elastic half space. 105

5.2 The dispersion curves for surface waves on the half plane coated with rod-like resonators, using physical parameters from Table 5.1. The solid blue lines show the dispersion curve of the full unimodal solution from (5.1.18) and the solid black lines the dispersion curve of the asymptotic solution from (5.1.17). The dashed orange and purple lines correspond to the shear and Rayleigh wave lines respectively. 108

5.3 The dispersion curves near the asymptotes for surface waves on the half plane coated with rod-like resonators, using physical parameters from Table 5.1. The solid blue lines show the dispersion curve of the full unimodal solution from (5.1.18) and the solid black lines the dispersion curve of the asymptotic solution from (5.1.17). The dashed orange and purple lines correspond to the shear and Rayleigh wave lines respectively. 109

6.1 An array of beam-like resonators of length L and diameter h_b periodically attached with spacing l to the surface of a semi-infinite linearly elastic half space. 119

6.2 The dispersion curves for surface waves on the half-space coated with simply supported beam-like resonators, using physical parameters from Table 6.1. The solid blue lines show the dispersion curve of the full unimodal solution from (6.2.11) and the solid black lines the dispersion curve of the asymptotic solution from (6.2.17). The dashed green, orange and purple lines correspond to the longitudinal, shear and Rayleigh wave lines respectively. 125

6.3 The dispersion curves for surface waves on the half-space coated with beam-like resonators supported by rails, using physical parameters from Table 6.1. The solid blue lines show the dispersion curve of the full unimodal solution from (6.3.8) and the solid black lines the dispersion curve of the asymptotic solution from (6.3.13). The dashed green, orange and purple lines correspond to the longitudinal, shear and Rayleigh wave lines respectively. 129

6.4 The dispersion curves for surface waves on the half-space coated with fully matched beam-like resonators, using physical parameters from Table 6.1. The solid blue lines show the dispersion curve of the full unimodal solution from (6.4.8) and the solid black lines the dispersion curve of the asymptotic solution from (6.4.13). The dashed green, orange and purple lines correspond to the longitudinal, shear and Rayleigh wave lines respectively. 133

6.5 The dispersion curves for surface waves on the half-space coated with fully matched beam-like resonators, using physical parameters from Table 6.1. The solid blue lines show the dispersion curve of the full unimodal solution from (6.4.8) and the solid red lines the dispersion curve of the asymptotic solution with stress interaction term from (6.4.20). The dashed green, orange and purple lines correspond to the longitudinal, shear and Rayleigh wave lines respectively. 136

7.1 The values for Γ_R (7.2.28) for varying Poisson ratio ν. 144

7.2 A comparison of the leading and second order asymptotic models with the exact solution for the scaled potential ϕ_s near the Rayleigh speed. Here the leading order and second order asymptotic solutions correspond to the dashed grey and solid grey lines respectively and the exact solution is denoted by the solid black line. 149

7.3 A comparison of the leading and second order asymptotic models with the exact solution for the scaled stress S_{33} near the Rayleigh speed for $\xi = 0.2$. Here the leading order and second order asymptotic solutions correspond to the dashed grey and solid grey lines respectively and the exact solution is denoted by the solid black line. 152

7.4 The second order asymptotic solution (7.3.25), denoted by the grey curve, for a 2D system of rod like resonators. The Rayleigh line is plotted in dashed purple and the shear wave line in dashed orange. . . 154

7.5 The dispersion relation near the first two resonances for a 2D system of rod like resonators. The second order asymptotic solution (7.3.25) is denoted by the solid grey curve, the full unimodal solution (7.3.22) by the solid black curve, and the first order asymptotic solution (7.3.24) by the dashed grey curve. The Rayleigh line is plotted in dashed purple and the shear wave line in dashed orange. 155

A.1 A schematic representation of the system junction conditions, showing the end of the beam above the edge of the half-space. The relevant half-space quantities and corresponding beam quantities are indicated with a single arrow indicating a dimension of length and a double arrow indicating a dimension of stress. 183

List of Tables

3.1 Values for σ (3.2.32) for a Jacobi ϑ_3 forcing with Fourier coefficients (3.2.45) with varying incident wavelengths λ and peak relative half widths d. 56

5.1 The numerical system parameter values for the rod resonators and half-space used to produce the dispersion relation curves of Figs. 5.2 and 5.3. 107

5.2 The solutions to partial evaluations of (5.2.17) for given intervals of n with $m = 0$, $\omega = 100$, for system parameters from Table 5.1. 112

6.1 The numerical system parameters for the beam resonator and half-space used to produce the dispersion curves shown in Figs. 6.2– 6.5. 124

CHAPTER 1

Introduction

1.1 Literature Review

It is known that for a point forcing on the surface of a semi-infinite soil layer, localised surface waves, or 'Rayleigh waves' can account for around 67% of the energy carried by a seismic wave, dominating over shear and pressure waves [110]. These Rayleigh waves propagate only along the surface, with amplitude decreasing exponentially with depth into the bulk [2]. This allows them to travel further and decay more slowly than so called 'bulk waves' which propagate in all directions.

The human and financial costs of such seismic surface waves are well documented. The 2011 New Zealand earthquake in Christchurch alone reportedly cost an estimated 16.5 billion NZD [84] while after the 2008 Sichuan earthquake in China, 69,197 people were listed as having died, with many more injured or missing [101]. On a smaller scale, ground vibrations from building work, roads and train lines can cause significant damage to nearby buildings [102].

Recently there has been a significant increase in the amount of work produced with the aim of redirecting or suppressing waves in a wide array of systems. This follows a long tradition of attempting to control wave propagation, including the use of mirrors

and basic lenses to focus and redirect optical wavelengths of electromagnetic radiation. Following the discovery of microwaves in the late 19th Century there were attempts to control the newly discovered electromagnetic waves using waveguides and differently shaped antennae [95], while the use of seismic lensing by changing the refractive index of the ground has been investigated more recently [21]. The approach to controlling propagation has often been considered as a lattice problem, and numerous investigations have used or produced waveguides for which the dispersion relation shows band gaps, also known as stop bands or filter bands, which are ranges of frequencies for which waves cannot propagate through the material. Such waveguides have been produced for optical [36, 56, 90], acoustic [96], elastic [29, 30, 78] and flexural [23, 46] waves.

Of particular interest is the use of periodic structures which can change the behaviour of waves passing through a continuous material. This includes wave gratings, periodic structures classically originating in optics [37] used in elasticity to filter and control wave propagation [109, 51]. More recently the effect that so called 'structured interfaces', periodic connections between continuous materials, have on wave motion has been investigated [6, 7]. These structures are capable of exhibiting behaviour such as wave filtering [11] and polarisation [12]. Particular attention is given to structured interfaces and gratings intended to enhance transmission using the resonance of successive internal reflections [55, 54].

These waveguides have been complemented by recent advancements in the field of so-called 'metamaterials'. A metamaterial is any artificial construct which can behave like a new effective material, usually with the aim of producing material parameters or behaviours which are not found naturally or not possible with classical materials [58]. As such, metamaterials have a wide range of other uses in multiple systems. A subsection of metamaterials of particular interest for an elastic half-plane are 'meta-

surfaces' [77]. As a metamaterial can be used to control bulk waves, metasurfaces are constructed on the edge of a bulk and can be used to control surface waves. These metasurfaces have the advantage of being easier to construct and insert into a physical system and are easier to manufacture [114].

The development of materials which can exhibit behaviours not possible for natural materials has renewed interest in designing materials to control waves using coordinate transforms, including the study of cloaking. This recent development has numerous practical uses and a great deal of vibrant research. These rely on metamaterial designs since, to produce the transformation effect, material parameters are assumed to have the form of an anisotropic matrix. This requirement is difficult, or even impossible, with classical materials [17]. The original work on coordinate transformations was developed in an electromagnetic system by Ward and Pendry [106], although work on the topic had been undertaken previously at a purely theoretical level.

The aim of transformation cloaking is to create a region, or 'inclusion', surrounded by some cloak which diverts incident waves around it, such that the inclusion is undisturbed and the wave pattern outside the cloak is identical to a wave pattern where no cloak or inclusion is present. This has previously been achieved by the use of coordinate transforms, where the cloak describes a deformed space which replicates the wave equation of the undeformed region. Following the work by Pendry [93] on optical cloaks there has been great interest in extending these ideas to other systems.

Many of the approaches in these problems require the treatment of multiscale problems. The forcing at the interface between the two materials is classically modelled as a point forcing, using a Dirac delta function. However, such point actions are often incompatible with the exact treatment of a continuous boundary [103] and so other models must be chosen for real-world relevance. Previous efforts to solve multiscale

problems have included matched asymptotics [104], the so-called 'Arlequin method' [5, 69] and homogenisation (for examples, see [26, 53] and references within). While the Arlequin method matches work done in the system, the treatment of the boundaries in this thesis involves either homogenisation or Fourier series expansions to match displacement and conserve tensions along the boundary. For more complicated systems such treatments may not be possible or will not give an appropriate degree of accuracy.

1.1.1 Metamaterials

A metamaterial is an artificial construct which can behave like a new effective material, usually with the aim of producing material parameters or behaviours which are not found naturally or not possible with classical materials [58]. Many of the examples provided below approximate a continuous material using a lattice structure. While in optical systems these lattices are static, in a moving system such as an acoustic or elastic system the lattice elements will be mobile. In more complicated systems this may cause effects that cannot occur in an ideal continuous material. Furthermore, if the metamaterial is a lattice and is embedded in a continuous material, then there will be point forcing at the boundary between the two materials leading to discontinuity effects.

Colquitt et al. [27] produced a comprehensive discussion of elastic waves in periodic materials, with discussion on types of lattices, defects, standing waves, and frequency dependent focusing and filtering. While in this treatment the lattice is a large structure, something which may not be achievable in all situations, the results can still be useful. Of particular interest are the presence of stop bands and filter bands; having wave frequencies which do not propagate through a system will be useful for controlling or suppressing waves but would disrupt attempts at ideally reproducing them. Pro-

ducing stop bands has also been extensively discussed for different shapes of lattice by Martinsson and Movchan, [78] including unusual designs such as ordinary lattice shapes with small periodically inserted oscillators. For these lattices, clear band gaps should theoretically exist.

A broad range of metamaterials have been produced or theorised for a number of applications. One of the first and leading uses of metamaterials, particularly in optics, is to produce a 'negative index material' which appears to have a negative refractive index [99] and can be used to create a perfect lens [91]. Such materials have also been physically constructed and experimentally verified for limited wavelengths [57, 100]. These are credited by Pendry et al. [93] as indicating electric permittivity and magnetic permeability can be can be arbitrarily varied by a tailored material, therefore making optical transformation cloaking conceivable.

Optical metamaterials are largely based on utilising well established properties of electromagnetism. Several designs use a 'Split Ring Resonator' design, a periodic array which uses induction laws to produce an effective magnetic permeability [92]. Such a design has already been experimentally verified for cloaking at microwave frequencies [98]. For three dimensional cloaks, however, the majority of experimentally verified cloaks are carpet cloaks for microwave [73] and visible [44, 45, 48, 50] frequencies. These can be made using simpler designs with dielectric components such as a lattice constructed from polymers with a variable cell filling factor controlling the local refractive index [44, 45, 48] or with nanoscale silicon rods which have a placement density proportional to the refractive index [50].

Following developments in optics and electromagnetism, metamaterials have been extended to a broad range of different fields [58] including acoustics [71, 74, 83], elasticity [81, 114], flexural plate waves [24, 108, 112] and most notably for this thesis,

seismic waves [8].

Many of the results for acoustic metamaterials are applications of results for optical systems, with Li et al. [71] producing negative index materials and negative effective material parameters and Movchan and Guenneau [83] considering acoustic analogues to Split Ring Resonators. Guenneau et al. [52] build on the same ideas to produce so called 'Double C Resonators' consisting of rigid discs connected by thin ligaments to produce negative refractive index and phase velocity for a given frequency band, allowing for a limited wave trapping effect. A similar system has also been considered using periodically arranged plates inserted into a fluid [94], where the fluid waves exhibit negative refraction and 'waveshifting' properties.

Developments in elastic metamaterials follow a similar methodology of using periodic inclusions, including the use of periodically inserted coated spheres and finite mass-spring systems to create negative bulk and shear moduli [114]. Milton and Willis [81] consider embedded mass-spring systems and spinning rings to create overall effective bulk parameters and show that, as well as giving tunable material parameters, the resulting form of the equations take a similar form to Maxwell's electromagnetic field equations, allowing previous results in electromagnetism to be replicated for elasticity.

As with metamaterials, the original work and subsequent focus for metasurfaces has been electromagnetism [114]. Following the previous success of extending other metamaterials to other systems, metasurfaces have started to be applied to other physical systems, including acoustics [85, 113] and flexural waves [24, 108, 112]. Each of these flexural wave metamaterials make use of different types out-of-plane resonators. Xiao et al. used an array of 'lumped resonators' consisting of masses on the end of out-of-plane springs [112], with Williams et al. using the same type of array but utilising rod-like resonators [108] and Colombi et al. using beam-like resonators [24]. Each of

these systems showed stop bands or band gaps in the dispersion of incident flexural waves, with Williams et al. [108] verifying the results with an experimental setup. Similar out-of-plane resonators have also been applied to elastic surface waves, termed 'seismic metasurfaces'.

1.1.2 Seismic Metasurfaces

The development of seismic metasurfaces has been driven by large scale experiments. In the first of these, Brûlé et al. [8] experimentally verified the existence of stop bands to decrease the motion caused by earthquakes or man-made ground vibrations. Using a test site in silty soil, a metamaterial lattice was constructed with periodic 5 metre deep boreholes and the ground excited by a 50 Hz seismic source. In this system, it was shown that regions near the lattice experienced a significant reduction in the seismic energy received.

A similar seismic metasurface was treated analytically, using a buried lattice structure of rods [1]. This refined model took into account the effects of sub-soil structure, and is particularly notable for being able to produce zero-frequency band gaps by clamping the rods to a fixed bedrock. Further schemes have proposed constructing buildings over specialised metamaterials to protect structures from seismic waves [13, 105].

In contrast to these embedded metasurfaces, the seismic experiment undertaken by Colombi et al. [22] considered a natural array of trees. This was experimentally shown, with numerical verification, to exhibit stop band behaviour and to cause reduction of wave amplitude at certain frequencies. Usually in such systems, sub-wavelength resonant arrays are only capable of producing very narrow band gaps [114] and, as a result, it is challenging to make use of these band gaps in the design of filters and

other wave control devices. Therefore, much of the existing work involves predicting and controlling the locations of these band gaps, and also in enhancing the 'size' of the stop bands to suppress a wider range of wave frequencies.

In further work by Colombi et al. [20] such an array with gradually varying system parameters was shown to either 'trap' waves in the resonators or convert the surface wave into a bulk wave. The overall effect of either of these is that the surface wave can no longer propagate. This so called 'metawedge', typically characterised by increasing or decreasing resonator heights, has been experimentally shown in a small scale ultrasonic regime to cause conversion from Rayleigh waves to bulk waves [19]. This metawedge design has also been applied to the energy harvesting [35] with the mode trapping effect significantly increasing the energy yield.

In previous analytic treatment this type of array was modelled by Colquitt et al. as an array of vertical rod-like resonators ideally attached at periodic intervals [25], considering only longitudinal wave motion. This treatment provides analytic verification for the band gap behaviour shown experimentally. However recent experimental data obtained for a dense forest of pine trees, acting as subwavelength resonators, suggests that the flexural resonances and junction conditions [97] may play an important role. In the current literature, however, little attention has thus far been given to the junction condition joining the resonators to the substrate.

1.1.3 Wave Cloaking

There are several different effects which are all referred to as cloaking. The most general meaning of cloaking is for waves to 'ignore' some defect or inclusion, leaving the wave pattern to appear as though the region being cloaked is not present. For transformation cloaking, the cloak redirects the incident waves in such a way as to

make both the object and the cloak undetectable. A related effect termed 'carpet cloaking' covers an object with a transformation cloak and conceals any distortion or bump caused by the inclusion, making the cloak appear to be flat [58]. The carpet cloak is a type of transformation cloak, but instead of mapping the inclusion onto an infinitely small point or line, the inclusion is mapped onto an infinitely thin sheet [16]. Since the transformation is simpler, this type of cloak can be produced from isotropic dielectric materials and so has a simpler construction. While it is capable of concealing an object, it does not prevent the cloak itself from causing reflections or scattering [72].

Cloaking of the Helmholtz equation was first solved in the short wavelength limit by Leonhardt [70], making use of geometric optics to alter the refractive index to divert rays around an inclusion. A more complete solution to the problem was given by Norris [88], who advanced previous work done in producing cloaks for acoustic waves [16, 32, 33]. In this Norris derived a relation for a cloak for acoustic waves based around a metamaterial termed a "pentamode material", originally posited by Milton and Cherkaev [80] while discussing what properties can be artificially created in metamaterials using only ordinary materials. The original physical design for such a material is a lattice where each unit cell consists of four linkages meeting at a single point, with the stress determined by the width of the linkages and the location of the meeting point. The first theoretical use of pentamode materials in cloaking was in a paper by Milton et al. [79] attempting to cloak the elasticity equations in an investigation into the transform invariance of different physical equations. This result was shown to be a special case of both acoustic cloaking [88] and elastic cloaking [89].

The main results obtained by Norris [88] are general for any coordinate transform and can be applied to other physical systems. Colquitt et al. [28] applies the results to the vertical displacement of an elastic membrane and due to the prevalence of the

Helmholtz equation in physical systems, it is likely they will be similarly useful in many other situations. There are also equations which can be expressed in a Helmholtz-like form, which can also use these results to achieve cloaking.

Several schemes have also attempted to cloak flexural waves in a Kirchoff-Love plate, despite the fact that these waves are governed by a fourth order equation instead of second order. Brun et al. [9] disregard terms lower than 4th order to reduce the equation to a form suitable for transformation cloaking, using a similar technique to acoustic cloaking. As before this requires the material parameters of the system to be changed according to the cloaking transformation variables. The second approach, proposed by Colquitt et al. [31], instead introduces in-plane forces to the system. The final approach by Farhat et al. [47], which uses established plate theory to simplify the form of the governing equation using only homogenised layered isotropic materials. While each cloaking is shown to be successful the effect is either not broadband or otherwise restricts the cloaking. However a computational model of the cloak by Farhat et al. confirms that for the required frequency band a cloak with as few as 10 isotropic layers can have a good cloaking effect.

Cloaking has also been arbitrarily achieved for elasticity by Norris and Shuvalov [89], in a generalisation of two earlier schemes for elastic cloaking, termed 'Cosserat' [10] and 'Willis' [79]. While this can lead to a perfect cloaking of all elastic waves, the strict requirements for the construction of such a cloak leaves scope for simpler cloaks oriented at limited cloaking of individual wave types.

While much focus has been on transformation cloaking, other schemes have been developed to cloak Rayleigh and Seismic waves. As a concept Colombi et al. [21] proposed the construction of a Luneburg lens, a classical lens with variable refractive index to redirect waves around the centre. However this cloak cannot cloak for arbitrary

incidences.

1.1.4 Rayleigh Waves

In contrast to the modern fields of cloaking and metamaterials, elasticity and Rayleigh waves are firmly established and thoroughly investigated branches of mathematics. The first major mathematical discovery in elasticity was Hooke's Law in the 17th Century and at the time of Rayleigh there was a firm foundation of research on which to build [76]. Of particular interest is Rayleigh's research into surface waves on an elastic half-space [75], now referred to as Rayleigh waves [2]. A succinct derivation of the Rayleigh wave form is given by Kaplunov and Prikazchikov [60].

As mentioned previously these waves occur on the surface of an elastic half-space and, in contrast to shear and longitudinal bulk waves, propagate only along the surface and so for a point forcing will have an inverse square decay. Since they decay much more slowly, Rayleigh waves have a higher amplitude than body waves at distances far from the source [2]. However, unlike bulk waves, these surface waves do not have an explicit wave equation; they are instead 'hidden' through the equations of linear elasticity. This makes both finding the exact solution or undertaking numerical analysis for a system dominated by surface waves difficult. Previous results have shown that the displacement potentials can be expressed as a single function related through harmonic conjugates [49], allowing the Rayleigh wave to be easily found in an arbitrary form [14]. This has been extended to surface waves in linear elasticity with general depth dependence [3, 68, 67].

Rayleigh waves are notable for having many practical applications, beginning with the discovery that seismic waves from man-made ground vibrations or from earthquakes include Rayleigh waves [4]. There are also similar surface waves which have been used

in non-destructive testing [18], electrical components such as transducers [82], and also in materials with a piezoelectric coating, where applied stress causes an electrical current [64].

Taking advantage of the relation between displacement potentials, an asymptotic model for the Rayleigh wave was first proposed by Kaplunov and Kossovich [66] with the aim of reducing the full equations of elasticity and surface boundary conditions to an elliptic bulk equation and a hyperbolic surface condition. This model predicts the leading order Rayleigh-type waves produced by forcing along the surface of a linearly elastic half plane, for example see [63]. This model has been applied to multiple problems including: Plane-strain and moving load systems [59, 61], mixed boundary problems [42] and embedded point forces [38]. Special attention has also been given to coated half-space problems [34, 43, 62]. For more general works and further examples see also [63, 87]. In each, the asymptotic model has produced a simple but remarkably accurate approximation of the exact solution. This system could also be further developed by considering the near-surface effect of coupled stresses. Furthermore, the effect of microstructure, including non-local effects, have previously been considered for near-surface wave motion [15] and, as might be expected, are asymptotically secondary for treating Rayleigh-type waves.

The same asymptotic expansion method has also been applied to produce similar models for interfacial waves in linear elasticity and edge waves on plates [60], piezo-electric waves [64] and plates with surface loading [41] with similar success. The hyperbolic-elliptic form of equations has also been shown to be present in the asymptotic formulation of other physical systems. A further paper by Kaplunov and Prikazchikov [60] details results for moving load problems on interfacial waves which again have a hyperbolic-elliptic form, and for edge bending waves on thin elastic plates

which instead have a parabolic-elliptic form. The same result for a surface wave in an elastic material with surface stresses is extended by Ege et al. [40] for purely tangential loads, but considering a fully 3D system with surface stresses acting in any direction parallel to the surface. This system again shows equations of a hyperbolic-elliptic form and a concise set of equations from which the displacement potentials in the elastic half plane are produced. A similar result has been produced by Kaplunov and Prikazchikov for piezoelectric Bleustein-Gulyaev waves [64], a surface wave where displacement in the material and electric potential are strongly linked, which again displays a hyperbolic-elliptic form.

1.2 Thesis Overview

The aim of this thesis is to demonstrate how wave propagation in continuous elastic media can be controlled or suppressed using periodic structures. These metamaterials will fall into two categories: The first, metasurfaces, are periodic arrays attached to the surface of an elastic half-plane, while the second, bridges, are periodic arrays inserted into a void between two halves of a continuous media. Since the treatment of the metasurfaces makes extensive use of an existing asymptotic model for surface wave propagation, this model will also be further investigated and developed.

This thesis will be organised as follows. Chapter 2 begins by establishing different wave carrying materials and the homogenisation technique which will be used extensively in this thesis. In Chapter 3 a novel method for transferring waves across a gap between two thin elastic membranes using 1D strings is proposed. In Chapter 4 the same formulation is extended to a 3D case using linear elasticity, with bulk waves transferred in §4.1 and surface waves in §4.2. Chapters 5 and 6 will then propose

metasurfaces for linearly elastic half spaces to control wave propagation; Chapter 5 will make use of the asymptotic model to discuss the effects of an array of vertical rod-like resonators ideally attached to the surface and Chapter 6 will consider a similar novel array with beam-like resonators with a variety of boundary conditions. Following this, Chapter 7 uses the previous methodology used to produce the asymptotic model for Rayleigh-type waves to extend the previous leading order model into a second order model. Following the derivation, previous example situations are used to demonstrate the improved accuracy of the new model. The work will then be concluded in Chapter 8 with a final discussion of each of the problems with possibilities for future work considered.

CHAPTER 2

Preliminaries

In the work that follows there will be a selection of different materials and techniques which will be made repeated use of. For convenience these will be described in this section and referred back to as required.

2.1 1D and 2D Material Descriptions

A large component in this work is the theoretical construction of metamaterials and metasurfaces for a bulk using a periodic array of lower-dimension objects. For this it is necessary to make use of a range of 1D and 2D materials, both for bridging problems and to act as surface resonators. For brevity, each will be detailed here. Since several of these materials will be used in multiple different systems introduce an arbitrary 2D Cartesian coordinate system (ζ, η) and transpose into the new coordinates for each case as required. For consistency, define Ω as some constant angular frequency for the wave motion.

2.1.1 Infinitely Thin String

First the linearly elastic behaviour of an infinitely thin string will be detailed. Such a string is a 1D object and has only out-of-plane wave motion. Represent the horizontal plane by the arbitrary orthonormal co-ordinate system (ζ, η) such that the string motion is perpendicular to both the ζ-axis and η-axis and denote the vertical displacement by u_s. Then if the ends of the string are fixed at $(\zeta_1, \eta_1), (\zeta_2, \eta_1)$ the string exists only in the domain $\zeta_1 < \zeta < \zeta_2,\ \eta = \eta_1$.

For these co-ordinates the equation of motion for vertical displacement is given by,

$$\rho_s \frac{\partial^2 u_s}{\partial t^2} = T_s \frac{\partial^2 u_s}{\partial \zeta^2}, \tag{2.1.1}$$

where ρ_s and T_s are the mass per unit area and average tension per unit length of the strings respectively. At the ends of the string the vertical tension per unit length, P, is given by,

$$P = T_s \frac{\partial u_s}{\partial \zeta}. \tag{2.1.2}$$

This leads to harmonic wave solutions along the string of the form,

$$u_s = A_s e^{i[K_s \zeta \ \pm \ \Omega t]} \tag{2.1.3}$$

where the amplitude A_s and wavenumber K_s are arbitrary constants arising from the boundary conditions, and where K_s is determined by,

$$\frac{\Omega}{K_s} = c_s = \sqrt{\frac{T_s}{\rho_s}}, \tag{2.1.4}$$

where c_s is the wave speed in the string. The choice of sign in the exponent depends on whether the wave solution is right- or left-travelling.

2.1.2 Stiff Elastic Rod

Next consider a stiff elastic rod. In the same way that the string can only support out-of-plane motion, a stiff elastic rod is inflexible and only supports in-plane longitudinal waves. Reusing the same arbitrary Cartesian (ζ, η) coordinates, with ends fixed at $(\zeta_1, \eta_1), (\zeta_2, \eta_1)$ the rod again exists only in the domain $\zeta_1 < \zeta < \zeta_2,\ \eta = \eta_1$. In this domain the rods have governing equation,

$$\rho_r \frac{\partial^2 u_r}{\partial t^2} = E_r \frac{\partial^2 u_r}{\partial \zeta^2}, \tag{2.1.5}$$

where E_r and ρ_r are the Young Modulus and the density of the rod respectively. For a cylindrical rod with diameter h_r, the ends of the rod experience an in-plane force V,

$$V = -\frac{\pi h_r^2}{4} E_r \frac{\partial u_r}{\partial \zeta}, \tag{2.1.6}$$

which again leads to wave solutions of the form,

$$u_r = A_r e^{i[K_S \zeta \pm \Omega t]}, \tag{2.1.7}$$

where A_r is the wave amplitude, determined by the boundary conditions, and the wavenumber K_r comes from the dispersion relation,

$$\frac{\Omega}{K_r} = c_r = \sqrt{\frac{E_r}{\rho_r}}, \tag{2.1.8}$$

where c_r is the speed of longitudinal waves in the rod.

2.1.3 Flexural Beam

In contrast to the stiff rod which can only support longitudinal waves, next introduce a beam which can only support flexural motion. Again use the arbitrary Cartesian

coordinates (ζ, η) and take a beam as occupying the domain $\zeta_1 < \zeta < \zeta_2,\ \eta = \eta_1$. The classical Euler-Bernoulli beam model yields the governing equations for flexural motion of a beam as,

$$M_b \frac{\partial^2 u_\eta}{\partial t^2} = -B_b I_b \frac{\partial^4 u_\eta}{\partial \zeta^4}, \tag{2.1.9}$$

where u_η is a component of the displacement vector perpendicular to the beam, B_b and M_b are the bending stiffness and mass per unit length of the resonators respectively, and I_b is the area moment of inertia of the beams. If the beam is cylindrical I_b is given by,

$$I_b = \frac{\pi h_b^4}{64}, \tag{2.1.10}$$

where h_b is the diameter of a beam and for a beam B_b is given by

$$B_b = \frac{E_b}{1 - \nu^2} \tag{2.1.11}$$

where E_b and ν are the Young modulus and Poisson ratio respectively of the beam. Unlike for the previous materials, a flexural beam has four boundary conditions at the ends with the beam displacement and its first, second and third derivatives corresponding to displacement, bending angle, moment and horizontal stress respectively. These boundary conditions are;

$$\frac{\partial u_\zeta}{\partial \eta} = \frac{\partial u_\eta}{\partial \zeta}, \qquad \frac{\partial \sigma_{\zeta\zeta}}{\partial \eta} = -B_b \frac{\partial^2 u_\eta}{\partial \zeta^2}, \qquad H = I_b B_b \frac{\partial^3 u_\eta}{\partial \zeta^3}, \tag{2.1.12}$$

where u_ζ is the in-plane displacement, $\sigma_{\zeta\zeta}$ the in-plane stress and H is the out-of-plane force in the η direction. A more detailed explanation for each of these is given in the appendix §A.1. Also unlike the previous materials the wave speed is not a material constant, instead being given by,

$$\frac{\Omega}{K_b} = c_b = \left(\frac{B_b \pi h_b^4}{64 M_b}\right)^{\frac{1}{4}} \sqrt{\Omega}, \tag{2.1.13}$$

which has a clear frequency dependence.

2.1.4 Infinitely Thin Membrane

Similar to the 1D string outlined previously, an infinitely thin membrane has only vertical out-of-plane motion with displacement u_M but unlike the string fills a 2D domain of any shape. Utlising the previous Euclidean coordinates a rectangular membrane has co-ordinates $\zeta_1 < \zeta < \zeta_2,\ \eta_1 < \eta < \eta_2$. On this domain the out-of-plane displacement for a membrane which has mass per unit volume ρ_M and internal tension per unit area T_M is given by the solutions to,

$$\rho_M \frac{\partial^2 u_M}{\partial t^2} = T_M \left(\frac{\partial^2 u_M}{\partial \zeta^2} + \frac{\partial^2 u_M}{\partial \eta^2} \right). \tag{2.1.14}$$

and at the edges $\zeta = \zeta_1, \zeta_2$ of the rectangular membrane the out-of-plane stress, $\sigma_{\zeta 3}$, is given by,

$$\sigma_{\zeta 3} = T_M \frac{\partial u_M}{\partial \zeta}. \tag{2.1.15}$$

As with the string this gives harmonic solutions,

$$u_M = A_M e^{i[K_M(\zeta \cos\theta + \eta \sin\theta)\ \pm\ \Omega t]}, \tag{2.1.16}$$

where as before the amplitude A_M and wavenumber K_M are arbitrary constants and again the choice of sign in the exponent denotes a right or left travelling wave. This is clearly the 2D analogue of the 1D string solution (2.1.3) with wave propagation at an angle θ to the ζ-axis. The frequency and wavenumber are also related to the membrane wave speed, c_M, by the expression,

$$\frac{\Omega}{K_M} = c_M = \sqrt{\frac{T_M}{\rho_M}}, \tag{2.1.17}$$

which is similar to the string dispersion relation (2.1.4).

2.1.5 Thin Stiff Sheet

As the infinitely thin membrane is a 2D generalisation of the 1D infinitely thin string, introduce the thin stiff sheet to be the 2D analogue to the 1D stiff elastic rod. Since it is stiff there is no flexural bending of the sheet and so only in-plane waves propagate through the system. Unlike a rod however, an in-plane shear force on the boundary could produce a shear wave and so in the work that follows this sheet will only be used to consider a normally incident longitudinal wave.

Since only plane waves normally incident on the edge of the sheet are being considered, for a rectangular sheet with domain $\zeta_1 < \zeta < \zeta_2,\ \eta_1 < \eta < \eta_2$ and a wave incident at $\eta = \eta_1$ propagating in the ζ direction only, the governing equation of waves is,

$$\rho_S \frac{\partial^2 u_S}{\partial t^2} = E_S \frac{\partial^2 u_S}{\partial \zeta^2}, \tag{2.1.18}$$

where u_S is the displacement in the ζ direction, and ρ_S and E_S are the mass density per unit volume and Young modulus of the sheet respectively. Similar to the stiff rod (2.1.6), this has in-plane stress at the edge,

$$\sigma_{\zeta\zeta} = E_S \frac{\partial u_S}{\partial \zeta}. \tag{2.1.19}$$

Since only 1D propagation of waves through the sheet are allowed, the harmonic wave form,

$$u_S = A_S e^{i[K_S\zeta \,\pm\, \Omega t]}, \tag{2.1.20}$$

is similar to that of the string (2.1.3), again with A_S, K_S and Ω being arbitrary constants determined by the boundary conditions with dispersion relation,

$$\frac{\Omega}{K_S} = c_S = \sqrt{\frac{E_S}{\rho_S}}, \tag{2.1.21}$$

where c_S is the speed of the longitudinal waves.

2.2 Linear Elasticity Formulation

Although not detailed here, the previous materials are specific examples of linearly elastic materials in limiting cases. In order to consider waves in a semi-infinite elastic bulk it is necessary to use the general equations for linear elasticity. In each case the materials used will be treated in 2D or 3D Cartesian coordinates. For the 2D systems take $x_1 = x$ and $x_2 = y$ and for the 3D systems take $x_1 = x$, $x_2 = y$ and $x_3 = z$. For most of the 3D cases it will be assumed that there is uniform motion in the y-direction.

Start with with the classical equations of motion in 3D elasticity [2];

$$\rho \frac{\partial^2 u_i}{\partial t^2} = \frac{\partial \sigma_{im}}{\partial x_m}, \quad i = 1, 2, 3, \tag{2.2.1}$$

where ρ is the mass volume density, σ_{im} are components of the stress tensor and u_i are components of the displacement vector $\boldsymbol{u}$. Linear elasticity has the constitutive relations,

$$\sigma_{ik} = \delta_{ik}\ \lambda\ \mathrm{div}\boldsymbol{u} + \mu \left(\frac{\partial u_i}{\partial x_k} + \frac{\partial u_k}{\partial x_i} \right), \tag{2.2.2}$$

where λ and μ are the first and second Lamé parameters respectively and δ_{ik} is the Kronecker delta. These when combined with the equations of motion yields the particular vector equation of motion as,

$$\rho \frac{\partial^2 \boldsymbol{u}}{\partial t^2} = (\lambda + \mu)\ \mathrm{grad}\ \mathrm{div}\boldsymbol{u} + \mu \Delta \boldsymbol{u}, \tag{2.2.3}$$

where grad, div and Δ are the usual 3D differential operators. For most uses of an elastic bulk in this work, assume that waves propagate in the x- and z-directions with uniform motion in the y-axis. Then introduce two displacement potentials, ϕ, ψ, such that,

$$u_1 = \frac{\partial \phi}{\partial x} - \frac{\partial \psi}{\partial z}, \qquad u_3 = \frac{\partial \phi}{\partial z} + \frac{\partial \psi}{\partial x}, \tag{2.2.4}$$

so the equations of motion for the half-space (2.2.3) can be rewritten in terms of the displacement potentials as,

$$\frac{\partial^2\phi}{\partial x^2}+\frac{\partial^2\phi}{\partial z^2}-\frac{1}{c_1^2}\frac{\partial^2\phi}{\partial t^2}=0, \qquad \frac{\partial^2\psi}{\partial x^2}+\frac{\partial^2\psi}{\partial z^2}-\frac{1}{c_2^2}\frac{\partial^2\psi}{\partial t^2}=0, \tag{2.2.5}$$

where the longitudinal and shear wave speeds, c_1 and c_2, have equations,

$$c_1=\frac{\lambda+2\mu}{\rho}, \qquad c_2=\frac{\mu}{\rho}. \tag{2.2.6}$$

Neglecting the y-plane motion the linear elastic bulk has stresses,

$$\begin{aligned}
\sigma_{11}&=(\lambda+2\mu)\frac{\partial^2\phi}{\partial x^2}+\lambda\frac{\partial^2\phi}{\partial z^2}-2\mu\frac{\partial^2\psi}{\partial x\partial z},\\
\sigma_{13}&=2\mu\frac{\partial^2\phi}{\partial x\partial z}-\mu\frac{\partial^2\psi}{\partial z^2}+\mu\frac{\partial^2\psi}{\partial x^2},\\
\sigma_{33}&=(\lambda+2\mu)\frac{\partial^2\phi}{\partial z^2}+\lambda\frac{\partial^2\phi}{\partial x^2}-2\mu\frac{\partial^2\psi}{\partial x\partial z},
\end{aligned} \tag{2.2.7}$$

where for boundaries parallel to the x-axis conserve σ_{13} and σ_{33}, and parallel to the z-axis conserve σ_{11} and σ_{13}. The following work will involve both elastic bulk and surface waves, the formulation of which will both now be detailed.

2.2.1 Elastic Bulk Waves

When the linearly-elastic bulk is infinite in all directions the only propagating wave types are bulk waves. In any elastic bulk these are given by wave solutions to the displacement potentials,

$$\phi=A_\phi e^{i[K_\phi(x\cos\theta_1+z\sin\theta_1)\ \pm\ \Omega_\phi t]}, \tag{2.2.8}$$

$$\psi=A_\psi e^{i[K_\psi(x\cos\theta_2+z\sin\theta_2)\ \pm\ \Omega_\phi t]}, \tag{2.2.9}$$

where,

$$\frac{\Omega_\phi}{K_\phi}=c_1, \qquad \frac{\Omega_\psi}{K_\psi}=c_2, \tag{2.2.10}$$

and A_ϕ and A_ψ are arbitrary constants. As before, θ_1 and θ_2 are the angles between each wave and the x-axis and the choice of sign in the exponent denotes a right or left travelling wave. If both waves share the same angular frequency,

$$\Omega_\phi = \Omega_\psi = \Omega, \tag{2.2.11}$$

then the wavenumbers and propagation angles are related by,

$$K_\psi \sin\theta_2 = K_\phi \sin\theta_1, \tag{2.2.12}$$

$$\sin\theta_2 = \frac{K_\phi}{K_\psi}\sin\theta_1, \tag{2.2.13}$$

$$= \frac{c_2}{c_1}\sin\theta_1. \tag{2.2.14}$$

where c_2/c_1 is a fixed material parameter where for conventional materials,

$$0 \leq \frac{c_2}{c_1} \leq \frac{1}{\sqrt{2}}. \tag{2.2.15}$$

2.2.2 Rayleigh Waves

If the elastic bulk is semi-infinite with a surface at $z = 0$ then there are wave solutions, termed "Rayleigh waves", which propagate along the surface and decay into the bulk. In the case of a free surface, at $z = 0$ stress free boundary conditions are imposed yielding,

$$\sigma_{3i} = 0, \quad i = 1, 2, 3. \tag{2.2.16}$$

Assuming a wave propogating in the x-direction this produces a single wave with both shear and longitudinal components of the form,

$$\phi = A_\phi\, e^{i[Kx \,\pm\, \Omega t] - K\alpha z}, \qquad \psi = A_\psi\, e^{i[Kx \,\pm\, \Omega t] - K\beta z}, \tag{2.2.17}$$

where A_ϕ, A_ψ, K and Ω are constants and α and β are given by,

$$\alpha = \sqrt{1 - \left(\frac{\Omega}{c_1 K}\right)^2}, \qquad \beta = \sqrt{1 - \left(\frac{\Omega}{c_2 K}\right)^2}. \tag{2.2.18}$$

Substituting these assumed solution forms into the stress free surface conditions yields the Rayleigh determinant,

$$4\alpha\beta - (1+\beta^2)^2 = 0 \tag{2.2.19}$$

which has a unique solution for wave speed,

$$c_R = \frac{\Omega}{K} \tag{2.2.20}$$

termed the Rayleigh speed where the Rayleigh decay constants are subsequently given by,

$$\alpha = \sqrt{1 - \left(\frac{c_R}{c_1}\right)^2} \triangleq \alpha_R, \qquad \beta = \sqrt{1 - \left(\frac{c_R}{c_2}\right)^2} \triangleq \beta_R. \tag{2.2.21}$$

The stress free surface also gives the relations between the two displacement potentials at the surface,

$$\frac{\partial\psi}{\partial x} = -\frac{2}{1+\beta_R^2}\frac{\partial\phi}{\partial z}, \quad \frac{\partial\psi}{\partial z} = \frac{1+\beta_R^2}{2}\frac{\partial\phi}{\partial x} \tag{2.2.22}$$

2.2.3 Asymptotic Rayleigh Wave Model

Next introduce the asymptotic model from Kaplunov and Prikazchikov [60] for a near-Rayleigh surface wave. While here only 2D systems are considered, the same asymptotic model applies for a 3D system. For details and other examples of this model, see [63] and references within. A short derivation is also given in the appendix §A.2. In this model for a near-Rayleigh wave, the equations for the bulk are simplified to,

$$\frac{\partial^2\phi}{\partial z^2} + \alpha_R^2\frac{\partial^2\phi}{\partial x^2} = 0, \qquad \frac{\partial^2\psi}{\partial z^2} + \beta_R^2\frac{\partial^2\psi}{\partial x^2} = 0. \tag{2.2.23}$$

which then leads to the previous travelling wave solutions (2.2.17) becoming,

$$\phi = A_\phi\, e^{i[Kx \,\pm\, \Omega t] - K\alpha_R z}, \qquad \psi = A_\psi\, e^{i[Kx \,\pm\, \Omega t] - K\beta_R z}. \tag{2.2.24}$$

Depending on the applied surface stress, the model is formulated in terms of either the longitudinal or shear wave potential. When $\sigma_{33} = 0$, the model is oriented at solving for the shear wave potential and so leads to the condition for the wave along the surface $z = 0$,

$$\frac{\partial^2 \psi}{\partial x^2} - \frac{1}{c_R^2}\frac{\partial^2 \psi}{\partial t^2} = -\frac{1+\beta_R^2}{2\mu B}\sigma_{31}, \tag{2.2.25}$$

whereas for $\sigma_{31} = 0$ the model is oriented at solving for the longitudinal wave potential and so leads to the surface condition at $z = 0$,

$$\frac{\partial^2 \phi}{\partial x^2} - \frac{1}{c_R^2}\frac{\partial^2 \phi}{\partial t^2} = \frac{1+\beta_R^2}{2\mu B}\sigma_{33}, \tag{2.2.26}$$

where

$$B = \frac{\beta_R}{\alpha_R}(1-\alpha_R^2) + \frac{\alpha_R}{\beta_R}(1-\beta_R^2) - (1-\beta_R^4), \tag{2.2.27}$$

and the displacement potentials are related along the surface by (2.2.22) allowing for the full solution for the system to be obtained.

Not only is this form of the surface equations much simpler than the exact form of the equations, but for a known stress they will each only require the solving of a single hyperbolic scalar problem along the surface with the explicit Rayleigh wave speed.

This asymptotic model is a leading order perturbation of the equations of motions (2.2.5) around the Rayleigh wave eigensolution above (2.2.19). Here, a surface stress is imposed which causes a small deviation from the Rayleigh speed. This expansion relies on the small parameter condition,

$$\epsilon = \left|1 - \frac{\omega}{c_R k}\right| \ll 1, \tag{2.2.28}$$

so the solution is known to be valid only if $\frac{\omega}{k} \sim c_R$. From inspection of the surface conditions this is equivalent to both of the surface stresses tending to zero.

As mentioned before, the asymptotic model used is a simplification of the more general 3D model. To recover the 3D model from the 2D one, add a second shear potential ψ_2 to correspond to the stress σ_{32} and replace any second order x derivatives with the two dimensional Laplace operator, Δ. For example the vertical surface relation (2.2.26) in full 3D form becomes,

$$\Delta\phi - \frac{1}{c_R^2}\frac{\partial^2\phi}{\partial t^2} = \frac{1+\beta_R^2}{2\mu B}\sigma_{33}. \tag{2.2.29}$$

Finally, replace the surface potential relations (2.2.22) by the 3D equivalents,

$$\phi_{,i} = \frac{2}{1+\beta_R^2}\psi_{i,3}\ , \quad \phi_{,3} = -\frac{1+\beta_R^2}{2}\left(\psi_{1,1}+\psi_{2,2}\right)\ , \quad i=1,2. \tag{2.2.30}$$

where as usual, a subscript after the comma denotes differentiation.

2.3 Homogenisation Procedure

Throughout this work periodic arrays are attached to a continuous material. While it is possible to conduct an exact analysis of these systems, it is more convenient to make a long wave assumption and homogenise any stresses along the boundary. Furthermore, as previously mentioned, such point actions are often inconsistent with continuous media [103], and using homogenisation to distribute the point forcing removes this inconsistency. For simplicity, introduce a new periodic delta function $\delta^{(l)}$ given by,

$$\delta^{(l)}(\eta) = \sum_{n=-\infty}^{\infty}\delta(\eta+nl), \tag{2.3.1}$$

If the spacing between the bridges is sufficiently small then for a wave passing through the system the boundary will appear near-continuous and to a high degree of accuracy the point loading can be distributed over the unit cell to obtain a continuous tension. This distribution is obtained by integrating the stresses at the boundary over

the unit cell and assuming that on these short scales the changes in displacement is negligible,

$$\int_{(n-\frac{1}{2})l}^{(n+\frac{1}{2})l} P\delta(\eta + nl)\ d\eta = \int_{(n-\frac{1}{2})l}^{(n+\frac{1}{2})l} \sigma\ d\eta, \tag{2.3.2}$$

$$P|_{\eta=nl} \approx \sigma l. \tag{2.3.3}$$

This can then be distributed across the entire boundary to give the homogenised boundary condition,

$$P = \sigma l. \tag{2.3.4}$$

It is worth noting that the Fourier series for a periodic delta function of this type is,

$$\delta^{(l)}(\eta) = \sum_{j=-\infty}^{\infty} \frac{1}{l} e^{i\ 2j\pi\frac{\eta}{l}}, \tag{2.3.5}$$

for which the above homogenisation gives the leading order coefficient.

CHAPTER 3

Membrane Bridging

This chapter introduces a novel method for transferring waves across a void between two halves of a membrane. While this approach is intended to perfectly reproduce the wave pattern as though the region were filled, it is distinct from transformation cloaking and so throughout this new approach is referred to as 'bridging'. While cloaking has already been achieved for a membrane [28] this bridging method does not require anisotropic material parameters and so is much simpler to construct. It is also directly oriented at concealing infinite voids rather than finite inclusions. This will be used as a sample problem on which to build similar bridges for more complicated systems, as well as to verify the use of the homogenisation procedure.

The system considered in this chapter consists of two half-membranes which occupy the regions $-\infty < x < 0$ and $d < x < \infty$, $-\infty < y < \infty$. Then consider an array of 1D strings held at an angle ϑ which have end points $(0, nl)$ and $(d, nl + d\tan\vartheta)$, $n \in \mathbb{Z}$ which connect the edges of the two membranes, as shown in Fig. 3.1. A wave travelling on the membrane incident on the boundary will transfer some energy to the strings which will be carried on as wave motion, and then be transmitted again into the membrane on the other side of the void, carrying some component of the wave motion across the gap.

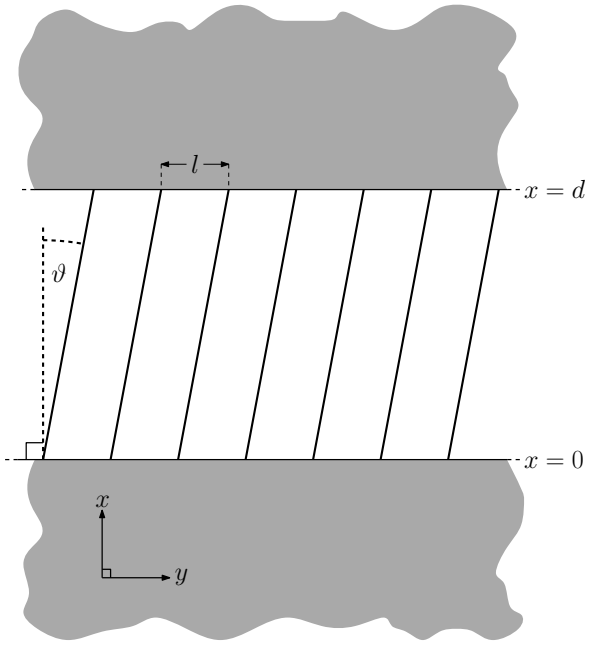

Figure 3.1: An infinite elastic membrane with periodically inserted 1D strings bridging a void between $x = 0$ and $x = d$.

If it is assumed that the strings are infinitely thin and are ideally connected to the membrane then from the boundary conditions (2.1.2, 2.1.15) this leads to a boundary condition at $x = 0$ and $x = d$,

$$T_s \frac{\partial u_s}{\partial x} \delta^{(l)}(y) = T_M \frac{\partial u_M}{\partial x}. \tag{3.0.1}$$

This can be solved either through homogenisation or taking the Fourier series of the delta function. Consider the homogenised problem first in §3.1 and then verify these results in §3.2 using a Fourier series boundary.

3.1 Homogenised Boundary

Begin by making use of the homogenisation procedure in §2.3, which when applied to the boundary condition (3.0.1) leads to the homogenised boundary condition,

$$\frac{T_s}{l} \frac{\partial u_s}{\partial x} = T_M \frac{\partial u_M}{\partial x}. \tag{3.1.1}$$

Since the connections at the boundary are fixed it is necessary to conserve displacements at the boundary, such that at the connection points between the bridge and the membrane,

$$u_s = u_M. \tag{3.1.2}$$

The solution of this system then depends on the incident wave pattern. Start with a normally incident wave and then analyse increasingly complicated systems with the aim of perfectly reproducing the incident wave pattern on the other side of the void.

3.1.1 Normal Incidence

First consider the simplest system, that of a wave normally incident to the boundary propagating through the membrane. For simplicity, denote the incident, reflected and transmitted wave components by superscript (i), (r) and (t) respectively. From the general solution (2.1.16) define the incident component of the wave as $u_M^{(i)}$ where,

$$u_M^{(i)} = A_i e^{i[kx-\omega t]}, \tag{3.1.3}$$

where A_i is an arbitrary constant and ω and k are the wave angular frequency and wavenumber respectively, which have the usual relation (2.1.17). Similarly the solution for the transmitted waves in the strings (2.1.3) is,

$$u_s^{(t)} = A_t e^{i[Kx-\Omega t]} \tag{3.1.4}$$

where as above A_t is a constant, and the angular frequency Ω and wavenumber K are related by (2.1.4).

Assume also that there is a reflected component to the wave, which has the same form as the incident wave but propagating in the opposite direction and with a different

amplitude, given by

$$u_M^{(r)} = A_r e^{-i[kx+\omega t]}, \tag{3.1.5}$$

where the overall membrane displacement is,

$$u_M = u_M^{(i)} + u_M^{(r)}. \tag{3.1.6}$$

Substituting the displacements into the stress boundary condition between the strings and the membrane (3.1.1) and letting $x = 0$ gives,

$$i\ l\ T_M k(A_i - A_r)e^{-i\omega t} = iT_s K A_t e^{-i\Omega t}. \tag{3.1.7}$$

From this, it is clear that the only term dependent on time is in the exponent part of the wave solution. Therefore,

$$e^{-i\Omega t} = e^{-i\omega t}, \tag{3.1.8}$$

and hence $\Omega = \omega$. So,

$$A_i - A_r = \gamma A_t, \tag{3.1.9}$$

where

$$\gamma = \frac{T_s c_M}{l\ T_M c_s}. \tag{3.1.10}$$

Conserving the displacements (3.1.2) gives the condition,

$$A_i + A_r = A_t. \tag{3.1.11}$$

Therefore by rearranging and substituting the expressions for the transmission and reflection amplitudes in terms of the incident amplitude and γ can be obtained,

$$A_r = \frac{1-\gamma}{1+\gamma}\ A_i, \qquad A_t = \frac{2}{1+\gamma}\ A_i. \tag{3.1.12}$$

This procedure can then be repeated for the second boundary, with an incident wave on the strings being transmitted into the membrane with some component reflecting back into the strings. For simplicity, since the wave is fully periodic with time and position, the co-ordinate system can be arbitrarily moved with only a change in phase. Since the main motivation is preserving wave amplitudes, for now disregard phase changes and define the boundary currently being treated as $x = 0$. Assume then that the incident, reflected and transmitted waves respectively have the form,

$$u_s^{(i)} = B_i \; e^{i[Kx-\omega t]}, \tag{3.1.13}$$

$$u_s^{(r)} = B_r \; e^{-i[Kx+\omega t]}, \tag{3.1.14}$$

$$u_M^{(t)} = B_t \; e^{i[kx-\omega t]}, \tag{3.1.15}$$

where the overall string displacement is,

$$u_s = u_s^{(i)} + u_s^{(r)}, \tag{3.1.16}$$

and as before B_i, B_r and B_t are constants representing the incident, reflection and transmission amplitudes respectively. Substituting into the stress boundary condition (3.1.1) as before yields the expression,

$$B_i - B_r = \frac{1}{\gamma} \; B_t, \tag{3.1.17}$$

where γ is defined as before (3.1.10). Rearranging these and substituting into (3.1.2) gives the reflection and transmission amplitudes in terms of the incident amplitude,

$$B_r = \frac{\gamma - 1}{\gamma + 1} \; B_i, \qquad B_t = \frac{2\gamma}{\gamma + 1} \; B_i. \tag{3.1.18}$$

To obtain the overall effect of the bridging, consider the ratio of the transmission from the second boundary to the initial incident wave amplitude. Furthermore, the amplitude of the wave incident on the second boundary will be given by the transmitted

amplitude from the first boundary. Hence the overall transmission of the system in terms of the initial wave amplitude A_i will be given by,

$$\frac{B_t}{A_i} = \frac{B_t}{B_i}\frac{A_t}{A_i} = \frac{4\gamma}{(1+\gamma)^2}. \tag{3.1.19}$$

For positive γ, this transmission ratio has a maximum at $\gamma = 1$, for which the transmitted wave has the same amplitude as the incident wave, representing a perfect transmission. As γ tends to zero or infinity however, the transmission through the system tends to zero with the parameter contrast making the wave unable to propagate.

3.1.2 Oblique Incidence

Suppose now that the incident wave is propagating at some angle θ to the boundary normal, and has the form,

$$u_M^{(i)} = A_i e^{i[k(x\cos\theta + y\sin\theta) - \omega t]}, \tag{3.1.20}$$

where k and ω again satisfy the dispersion relation (2.1.17). Assume also that the transmitted waves into the strings have the form,

$$u_s^{(t)} = A_t e^{i[Kx + \chi y_0 - \omega t]}. \tag{3.1.21}$$

where K and Ω satisfy the string dispersion relation (2.1.4) where for $y_0 = nl,\ n \in \mathbb{Z}$ then χ is introduced to match the form of the exponent at the connections where for each string $y = y_0$. Following the same procedure as before then at the connections,

$$P(y,t) = Pe^{i\chi y_0 - i\Omega t} = Pe^{iky_0\sin\theta - i\omega t}, \tag{3.1.22}$$

from which it readily follows that $\chi = k\sin\theta$. Since χ is real, this represents a change in phase between successive strings. As the displacement along the boundary must be continuous and it is assumed that there is only one transmitted wave direction then it

equally follows that the reflected wave has the form,

$$u_M^{(r)} = A_r e^{-i[k(x\cos\theta - y\sin\theta)+\omega t]}. \tag{3.1.23}$$

As expected the angle of incidence is equal to the angle of reflection. On substituting these assumed wave solutions into the stress boundary condition (3.1.1),

$$A_i - A_r = \tilde{\gamma}\ A_t, \tag{3.1.24}$$

where

$$\tilde{\gamma} = \frac{\gamma}{cos\theta}. \tag{3.1.25}$$

Using the displacement continuity (3.1.2), the transmission and reflection coefficients are,

$$A_r = \frac{1-\tilde{\gamma}}{1+\tilde{\gamma}}\ A_i, \qquad A_t = \frac{2}{1+\tilde{\gamma}}\ A_i. \tag{3.1.26}$$

Repeating the procedure at the second boundary assuming incident, reflection and transmission amplitudes respectively of the form,

$$u_s^{(i)} = B_i\ e^{i[Kx+ky_0\sin\theta-\omega t]}, \tag{3.1.27}$$

$$u_s^{(r)} = B_r\ e^{-i[Kx-ky_0\sin\theta+\omega t]}, \tag{3.1.28}$$

$$u_M^{(t)} = B_t\ e^{i[k(x\cos\theta+y\sin\theta)-\omega t]}, \tag{3.1.29}$$

which yields the boundary condition,

$$i\ T_s K(B_i - B_r) = i\ l\ T_M k\cos\theta B_t, \tag{3.1.30}$$

$$B_i - B_r = \frac{1}{\tilde{\gamma}}\ B_t. \tag{3.1.31}$$

And so similar to before the reflection and transmission coefficients are,

$$B_r = \frac{\tilde{\gamma}-1}{\tilde{\gamma}+1}\ B_i, \qquad B_t = \frac{2\tilde{\gamma}}{\tilde{\gamma}+1}\ B_i, \tag{3.1.32}$$

and the overall transmission through the system is,

$$\frac{B_t}{A_i} = \frac{4\tilde{\gamma}}{(1+\tilde{\gamma})^2}. \tag{3.1.33}$$

This is similar in form to the normal incidence result and as expected reduces to the previous result (3.1.19) when $\theta = 0$. This angular dependence does indicate that this system cannot be used to simultaneously bridge a range of waves with different incidences without causing reflections and losing transmission. Instead it is limited to perfectly bridging waves from one particular angle.

3.1.3 Oblique Boundary

Finally, consider the effect of having the strings connected at some angle ϑ to the boundary, instead of perfectly perpendicular. These strings will now have connection points to the membrane at $(0, nl)$ and $(d, nl + d\tan\vartheta)$. The formulation follows in the same way as before for the membranes but the governing equation for the strings instead becomes (2.1.1),

$$\rho_s \frac{\partial^2 u_s}{\partial t^2} = T_s \frac{\partial^2 u_s}{\partial \xi^2}, \tag{3.1.34}$$

where $\xi = x\cos\vartheta + y\sin\vartheta$ and so on matching the vertical tension, the altered boundary condition is given by,

$$T_M \frac{\partial u_M}{\partial x} = T_s \frac{\partial u_s}{\partial \xi}\delta^{(l)}(y), \tag{3.1.35}$$

which can be homogenised to produce,

$$T_M \frac{\partial u_M}{\partial x} = \frac{T_s}{l}\frac{\partial u_s}{\partial \xi} \tag{3.1.36}$$

From these expressions the displacement in the string is given by,

$$u_s^{(t)} = A_t e^{i[K\xi - \Omega t]} e^{i\chi y_0} = A_t e^{i[K(x\cos\vartheta x + y\sin\vartheta) - \Omega t]} e^{i\chi y_0}, \tag{3.1.37}$$

where K and Ω are related by (2.1.4) and to match the form of the exponents at the connections, $\chi = k_m \sin\theta - k_s \sin\vartheta$. It is clear that matching the displacements and tensions at the boundary in the same way as before will yield the same amplitude expressions as previously (3.1.24, 3.1.31), resulting in the same expressions for $\tilde{\gamma}$ and transmission and reflection coefficients (3.1.26, 3.1.32) but with an added phase change. Instead this system will be used to determine the wave phase shifts caused by the bridging. For this define two different phase shifts, a reflection phase shift, φ, and a transmission phase shift φ'.

The reflection phase shift refers to the phase shift undergone by a wave travelling from one end of the string to another. This is referred to as the reflection phase shift since a wave reflected at the right boundary will be out of phase with the incident wave by a factor of 2φ when it returns to the left boundary. The transmission phase shift will instead concern the right boundary of the system, representing the difference in phase of waves produced by the bridge and the phase of the corresponding wave produced by a system where the entire space is filled by the elastic membrane.

Begin by considering an arbitrary point of the left boundary, and set this to be the new origin of the coordinate system. Since all waves share the same frequency disregard the variation of phase with time and only consider spatial phase changes. At the origin then, define the phase to be 0. For a wave travelling along a string, the change in phase will simply be,

$$\varphi = Kd\cos\vartheta + Kd\sin\vartheta\tan\vartheta, \tag{3.1.38}$$

$$= \frac{\omega d}{c_s \cos\vartheta}, \tag{3.1.39}$$

which has no dependence on the angle of the incident wave. Thus by only knowing the frequency of an incoming wave it is possible to tune the phase changes and control wave interference. In the long wave limit the width of the gap will be much smaller

than the wavelength so $kd \ll 1$. With the exception of $\vartheta \to \pm\pi/2$, at this limit the reflection phase difference will tend to 0.

Next attempt to determine the transmission phase shift. An unbridged wave propagating from the origin would have a phase shift φ'_0 of,

$$\varphi'_0 = kd\cos\theta + kd\sin\theta\tan\theta, \tag{3.1.40}$$

$$= \frac{\omega d}{c_M\cos\theta}, \tag{3.1.41}$$

The corresponding 'originator' point on the left boundary for a bridged wave will be $(0, d\tan\theta - d\tan\vartheta)$. Since the change in phase along a string has already been calculated, the overall phase difference will be,

$$\varphi' = kd\sin\theta(\tan\theta - \tan\vartheta) + \varphi - \varphi'_0, \tag{3.1.42}$$

$$= \frac{\omega d}{c_M}\left(\frac{1}{\cos\vartheta}\left(\frac{c_M}{c_s} - \sin\theta\sin\vartheta\right) - \frac{1}{\cos\theta}\right), \tag{3.1.43}$$

which has the trivial solution of $\varphi' = 0$ for normal incidence on strings perpendicular to the boundary, where $c_M = c_s$. It also shows an infinite phase difference as the string angle $\vartheta \to \pm\pi/2$, representing the infinite increase of the string length. When the strings are held perpendicular to the boundary this simplifies to,

$$\varphi' = \frac{\omega d}{c_M}\left(\frac{c_M}{c_s} - \frac{1}{\cos\theta}\right). \tag{3.1.44}$$

Again in the long wave limit $kd \ll 1$ for a non-zero string wave speed, or an incident wave not parallel to the boundary, this gives $\varphi' \to 0$.

3.1.4 Perfect transmission

In many of the physical situations where a periodic bridge would be required, it is desirable that the system behaves as though there were no bridge present. For this

perfect transmission, it is required that the wave behaviour after the bridge is identical to the behaviour before the bridge. Most importantly, this means that both the amplitude and phase of the wave must be unchanged.

Both the cases for normal and oblique incidence have a single parameter which determine the transmission and reflection in the system, and both (3.1.19, 3.1.33) are an equation of the form,

$$T(\Gamma) = \frac{4\Gamma}{(1+\Gamma)^2}, \tag{3.1.45}$$

where Γ represents some unspecified bridging parameter such that $\Gamma = \gamma$ for normal incidence and $\Gamma = \tilde{\gamma}$ for oblique incidence. Then $T(\Gamma) = \frac{B_t}{A_i}$, plotted in Fig. 3.2 is the overall ratio of transmission. This function is a result of the transmissions and reflections from the first boundary, t_1 and r_1 (3.1.12, 3.1.26) and the second boundary, t_2 and r_2 (3.1.18, 3.1.32),

$$t_1 = \frac{2}{1+\Gamma}, \qquad r_1 = \frac{1-\Gamma}{1+\Gamma}, \tag{3.1.46}$$

$$t_2 = \frac{2\Gamma}{1+\Gamma}, \qquad r_2 = \frac{\Gamma-1}{\Gamma+1}. \tag{3.1.47}$$

It is clear both analytically from (3.1.45) and graphically from Fig. 3.2 that the

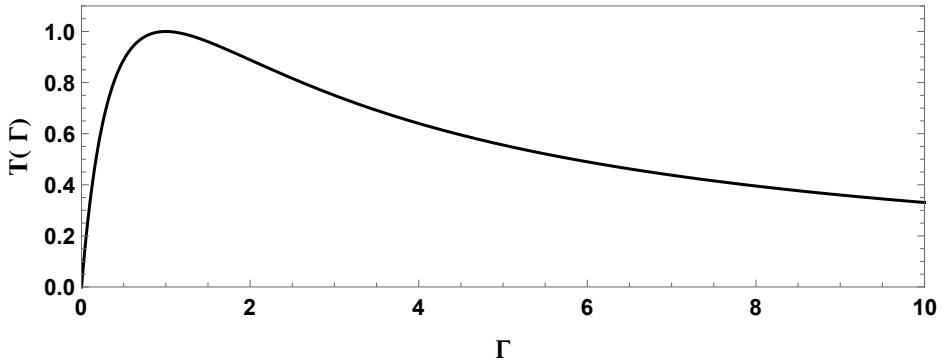

Figure 3.2: Ratio of amplitude of overall transmission to initial wave amplitude (3.1.45) against the parameter Γ.

transmission has a maximum of $T(\Gamma) = 1$ at $\Gamma = 1$. For normal incidence $\Gamma = \gamma$, which

has the special case of $\gamma = 1$ where the wave speeds across the two materials match and $T_M\ l = T_s$ (3.1.10). Physically this is the most intuitive system as it indicates that the tensions across the two materials match with perfectly balanced forces; the equivalent tension per unit area from the string acting on the membrane is equal to the tension per unit length divided by the length over which the tension is distributed, in this case l.

Since Γ varies with θ, it is not possible to construct a bridge such that $\Gamma = 1$ for all possible incident angles. Hence this system cannot be used to simultaneously bridge a range of waves with different incidences without losing transmission; instead it is limited to perfectly bridging waves from one particular angle. To find the average transmission over all incident angles, evaluate the integral,

$$\tilde{T}(\gamma) = \frac{1}{\pi}\int_{-\pi/2}^{\pi/2} T d\theta = \frac{1}{\pi}\int_{-\pi/2}^{\pi/2} \frac{4\Gamma\cos\theta}{(\cos\theta+\Gamma)^2}\, d\theta, \tag{3.1.48}$$

$$= \frac{8\Gamma}{\pi(1-\Gamma^2)}\left(2\frac{\tanh^{-1}\left(\sqrt{\frac{1-\Gamma}{1+\Gamma}}\right)}{\sqrt{1-\Gamma^2}} - 1\right) \tag{3.1.49}$$

which has a global maximum $\tilde{T} \approx 0.891$ for $\Gamma = 0.612871...$, compared to $\tilde{T} \approx 0.849$ for a bridge with $\Gamma = 1$ aimed at perfectly transmitting normally incident waves only. For some constant 'tuned' value of γ, transmission has a dependence with angle,

$$T(\theta) = \frac{4\Gamma\cos\theta}{(\Gamma+\cos\theta)^2} \tag{3.1.50}$$

which is shown for $\Gamma = 1$ and $\Gamma = 0.612871...$ in Fig. 3.3.

Both of the choices of parameter effectively transfer the wave amplitude from one side of the void to the other. While the maximised average tuning transmits the wave more effectively over a wider range of angles, the normal incidence tuning is more effective for small incident angles. Depending on the choice of system, either of these tuning choices may be more effective at bridging an incoming wave.

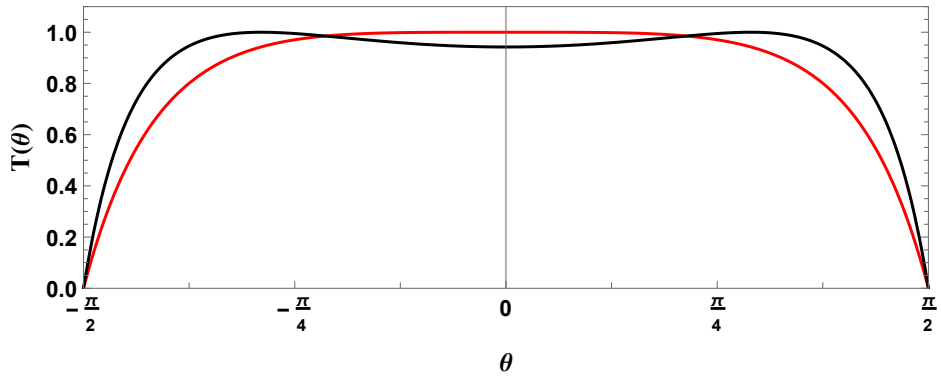

Figure 3.3: Ratio of amplitude of overall transmission to initial wave amplitude (3.1.50) for different incident angles θ on a string bridge. The two plot lines show different choices of parameter tuning, with normal incidence tuning, $\Gamma = 1$ denoted in red, and maximum average transmission tuning $\Gamma = 0.612871...$ denoted in black.

More generally, a wave tuned for perfect transmission for an angle θ has tuning parameter $\Gamma = \cos\theta$. If $\Gamma > 1$ then there is no perfect transmission for any incident angle, and transmission is decreased for all values of θ.

In this system, if the reflection at the second boundary is not perfect then there will be a part of the wave still present in the bridge, travelling back toward the first boundary. At this boundary it can again be transmitted or reflected, and the reflected component will again be incident on the second boundary, and so on. Therefore, as well as 'primary' reflection and transmission there will be an infinite number of reflections and transmissions at some fixed time intervals after the initial incidence, determined by the distance between the two boundaries and the wave speed in the strings.

Assuming that the two membrane halves are identical and that the properties of the string are constant, then from (3.1.46, 3.1.47), successive transmissions and reflections

from the bridges have coefficients,

$$R_n = \begin{cases} \dfrac{1-\Gamma}{1+\Gamma}\,, & n = 1 \\ \dfrac{4\Gamma}{(1+\Gamma)^2}\left(\dfrac{\Gamma-1}{\Gamma+1}\right)^{2n-3}, & n \geq 2 \end{cases} \tag{3.1.51}$$

$$T_n = \frac{4\Gamma}{(1+\Gamma)^2}\left(\frac{\Gamma-1}{\Gamma+1}\right)^{2n-2} \tag{3.1.52}$$

where R_n is the n^{th} reflection and T_n the n^{th} transmission, n being an integer denoting the number of reflections and transmissions the system has undergone. In this definition, $T(\Gamma) \equiv T_1$. These coefficients are plotted against the parameter Γ in Fig. 3.4 and show a clear decrease of amplitude for each successive R_n and T_n.

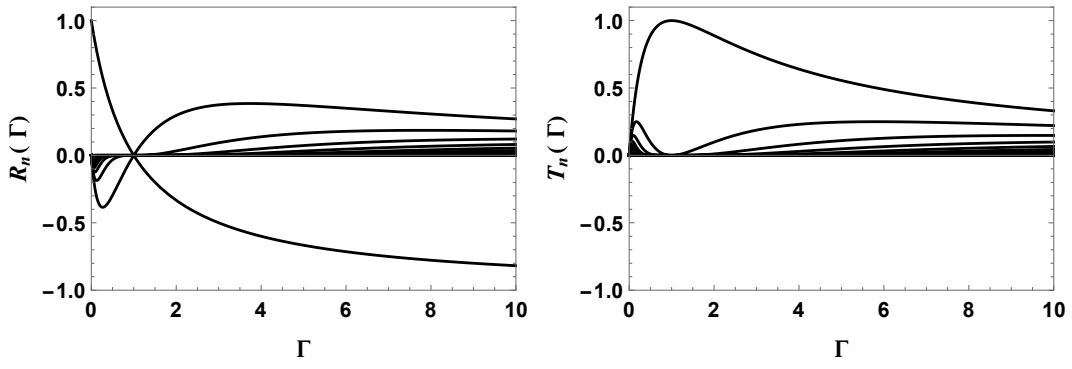

(a) Reflection Ratios, R_n **(b)** Transmission Ratios, T_n

Figure 3.4: Ratios of amplitudes of successive reflections (3.1.51) and transmissions (3.1.52) to initial wave amplitude against the parameter Γ.

This treatment only applies if there is a single wave packet incident upon the boundary. If the wave incident upon the bridge has an infinite number of successive wave packets then there will be wave interference between the successive reflections and transmissions. If the reflected waves or transmitted waves are in phase with each other as they exit the system then the overall amplitude will be the sum of all amplitudes.

These form the geometric series,

$$R_T = \frac{1-\Gamma}{1+\Gamma} + \sum_{n=2}^{\infty} \frac{4\Gamma}{(1+\Gamma)^2} \left(\frac{\Gamma-1}{\Gamma+1}\right)^{(2n-3)}, \tag{3.1.53}$$

$$T_T = \sum_{n=1}^{\infty} \frac{4\Gamma}{(1+\Gamma)^2} \left(\frac{\Gamma-1}{\Gamma+1}\right)^{(2n-2)}, \tag{3.1.54}$$

where R_T and T_T are the total reflection and transmission amplitude ratios respectively. Since these are geometric series the summation can be computed easily, and so regardless of the value of Γ,

$$R_T = 0, \qquad T_T = 1. \tag{3.1.55}$$

Therefore in an infinite system where the reflections and transmissions are kept in phase, the system will tend to having perfect transmission and no reflection.

However the successive transmitted and reflected waves are, in general, not in phase. When the waves are not kept in phase the amplitude of the overall wave is not equal to the summation of the amplitudes of the individual waves. To find the amplitude of the overall waves, assume the incident wave is of the form (3.1.20) and that each transmission across the strings adds a phase difference of φ (3.1.39) so that the transmitted wave is of the form,

$$u_M^{(t)} = \sum_{n=1}^{\infty} T_n A_i e^{i[k(x\cos\theta + y\sin\theta) - \omega t]} e^{i(2n-1)\varphi}, \tag{3.1.56}$$

and similarly the reflected wave is of the form,

$$u_M^{(r)} = \sum_{n=1}^{\infty} R_n A_i e^{-i[k(x\cos\theta - y\sin\theta) + \omega t]} e^{i(2n-2)\varphi}. \tag{3.1.57}$$

so the overall transmission and reflection ratios are,

$$R_T = \frac{1-\Gamma}{1+\Gamma} + \sum_{n=2}^{\infty} \frac{4\Gamma}{(1+\Gamma)^2} \left(\frac{\Gamma-1}{\Gamma+1}\right)^{2n-3} e^{i(2n-2)\varphi}, \tag{3.1.58}$$

$$T_T = \sum_{n=1}^{\infty} \frac{4\Gamma}{(1+\Gamma)^2} \left(\frac{\Gamma-1}{\Gamma+1}\right)^{2n-2} e^{i(2n-1)\varphi}, \tag{3.1.59}$$

where the previous T_T and R_T values (3.1.55) are for the particular case that $\varphi = 2m\pi$, $m \in \mathbb{Z}$. The magnitude of the ratio between successive terms in both of the infinite series are less than or equal to 1. When the ratio is 1 then there is already perfect transmission and R_n and T_n terms are zero for $n > 1$. In the other cases again treat these as a geometric series leading to,

$$R_T = \frac{1-\Gamma}{1+\Gamma}\left(\frac{1-e^{2i\phi}}{1-\left(\frac{1-\Gamma}{1+\Gamma}\right)^2 e^{2i\varphi}}\right), \tag{3.1.60}$$

$$T_T = \frac{4\Gamma}{(1+\Gamma)^2 e^{-i\varphi} - (1-\Gamma)^2 e^{i\phi}} \tag{3.1.61}$$

These have real wave amplitudes of,

$$|R_T| = \frac{1-\Gamma^2}{4\Gamma}\left(\frac{1}{2} + \left(\frac{1-\Gamma^2}{4\Gamma}\right)^2 \sin^2 2\varphi\right)^{-1/2} \sin 2\varphi, \tag{3.1.62}$$

$$|T_T| = \left(1 + \left(\left(\frac{1+\Gamma^2}{4\Gamma}\right)^2 - 1\right)\sin^2\varphi\right)^{-1/2}, \tag{3.1.63}$$

which are plotted in Fig. 3.5. From Fig. 3.5b it is clear that the overall transmission

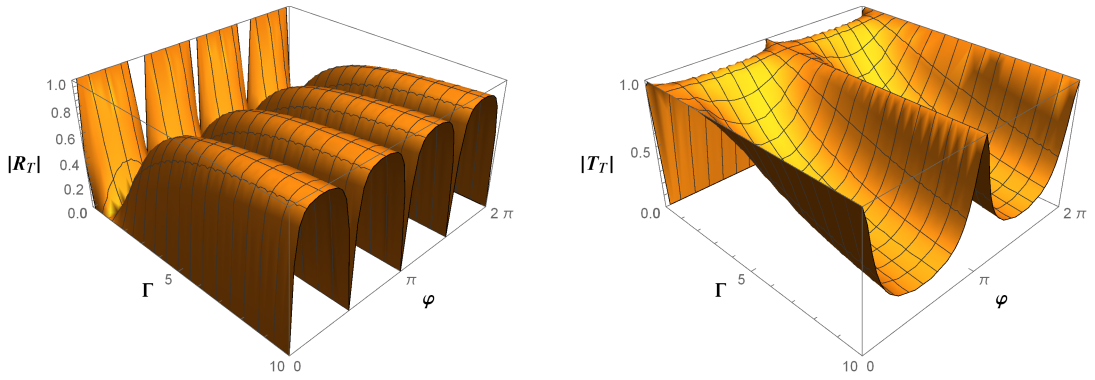

(a) Overall Reflection Ratio $|R_T|$ **(b)** Overall Transmission Ratio $|T_T|$

Figure 3.5: Ratios of amplitudes of overall reflection (3.1.62) and transmission (3.1.63) to initial wave amplitude against the parameter Γ and the added phase difference φ.

is only perfect for either $\Gamma = 1$ or when the phase difference φ is an integer multiple of π. Outside of these conditions the overall transmission decreases and the reflection increases. These two cases will be investigated individually.

When $\Gamma = 1$, it is not necessary to consider φ as there are no successive reflections and transmissions. In the long wave limit assuming c_M and c_s are both finite and that neither the incident wave or the strings are parallel to the boundary, both φ and φ' tend to 0, guaranteeing perfect matching of the wave.

If $\theta \to \pm\pi/2$ then the long wave assumption is no longer valid. Since perfect amplitude matching requires $\Gamma = 1$, then using the matching parameter for oblique incidence (3.1.24) gives $\Gamma = \tilde{\gamma}$ so,

$$\cos\theta = \gamma, \tag{3.1.64}$$

and to perfectly match the wave requires the overall phase change to be $\varphi' = 2m\pi,\ m \in \mathbb{Z}$. This leads to the relation for string angle to be,

$$\left(2m\pi\frac{c_M}{\omega d}\gamma + 1\right)\cos\vartheta = \gamma\left(\frac{c_M}{c_s} - \sqrt{1-\gamma^2}\sin\vartheta\right), \tag{3.1.65}$$

and if it is assumed that the strings are not held parallel to the boundary, $\cos\vartheta \neq 0$ so as $\gamma, \omega d \to 0$, the resulting wave matches if the wavelength and angle of the incident wave and size of the void satisfy,

$$\frac{d}{\lambda\cos\theta} \in \mathbb{N}, \tag{3.1.66}$$

where $\mathbb{N}$ is the set of natural numbers not including 0. Interestingly this condition is independent on the properties of the bridge itself, so this bridge construction cannot arbitrarily bridge any void for any incident wave.

In the case of an infinite number of incident wavefronts, when $\varphi = r\pi,\ r \in \mathbb{Z}$, $T_T = 1$ and $R_T = 0$. The overall wave, like each of the component waves, has a relative phase difference of 0. Hence the phase difference to the unbridged wave will be given by φ' (3.1.43). Since perfect matching requires that the bridged and unbridged waves be identical, $\varphi' = 2m\pi$, $m \in \mathbb{Z}$. Substituting φ from (3.1.39) gives,

$$\cos\vartheta = \frac{\omega d}{c_s r\pi}. \tag{3.1.67}$$

In the long wave limit this gives $\vartheta = 0$, $r \neq 0$.

$$2m\pi = \frac{\omega d}{c_M}\left(\frac{c_M}{c_s} - \frac{1}{\cos\theta}\right), \tag{3.1.68}$$

which gives the angle requirement,

$$\cos\theta = \frac{c_s}{c_M - \frac{m\lambda}{d}c_s}. \tag{3.1.69}$$

This will give different results depending on m. For $m = 0$ this gives the angle requirement,

$$\cos\theta = \frac{c_s}{c_M} \tag{3.1.70}$$

and for $m > 0$,

$$\frac{d}{\lambda\cos\theta} \in \mathbb{N}, \tag{3.1.71}$$

which is the same as the result for a single wave front.

Therefore for this system, whether a wave can be perfectly bridged or not depends only on the properties of the void and the incident wave. While a bridge exists for all angles of incidence which can ideally transfer the wave amplitude, for shallow incidence waves the change of phase cannot be controlled by changing bridge parameters. This is true for both a single incident wavefront and infinite wavefronts.

The system also produces no reflections for $\varphi = r\pi/2$, but unlike the other cases for no reflection there is still a loss in transmission. For this phase difference the overall transmission is,

$$T_T = \frac{4\Gamma}{(1+\Gamma)^2} \tag{3.1.72}$$

which is the same as the first wave transmission from the system (3.1.45). For this phase difference the R_n terms all cancel, and so do the T_n terms except T_0. Practically this

represents a wave suppression, where the wave pattern is replicated with no reflections but the amplitude is reduced.

Note also that the transmission for R_T and T_T is only valid for an infinite continuous wave. For a finite number of wavefronts, only the matching for $\Gamma = 1$ will give perfect transmission.

3.2 Fourier Series method

Complementary to the homogenisation approach above, this problem can also be treated using a Fourier Series approach. The purpose of this section is to show that the homogenisation technique is valid for this system given the periodic scale of the boundary is much smaller than the characteristic length scale of the wave, the wavelength λ.

3.2.1 Arbitrary Fourier Series

Since the above forcing is periodic, introduce an exact Fourier series to model the boundary. First start with the most general case of some arbitrary Fourier series with coefficients E_j and replace $\delta^{(l)}$ with the series,

$$\sum_{j=-\infty}^{\infty} \frac{E_j}{l} e^{-i\ j\pi \frac{y}{l}}. \tag{3.2.1}$$

so the boundary condition (3.0.1) takes the form,

$$T_M \frac{\partial u_M}{\partial x} = T_s \frac{\partial u_s}{\partial x} \sum_{j=-\infty}^{\infty} \frac{E_j}{l} e^{-i\ j\pi \frac{y}{l}}, \tag{3.2.2}$$

where E_j terms are constants with respect to the spatial and time variables. The incident wave is independent of the boundary so it is assumed that this has the same

arbitrary form as before,

$$u_M^{(i)} = A_i e^{i[k(x\cos\theta + y\sin\theta) - \omega t]}. \tag{3.2.3}$$

However, as the forcing along the boundary of the membrane contains a summation, to balance both sides of the equation it is assumed that the reflected component of the wave is an infinite summation. For the most simple matching assume that the summation takes the form,

$$u_M^{(r)} = \sum_{j=-\infty}^{\infty} A_{rj} e^{-i[k(\kappa_j x\cos\theta - y\sin\theta) - \omega t]} e^{i\ 2j\pi\frac{y}{l}}, \tag{3.2.4}$$

where to satisfy the governing equations,

$$k^2\cos^2\theta = k^2\kappa_j^2\cos^2\theta + \left(\frac{2j\pi}{l}\right)^2, \tag{3.2.5}$$

$$\kappa_j = \sqrt{1 - \left(\frac{j\lambda}{l\cos\theta}\right)^2}, \tag{3.2.6}$$

and as before λ is the wavelength of the incident wave and θ is the angle of incidence. Assume also that as before the transmitted waves into the strings have the form,

$$u_s^{(t)} = A_t e^{i[Kx + ky\sin\theta - \omega t]} \tag{3.2.7}$$

and so the boundary condition (3.2.2) becomes,

$$T_M e^{i[ky\sin\theta - \omega t]}\left(k\cos\theta A_i - \sum_{j=-\infty}^{\infty} k_j A_{rj} e^{i\ 2j\pi\frac{y}{l}}\right) = T_s K A_t e^{i[ky\sin\theta - \omega t]} \sum_{j=-\infty}^{\infty} \frac{E_j}{l} e^{i\ 2j\pi\frac{y}{l}}, \tag{3.2.8}$$

which gives

$$A_i - \sum_{j=-\infty}^{\infty} \kappa_j A_{rj} e^{i\ 2j\pi\frac{y}{l}} = \tilde{\gamma} A_t \sum_{j=-\infty}^{\infty} E_j e^{i\ 2j\pi\frac{y}{l}}. \tag{3.2.9}$$

Since both sides have the form of a Fourier series, the summation coefficients are unique and each term on the left hand side will equal the corresponding term from the right hand side. For the waves arising from the higher order terms to propagate into the

material and not decay exponentially away from the boundary, the values of κ_j must be real. Since the incident wave is always propagating then the incident wave number $k\cos\theta$ must be real. Then for the j^{th} term of the summation to be real, from (3.2.6),

$$\frac{|j|\lambda}{l|\cos\theta|} \leq 1, \tag{3.2.10}$$

$$|j| \leq \frac{l|\cos\theta|}{\lambda}. \tag{3.2.11}$$

For the homogenisation, it was assumed that $\lambda \gg l$ and since $|\cos\theta| \leq 1$,

$$0 < \frac{l|\cos\theta|}{\lambda} \ll 1, \tag{3.2.12}$$

so for long incident waves, for all $j \neq 0$ the reflected waves will decay exponentially away from the boundary. Thus it is preferable to treat the $j = 0$ reflected wave, or the 'first reflection' separately. Therefore on matching the summation term by term,

$$A_i - A_{r0} = E_0\tilde{\gamma}A_t, \tag{3.2.13}$$

$$A_{rj}\kappa_j = E_j\tilde{\gamma}A_t, \ j \neq 0. \tag{3.2.14}$$

and introduce a new summation parameter, σ, to represent the effect of the waves from the $n \neq 0$ terms,

$$\sigma = \sum_{j=-\infty}^{-1} \frac{E_j}{E_0}\kappa_j^{-1} + \sum_{j=1}^{\infty} \frac{E_j}{E_0}\kappa_j^{-1}. \tag{3.2.15}$$

Using the continuity of displacement (3.1.2),

$$A_i + \sum_{j=-\infty}^{\infty} A_{rj} = A_t, \tag{3.2.16}$$

$$A_i + A_{r0} = (1 + E_0\sigma\tilde{\gamma})A_t. \tag{3.2.17}$$

These give the reflection and transmission coefficients of,

$$\frac{A_{r0}}{A_i} = \frac{1 - E_0\tilde{\gamma}(1-\sigma)}{1 + E_0\tilde{\gamma}(1+\sigma)}, \qquad \frac{A_t}{A_i} = \frac{2}{1 + E_0\tilde{\gamma}(1+\sigma)}. \tag{3.2.18}$$

For the second boundary, follow the same technique as above but assume incident, reflected and transmitted displacements respectively of the form,

$$u_s^{(i)} = B_i \; e^{i[Kx+ky\sin\theta-\omega t]}, \tag{3.2.19}$$

$$u_s^{(r)} = B_r \; e^{-i[Kx-ky\sin\theta+\omega t]}, \tag{3.2.20}$$

$$u_M^{(t)} = \sum_{j=-\infty}^{\infty} B_{tj} \; e^{i[k(\kappa_j x\cos\theta+y\sin\theta)-\omega t]}\frac{1}{l}e^{i\;2j\pi\frac{y}{l}}. \tag{3.2.21}$$

As before, only the $j = 0$ case will propagate and so this 'first transmission' case of B_{t0} will be treated separately. In this case the continuity of displacements (3.1.2) gives the condition,

$$B_{tj} = \frac{E_j}{E_0}\kappa_j^{-1}B_{t0}, \tag{3.2.22}$$

$$\sum_{j=\infty}^{\infty} B_{tj} = B_{t0}(1+\sigma). \tag{3.2.23}$$

Then by substituting into the stress boundary condition (3.2.2) and following the same procedure as before of matching terms in the Fourier series yields the expression,

$$T_s K(B_i - B_r)E_0 = l\; T_M k\cos\theta B_{t0}, \tag{3.2.24}$$

$$B_i - B_r = \frac{B_{t0}}{\tilde{E_0\gamma}}, \tag{3.2.25}$$

so then the coefficients of reflection and transmission are,

$$\frac{B_r}{B_i} = \frac{E_0\tilde{\gamma}(1+\sigma)-1}{E_0\tilde{\gamma}(1+\sigma)+1}, \qquad \frac{B_{t0}}{B_i} = \frac{2E_0\tilde{\gamma}}{E_0\tilde{\gamma}(1+\sigma)+1}, \tag{3.2.26}$$

which leads to the overall transmission through the system as being,

$$\frac{B_{t0}}{A_i} = \frac{4E_0\tilde{\gamma}}{(1+E_0\tilde{\gamma}(1+\sigma))^2}. \tag{3.2.27}$$

(3.2.27) is the more general case of (3.1.45), with $\tilde{\gamma}$ replaced with $E_0\tilde{\gamma}$, and the inclusion of σ to represent the effect of the leading order terms. Thus, when σ is small the transmission will be perfect for $E_0\tilde{\gamma} = 1$.

Next reintroduce the periodic delta function, for which the Fourier series is given by,

$$\delta^{(l)}(y) = \sum_{j=-\infty}^{\infty} \frac{1}{l} e^{i\ 2j\pi\frac{y}{l}}. \tag{3.2.28}$$

then for this forcing $E_j = E_0 = 1$ and $\kappa_j = \kappa_{-j}$ so the σ for this forcing, σ_δ, is given by

$$\sigma_\delta = 2\sum_{j=1}^{\infty} \kappa_j^{-1} \tag{3.2.29}$$

Using the delta function boundary therefore leads to the coefficient for overall transmission through the system as,

$$\frac{B_{t0}}{A_i} = \frac{4\tilde{\gamma}}{(1+\tilde{\gamma}(1+\sigma_\delta))^2}, \tag{3.2.30}$$

which replicates the homogenised results (3.1.45) for $\sigma_\delta = 0$. In order to verify the homogenisation, it is therefore necessary to investigate the behaviour of σ.

3.2.2 Fourier Series σ Analysis

The homogenised solution differs to the exact Fourier solution due to the presence of σ_δ, a parameter arising from the summation, dependent on the angle of incidence, wavelength of the incident wave, and the spacing of the strings and also independent of the material parameters of the membrane and string. It is clear on comparing the overall transmission coefficient for the homogenised system (3.1.45) and those for the exact Fourier solution (3.2.30) that the two sets of results coincide given $\sigma_\delta = 0$.

For the higher terms, as $j \to \infty$,

$$\kappa_j \to 2i\frac{l\cos\theta}{\lambda}\frac{1}{j}. \tag{3.2.31}$$

On a term by term analysis, all of the terms are vanishingly small and so can individually be discarded. However for large j, the series σ_δ will converge towards the

harmonic series, which is divergent. Therefore it can be supposed that this series is also divergent and so $\sigma_\delta \to \infty$. Substituting this into the previous coefficients shows that regardless of the value of $\tilde{\gamma}$, the overall transmission will tend to 0.

It can however be supposed that this non-physical result is a consequence of using the delta function, a non-physical representation of point loading which disregards material deformations along the boundary. To see if this is a problem with the system or a particular feature of using delta function forcing, next investigate σ in a more general case.

In the particular case that the forcing is both real and symmetric, the values of E_j must be given by $\{E_j \in \mathbb{R} | E_j = E_{-j}\}$. In this case, the expression for σ becomes,

$$\sigma = \sum_{j=1}^{\infty} \frac{2E_j}{E_0} \kappa_j^{-1}. \tag{3.2.32}$$

As with the case for the delta function, as $j \to \infty$ each term σ_j is given by,

$$\sigma_j \to 2i \frac{l \cos\theta}{E_0 \lambda} \frac{E_j}{j}, \tag{3.2.33}$$

and since it is necessary that the boundary Fourier series converges, then it follows that the sum $\sum_{j=1}^{\infty} E_j$ must converge. From this it can also be shown that the sum $\sum_{j=1}^{\infty} \frac{E_j}{j}$ converges and so σ will have a finite value.

As before, if $\lambda \cos\theta \gg l$ then the summation will have all imaginary terms and so when $\sigma \neq 0$, in general, $\frac{B_{t0}}{A_i} \neq 1$ since there will be some imaginary component. Hence for full amplitude transmission the argument of the overall transmission ratio must be equal to 1, with the imaginary part causing a phase shift in the wave.

In the case $\sigma = \sigma_r + i\ \sigma_i$, where σ_r and σ_i are both real,

$$\left| \frac{4E_0\tilde{\gamma}}{(1 + E_0\tilde{\gamma}(1 + \sigma_r + i\ \sigma_i))^2} \right| = 1. \tag{3.2.34}$$

When σ has no real part, $\sigma_r = 0$. If it is also assumed that the bridge parameters are

all strictly real and positive then the above condition can be simplified to,

$$\left|(1+E_0\tilde{\gamma})^2 - E_0^2\tilde{\gamma}^2\sigma_i^2 - 2i(1+E_0\tilde{\gamma})E_0\tilde{\gamma}\sigma_i\right| = \frac{\left((1+E_0\tilde{\gamma})^2 - E_0^2\tilde{\gamma}^2\sigma_i^2\right)^2 + 4(1+E_0\tilde{\gamma})^2E_0^2\tilde{\gamma}^2\sigma_i^2}{4E_0\tilde{\gamma}} \tag{3.2.35}$$

which has solutions,

$$E_0\tilde{\gamma} = \frac{3 \pm 2\sqrt{2+i\sigma_i} + i\sigma_i}{\sigma_i^2 - 1 - 2i\sigma_i}, \quad \frac{1 \pm 2(-1)^{3/4}\sqrt{\sigma_i} - i\sigma_i}{1 + 2i\sigma_i - \sigma_i^2}. \tag{3.2.36}$$

However, these solutions only give real positive values of $E_0\tilde{\gamma}$ for $\sigma_i = 0$. Thus even though a sufficiently small value of σ will lead to diminishingly small transmission losses there is no way to perfectly reproduce all aspects of the wave pattern even taking into account the coupling between the two materials.

Since perfect transmission is not possible solely by selecting bridge parameters, it is again possible to consider the effect of the summation of successive reflections and transmissions from the system as before. Like the simple case for homogenisation (3.1.51, 3.1.52) the Fourier series gives reflection and transmission coefficients of,

$$R_n = \begin{cases} \dfrac{A_{r0}}{A_i}, & n = 1 \\ \dfrac{B_{t0}}{A_i}\left(\dfrac{B_r}{B_i}\right)^{(2n-3)}, & n \geq 2 \end{cases} \tag{3.2.37}$$

$$T_n = \frac{B_{t0}}{A_i}\left(\frac{B_r}{B_i}\right)^{(2n-2)}, \tag{3.2.38}$$

for which the summations of R_n and T_n are again a geometric series. From equations (3.2.18, 3.2.26, 3.2.27), the total reflected and transmitted amplitudes, R_T and T_T respectively, are

$$R_T = \frac{\sigma}{1+\sigma}, \quad T_T = \frac{1}{1+\sigma}. \tag{3.2.39}$$

Unlike for the homogenised case, the reflection and transmission totals do not tend to a value. They are however still independent of the material parameters and instead

depend only on the nature of the coupling chosen. To recover the homogenised solution, when σ tends to zero, R_T again tends to 0 and T_T tends to 1. In a more general case the sum of the transmitted and reflected wave amplitudes is 1 which conserves energy in the system. Furthermore, if the phase of the transmission and reflection are disregarded and as before assume that $\sigma = i\sigma_i$, then the wave amplitudes are,

$$|R_T| = \frac{\sigma_i}{\sqrt{1+\sigma_i^2}}, \quad |T_T| = \frac{1}{\sqrt{1+\sigma_i^2}} \tag{3.2.40}$$

which again only equal 0 and 1 respectively when $\sigma_i = 0$. For any other value of σ_i the transmission decreases and reflection increases.

Therefore our perfect matching is fundamentally limited by the matching between the materials, and a 'good' matching can only be produced for a small value of σ. It is therefore necessary to examine more realistic models for the boundary to see if this condition can be met. To undertake short scale analysis it is necessary to replace the delta function for a more realistic coupling function.

3.2.3 Distributed Delta Function Boundary

To determine how valid the above approach is, choose a function to investigate which could represent forcing along the boundary in a real physical system. Since this analysis began using the delta function, it is a good starting point to choose a function which on larger length scales approximates or tends to the delta function. One such function is a capped exponential, which is given by,

$$f(y) = \frac{\sqrt{\alpha}}{\sqrt{\pi}\ \mathrm{erf}(\frac{\sqrt{\alpha}\ l}{2})} e^{-\alpha y^2} \tag{3.2.41}$$

where $\mathrm{erf}(x)$ is the error function of x and α is a tuning parameter to alter the width of the function. This function is positive over the whole domain and has a single peak at the origin. The integral of the function over $-\frac{l}{2}$ to $\frac{l}{2}$ is 1 and as α tends to infinity, $f(y)$

will tend to 0 everywhere except the origin. These conditions together are sufficient to define $f(y)$ as $\alpha \to \infty$ as the delta function.

To fully replicate the coupling this function needs to be periodic over l. While the function could be defined piecewise periodically, this would lead to a discontinuity of the gradients at $y = (m + \frac{1}{2})l$, $m \in \mathbb{Z}$. Instead, suppose that each connection between the string and the membrane causes a capped exponential. Then the overall function would be an infinite sum of periodically arranged capped exponentials, which can be expressed as a Jacobi ϑ_3 function [107],

$$\vartheta_3\left(\frac{\pi y}{l},\ e^{\frac{-\pi^2}{\alpha l^2}}\right) = l \sum_{m=-\infty}^{\infty} \sqrt{\frac{\alpha}{\pi}} e^{-\alpha(y+ml)^2}, \tag{3.2.42}$$

where the function is periodic and infinitely differentiable. Since physical strings cannot have point like connections and the forcing will depend on the width of the strings, it may be more convenient to use a tuning parameter which changes the width of the function. Hence choose h to be the relative half width of one peak, ie.,

$$\left\{h \in \mathbb{R} \mid d > 0,\ e^{-\alpha(\frac{hl}{2})^2} = \frac{1}{2}\right\}. \tag{3.2.43}$$

Defining this distributed delta function as $\delta^{(h,l)}(y)$ gives

$$\delta^{(h,l)}(y) = \tfrac{1}{l}\ \vartheta_3\left(\frac{\pi y}{l},\ e^{\frac{-\pi^2 h^2}{4\ln(2)}}\right), \tag{3.2.44}$$

where the function has been normalised so that again the integral of $\delta^{(h,l)}(y)$ over any one period, $\frac{m}{2}l$ to $\frac{(m+1)}{2}l$ is 1. Figure 3.6 shows how this function behaves for decreasing values of h/l, quickly converging to the delta function.

From the standard expression for Fourier series coefficients,

$$E_j = \int_{-l/2}^{l/2} \tfrac{1}{l}\ \vartheta_3\left(\frac{\pi x}{l},\ e^{\frac{-\pi^2 h^2}{4\ln(2)}}\right) e^{-i(j\pi y/l)} dy, \tag{3.2.45}$$

$$E_0 = \int_{-l/2}^{l/2} \tfrac{1}{l}\ \vartheta_3\left(\frac{\pi x}{l},\ e^{\frac{-\pi^2 h^2}{4\ln(2)}}\right) dy. \tag{3.2.46}$$

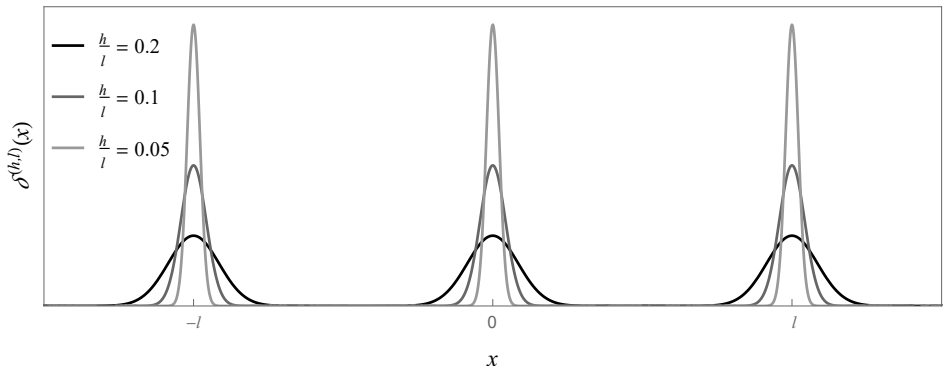

Figure 3.6: Comparisons of the distributed delta function $\delta^{(h,l)}(x)$ for different values of the half-thickness h, where l is the separation between successive strings.

It has already been established that the integral of the function equals 1, so regardless of the choice of parameters, $E_0 = 1$. Note that for the forcing to conserve tension along the boundary this integral should equal 1 and so $E_0 = 1$ in general.

To find the values for σ of the above $\delta^{(h,l)}(y)$, the sum of a numerical Fourier Series approximation can be made. For demonstration, a range of σ values for a normally incident wave with this type of boundary forcing are shown in Table 3.1 for different peak widths and incident wavelengths to an appropriate level of accuracy. From Table

		l/λ			
		1×10^{-1}	1×10^{-2}	1×10^{-3}	1×10^{-4}
h	1	0.0057 i	0.057 i$\times 10^{-2}$	0.057 i$\times 10^{-3}$	0.057 i$\times 10^{-4}$
	0.5	0.0854 i	0.850 i$\times 10^{-2}$	0.850 i$\times 10^{-3}$	0.850 i$\times 10^{-4}$
	0.1	0.3930 i	3.919 i$\times 10^{-2}$	3.919 i$\times 10^{-3}$	3.919 i$\times 10^{-4}$
	0.05	0.5312 i	5.301 i$\times 10^{-2}$	5.300 i$\times 10^{-3}$	5.300 i$\times 10^{-4}$
	0.01	0.8530 i	8.518 i$\times 10^{-2}$	8.518 i$\times 10^{-3}$	8.518 i$\times 10^{-4}$

Table 3.1: Values for σ (3.2.32) for a Jacobi ϑ_3 forcing with Fourier coefficients (3.2.45) with varying incident wavelengths λ and peak relative half widths d.

3.1 it is visible that smaller values of h lead to larger σ values. Alternately, for small d this function can be approximated by the delta function, and so the increasing σ will diverge. Similarly, for large d the forcing gradually becomes constant; in this instance the Fourier Series has no significant terms beyond the first and σ will tend to zero. Furthermore, from (3.2.33), for large $\frac{j\lambda}{l\cos\theta}$, the wave scaling parameter l/λ can be taken out of the terms of σ as a constant factor. Thus when the wavelength is much larger than the distance between the strings, σ is inversely proportional to λ.

Therefore, as $E_0 = 1$ and σ tends to 0 for large wavelengths, the homogenisation technique developed earlier reproduces the results of the exact solution while also being much simpler to solve. For the remainder of the bridging problems in this thesis, this homogenisation procedure will be assumed to be valid. Hence as the problems become more involved to solve, use this homogenisation procedure without additional verification from the exact result.

3.3 Net Bridge

Next, introduce a net of strings as described in [78] as a "membrane-like lattice". This square lattice consists of an infinite array of strings which we will insert into the void between membranes, as indicated in Figure 3.7. While this structure allows for both x and y-direction wave propagation in the bridge the size of the 'holes' are much smaller, meaning that the maximum size of inclusion which can be concealed by the bridge is correspondingly much smaller. Due to the connections between strings along the y-axis the wave propagation can be 2D in this structure. The dispersion of waves in such a net has already been studied, and for a harmonic wave of amplitude A_n being excited by a constant angular frequency ω the out-of-plane displacement waves in the net have

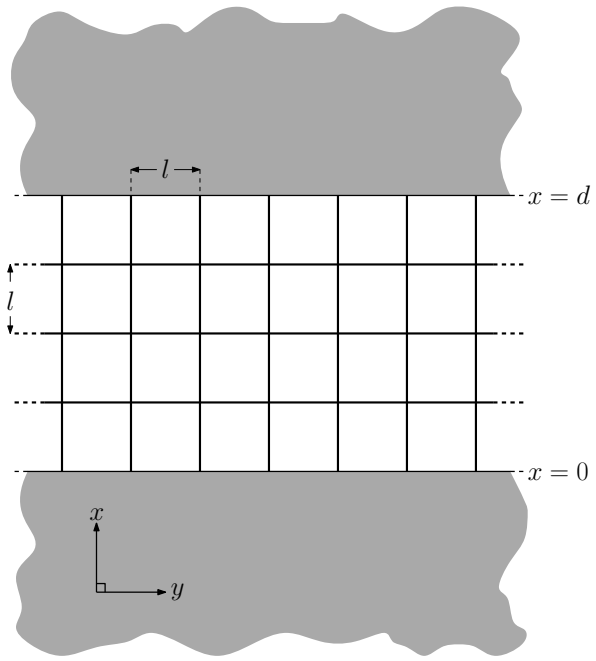

Figure 3.7: Schematic of an infinite elastic membrane with a square lattice of strings with separation l, bridging a void between $x = 0$ and $x = d$.

a form,

$$u_n = A_n e^{i[k_x x + k_y y - \omega t]}, \tag{3.3.1}$$

where k_x and k_y are the wavenumbers in the x and y-direction for waves in the net and in the notation of this thesis,

$$\cos(k_x l) + \cos(k_y l) = 2\cos\left(\frac{\omega l}{c_s}\right). \tag{3.3.2}$$

Using the same long wave assumption as before, if $\omega \ll c_s l$ then $k_x,\ k_y \ll l$ and so using the Taylor expansion of the cosine function yields,

$$k_x^2 + k_y^2 = \sqrt{2}\frac{\omega^2}{c_s^2}, \tag{3.3.3}$$

which is similar to the dispersion relation for a membrane (2.1.17). Defining a new wave speed c_n and wavenumber k_n by,

$$c_n = \frac{c_s}{\sqrt[4]{2}} = \frac{\omega}{k_n}. \tag{3.3.4}$$

For $c_M = c_n$ this net will have the same wave speed as the membrane. Following the same procedure as before yields the altered boundary conditions for forces and displacements respectively at $x = 0$ and $x = d$,

$$T_m \frac{\partial u_M}{\partial x} = T_s \frac{\partial u_n}{\partial x} \delta^{(l)}(y), \tag{3.3.5}$$

and

$$u_M = u_n. \tag{3.3.6}$$

Since we have already made use of a long wave assumption and shown the effectiveness of the homogenisation scheme for this boundary, consider only a homogenised boundary condition for this bridge. As before the homogenisation of the distributed delta function yields,

$$T_M \frac{\partial u_M}{\partial x} = \frac{T_s}{l} \frac{\partial u_n}{\partial x} \tag{3.3.7}$$

and on assuming waves in the membrane and net respectively of the form

$$u_M = A_i e^{i[k_m(x\sin\theta + y\cos\theta) - \omega t]} + A_r e^{i[k_m(-x\sin\theta + y\cos\theta) - \omega t]}, \qquad u_n = A_t e^{i(k_x x + k_y y - \omega t)}, \tag{3.3.8}$$

for which substitution into the boundary conditions at $x = 0$ yields,

$$A_r = \frac{1 - \gamma_n}{1 + \gamma_n} A_i, \qquad A_t = \frac{2}{1 + \gamma_n} A_i, \tag{3.3.9}$$

where in this case the bridging function $\gamma_n(\theta)$ is given by,

$$\gamma_n(\theta) = \frac{T_s}{T_M l} \sqrt{1 - \left(1 - \frac{c_M^2}{c_n^2}\right) \sec^2\theta}. \tag{3.3.10}$$

Similarly, taking the assumed wave forms,

$$u_n = B_i e^{i[k_x x + k_y y - \omega t]} + B_r e^{i[-k_x x + k_y y - \omega t]}, \qquad u_M = B_t e^{i[k_m(x\sin\theta + y\cos\theta) - \omega t]}, \tag{3.3.11}$$

and substituting into the boundary $y = d$ yields,

$$B_r = \frac{\gamma_n - 1}{\gamma_n + 1} B_i, \qquad B_t = \frac{2\gamma_n}{\gamma_n + 1} B_i. \tag{3.3.12}$$

for which the coefficients obtained from this system are identical to (3.1.26) and (3.1.32) with γ_θ replaced by γ_n and so the previous analysis also applies here, with the overall first wave transmission coefficient given by,

$$T_1(\gamma_n) = \frac{B_t}{A_i} = \frac{4\gamma_n}{(1+\gamma_n)^2}, \tag{3.3.13}$$

which has a maximum $T_1(\gamma_n) = 1$ at $\gamma_n = 1$. Unlike the previous string bridging problem, it is possible to ensure that perfect bridging can be obtained in this system regardless of incident angle since when $c_M = c_n$ there is no angular dependence on the value of γ_n. For this choice of material parameters the membrane formulation is the same as a distributed formulation for the net bridge and so in a long wave assumption the matching is trivial. Therefore, for this bridge the natural matching of tensions $T_M l = T_s$ gives $\gamma_n = 1$ and there is no phase change introduced, leading to a perfect bridging.

This bridging system also allows for tunable wave filtering based on incident angle. While the previous string bridging scheme had a decrease in transmission from angles away from the maximum, there was always some transmission from every incident wave angle. However, for this bridge system there are no propagating waves for

$$\sin\theta > \frac{c_M}{c_n} \tag{3.3.14}$$

so if $c_n > c_M$ there are always some waves which are not transmitted. To filter any waves with an incident angle greater than a previously defined filtering angle, θ_f, requires

$$\frac{c_M}{c_n} = \sin\theta_f \tag{3.3.15}$$

and to ensure a maximum at some given angle, θ_{max}, requires $\gamma_n = 1$ at this angle. Therefore on substitution the ratio of tensions must be given by,

$$\frac{T_M l}{T_s} = \sqrt{1 - \frac{\cos\theta_f}{\cos\theta_{max}}} \tag{3.3.16}$$

so by altering the tension and the wave speed of the strings proportional to the tension and wave speed in the membrane any incident wave can be fully bridged and any range of incident angles greater than a specified angle can be fully filtered. There is, however, no way to filter a range of angles less than a given angle.

Furthermore the previous discussion on the effect of successive transmissions and reflections remain valid where in this system if the propagation angle of the waves in the net is θ_n the reflection phase change φ_n is given by,

$$\varphi_n = d(k_n(\cos\theta_n + \sin\theta_n \tan\theta_n) - k_m \sin\theta \tan\theta) \tag{3.3.17}$$

$$= \frac{\omega d}{c_M}\left(\frac{c_M}{c_n}\left(1 - \frac{c_n^2}{c_M^2}\sin^2\theta\right)^{-1/2} - \sin\theta\tan\theta\right). \tag{3.3.18}$$

This phase change is much more involved than the previous phase changes due to the 2D wave propagation in the bridge. However, as before when φ_n is an integer multiple of π, wave superposition leads to the overall reflected wave tending to a relative amplitude of 0 and the transmitted wave tending to a relative amplitude of 1.

As before, however, this phase change depends on both the wave frequency and the incident wave angle so it is not possible to produce perfect transmission by internal reflections which is either broadband or angle independent.

3.4 Membrane Bridge Conclusion

For the above bridge system, it is demonstrated that two different periodic arrays of strings can carry wave behaviour across a void in an elastic membrane. Not only is

it possible to select material parameters for the strings to perfectly transmit a wave pattern incident from a single angle, but if the phase of the wave is correctly tuned, internal reflections on the bridge can interfere and for an infinite number of wavefronts either the same wave pattern or a suppressed wave can be transmitted across the void with no reflection. Importantly, all of the required material parameters are isotropic constants. This is unlike the scheme for membrane cloaking where the cloak stiffness and density were both spatially dependent and anisotropic.

It has also been shown that a homogenisation approach can be used to determine the wave transmission and reflection across the void caused by the periodic insertion of strings. Furthermore, it has been shown using a Fourier series to represent the forcing at the boundary that the transmission and reflection coefficients determined by this approach are accurate for long wavelength forcing. Thus, the homogenisation is not only practical to apply and use but the results are, to a good degree of accuracy, close to the exact solution. As a result this homogenisation can be applied to other more complicated schemes where the exact solution cannot be so easily obtained.

The scheme proposed does have limitations. While the results for the string bridge are broadband in the long wave limit, this bridge cannot ideally reproduce the wave pattern for all incident angles. Furthermore, while the net bridge produces a bridging scheme which can be both broadband and ideally reproduce the incident wave pattern for all incident angles, it strictly requires a matching of wave speeds $c_m = c_n$ which may not be possible in a physical system. The size of possible inclusions which can be concealed are also smaller than for the string bridge. While the 'holes' in the string bridge have area $d \times l$ the net bridge has significantly smaller holes of area l^2.

The net bridge can also produce a filtering effect, preventing the transmission of waves with an incidence angle greater than a critical angle, determined by system

parameters. This filtering effect also allows for perfect transmission of one incident angle, which can be changed by tuning the net parameters. However there is no way to perfectly transmit over a range of angles while filtering another. There is also no way to filter out small incident angle waves while allowing larger incident angle waves to be transmitted.

The simplicity of this bridging setup does however give scope for further development. The same type of metamaterial can also be proposed for other continuous media to extend the same bridging ideas to other systems. Notably, many other systems have the same Helmholtz governing equations, including the asymptotic leading order motion along the surface of a linearly elastic half plane [63], so the results obtained can potentially be extended to other systems.

CHAPTER 4

Linear Elasticity Bridging

Now consider a similar scheme as in Chapter 3 but with 3D waves in a linearly elastic bulk being bridged by 2D objects. The stresses from the bulk at each of the two boundaries come from the standard constituent equations (2.2.7), and the stresses from the bridges will depend on the bridge construction. As before the aim is to be able to perfectly reproduce an incident wave pattern on the other side of the void as though the bridges were not present.

This 'bridging' scheme is again distinct to transformation cloaking but has similar aims. Like cloaking the aim is to 'hide' a region, leaving the wave pattern undisturbed. Unlike the general cloaking scheme for elasticity [89] this relies on conventional isotropic materials and is much simpler to construct. It is also oriented at transferring waves over an infinite void rather than concealing a finite inclusion.

Begin in §4.1 by attempting to bridge bulk waves. First introduce two single mode bridges, each oriented at bridging only a single bulk wave type. These two single bridge types are then combined to produce a mixed mode bulk bridge intended to bridge both shear and longitudinal components of an incident wave. The same mixed mode bridge is then made use of to bridge surface waves in §4.2. Each section includes a conclusion specific to the wave types, with an overall discussion of the results at the end of the

chapter.

Each of the bridges connects two edges of a void in an elastic half plane between $x = 0$ and $x = d$ with 2D objects periodically inserted parallel to the $x - y$ plane, with constant spacing in the $z-$axis, as shown in Fig. 4.1. For each of the bridges make use

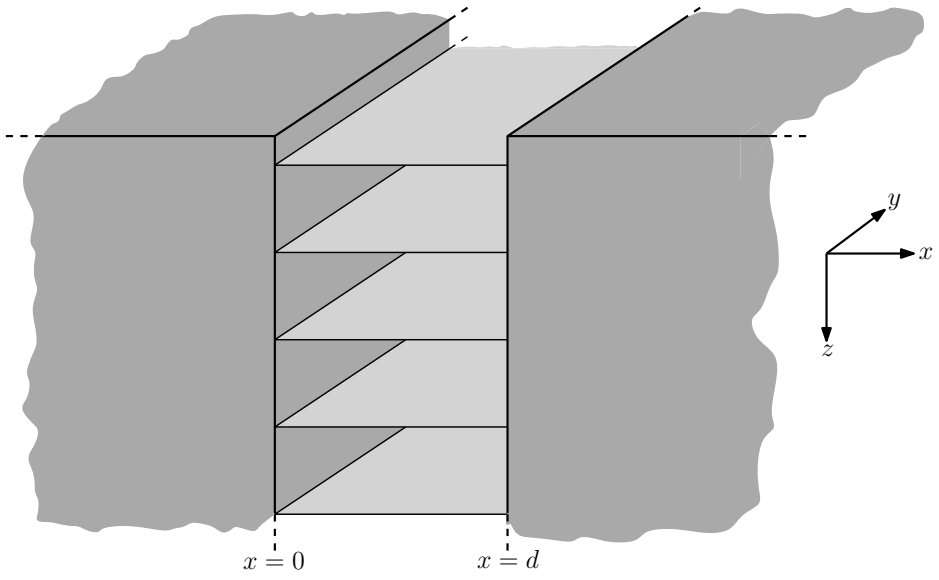

Figure 4.1: Cross-sectional view of an infinite linearly elastic bulk with periodically inserted 2D objects bridging a void between $x = 0$ and $x = d$.

of the homogenisation procedure §2.3 to turn the periodic point forcing at the edges into a distributed load.

4.1 Elastic Bulk Wave Bridging

To bridge bulk waves first establish two 3D linearly elastic structures with domains $\infty < y, z < \infty,\ \infty < x \leq 0,\ d \leq x < \infty$ with an array of 2D bridges connecting the two edges. The two bulk regions will both be able to support longitudinal and shear wave propagation with standard governing equations (2.2.5) and solutions (2.2.8, 2.2.9).

4.1.1 Single Material Bridges

First consider two different types of bridge, each oriented at bridging one type of bulk wave. To match a wave type to a bridge material, it is natural to attempt to bridge using a material which only supports that type of motion. Hence, for a longitudinal incident wave, use an array of thin stiff sheets, with governing equation (2.1.18), which are analogous to the 1D rod. Similarly, for transverse incident waves use an array of membranes with governing equation (2.1.14).

Longitudinal Bridging

To bridge longitudinal incident waves, first construct a bridge between the two elastic bulks, consisting of layers of sheets which each occupy $\infty < z < \infty,\ 0 \leq x \leq d,\ y = nl$, $n \in \mathbb{Z}$. Each n^{th} sheet is connected to the bulk at $-\infty < z < \infty,\ x = 0,\ x = d, y = nl$, and so from (2.1.18) have governing equations,

$$\rho_S \frac{\partial^2 u_S}{\partial t^2} = E_S \frac{\partial^2 u_S}{\partial x^2}. \tag{4.1.1}$$

In linear elasticity, the reflections from a single incident wave at a boundary wave can produce multiple reflected and transmitted waves. As in the previous chapter denote incident, reflected and transmitted waves by superscript (i), (r) and (t) respectively and begin with a longitudinal wave (2.2.8) with the form,

$$\phi^{(i)} = A_i e^{i[k(x\cos\theta_1 + z\sin\theta_1) - \omega t]}, \tag{4.1.2}$$

which transmits a horizontal displacement wave into the sheet bridge (2.1.20),

$$u_1^{(t)} = A_t e^{i[K_S x + kz\sin\theta_1 - \omega t]}, \tag{4.1.3}$$

where the sheet wave speed (2.1.21) and longitudinal wave speed (2.2.6) are given by,

$$c_S = \frac{\omega}{K_S}, \qquad c_1 = \frac{\omega}{k} \tag{4.1.4}$$

This produces reflected waves of the form (2.2.8, 2.2.9) with dispersion relation (2.2.14),

$$\phi^{(r)} = A_r e^{-i[k(x\cos\theta_1 - z\sin\theta_1)-\omega t]}, \tag{4.1.5}$$

$$\psi^{(r)} = B_r e^{-i[k(x\frac{c_1}{c_2}\cos\theta_2 + z\sin\theta_2)-\omega t]}, \tag{4.1.6}$$

where,

$$\phi = \phi^{(i)} + \phi^{(r)}, \qquad \psi = \psi^{(r)}. \tag{4.1.7}$$

Matching the horizontal displacements (2.2.4) at the boundary yields,

$$ik\cos\theta_1(A_i - A_r) - ik\sin\theta_1 B_r = A_t, \tag{4.1.8}$$

and matching the bridge stress (2.1.19) gives the boundary conditions,

$$\sigma_{11} = f_S E_S \frac{\partial u_1}{\partial x}\delta^{(l)}(y), \qquad \sigma_{13} = 0, \tag{4.1.9}$$

where f_S is the thickness of the sheets. Substituting the assumed wave to find the half plane stresses (2.2.7) and homogenising the delta function yields,

$$\sigma_{11} = \mu k\left(\left(2k\sin^2\theta_1 - k\frac{c_1^2}{c_2^2}\right)(A_i + A_r) + 2k\frac{c_1}{c_2}\cos\theta_2\sin\theta_1 B_r\right) \tag{4.1.10}$$

$$= i\frac{f_S}{l}E_S K_S A_t, \tag{4.1.11}$$

$$= i\mu k\frac{c_1^2}{c_2^2}\gamma_S A_t, \tag{4.1.12}$$

$$\sigma_{13} = \mu k\left(2k\cos\theta_1\sin\theta_1)(A_i - A_r) + \left(2k\sin^2\theta_1 - k\frac{c_1^2}{c_2^2}\right)B_r\right) = 0, \tag{4.1.13}$$

where γ_S is defined as,

$$\gamma_S = \frac{f_S}{l}\frac{c_1}{c_S}\frac{E_S}{\lambda + 2\mu}. \tag{4.1.14}$$

This gives the solutions,

$$A_t = ik\frac{2\frac{c_1^2}{c_2^2}\cos\theta_1\left(1-2\frac{c_2^2}{c_1^2}\sin^2\theta_1\right)\left(1-4\frac{c_2^2}{c_1^2}\sin^2\theta_1\right)}{\left(\frac{c_1^2}{c_2^2}-4\sin^2\theta_1\right)(\gamma_S\cos\theta_1+1)+4\sin^2\theta_1\left(\frac{c_2^2}{c_1^2}\sin^2\theta_1-\frac{c_2}{c_1}\cos\theta_1\cos\theta_2\right)}A_i, \tag{4.1.15}$$

$$A_r = \frac{\left(\frac{c_1^2}{c_2^2}-4\sin^2\theta_1\right)(\gamma_S\cos\theta_1-1)-4\sin^2\theta_1\left(\frac{c_2^2}{c_1^2}\sin^2\theta_1+\frac{c_2}{c_1}\cos\theta_1\cos\theta_2\right)}{\left(\frac{c_1^2}{c_2^2}-4\sin^2\theta_1\right)(\gamma_S\cos\theta_1+1)+4\sin^2\theta_1\left(\frac{c_2^2}{c_1^2}\sin^2\theta_1-\frac{c_2}{c_1}\cos\theta_1\cos\theta_2\right)}A_i, \tag{4.1.16}$$

$$B_r = \frac{4\cos\theta_1\sin\theta_1\left(2\frac{c_2^2}{c_1^2}\sin^2\theta_1-1\right)}{\left(\frac{c_1^2}{c_2^2}-4\sin^2\theta_1\right)(\gamma_S\cos\theta_1+1)+4\sin^2\theta_1\left(\frac{c_2^2}{c_1^2}\sin^2\theta_1-\frac{c_2}{c_1}\cos\theta_1\cos\theta_2\right)}A_i. \tag{4.1.17}$$

There are some immediate conclusions which can be seen from these coefficients. In the case of normal incidence, this system will behave similar to those considered for the membrane-string bridge system; replacing Γ with γ_S from the membrane first boundary (3.1.46) gives the same transmission coefficient while the reflection coefficient is the same amplitude but negative. This is due to the formulation being in terms of displacement potentials; in displacement terms this will represent the same coefficient as before.

From this, there are two cases for perfect reflection of the incident wave, (ie, where $A_i = A_r$), both of which only have dependence on the incident angle and the bulk parameters. The first is limiting case of a shallow incidence, where $\theta_1 \to \pi/2$. The second is given when the incident wave satisfies $\sin\theta_1 = \frac{c_1}{c_2\sqrt{2}}$, or alternately when the shear wave reflection would have the angle $\theta_2 \to \pi/4$. For these conditions there is neither a transmitted wave nor any reflected wave conversion.

It is also clear that these are the only angles for which there is no reflected wave conversion and that these depend solely on the material parameters and not on the properties of the bridge. However the angle condition for which there is no reflected

wave at all will depend both on the half plane and γ_S, which will be discussed in more detail later, also taking into account the overall transmission.

This boundary has one more condition for which there is no transmitted wave, for which the incident angle satisfies $\sin\theta_1 = \frac{c_1}{2c_2}$, or equivalently, $\theta_2 = \pi/6$. For conventional materials this will require the incident angle to be in the range $\pi/4 < \theta_1 < \pi/2$. This condition produces reflected waves with amplitude ratios,

$$\frac{A_r}{A_i} = \frac{\cos(\theta_1 - \theta_2)}{\cos(\theta_1 + \theta_2)}, \qquad \frac{B_r}{A_i} = \frac{c_2}{c_1}\frac{\sin(2\theta_1)}{\cos(\theta_1 + \theta_2)}, \tag{4.1.18}$$

which will clearly both have asymptotes at $\theta_1 = \pi/3$. This represents an infinitely large reflection with no transmission and can only occur in a material where $c_1/c_2 = \sqrt{3}$, or equivalently which has a Poisson ratio of 1/4. Physically this represents a system where the reflection forms standing waves. It is also not possible to entirely convert the longitudinal incident wave into a shear reflection since there is no value of θ_1 where $A_r = 0$. It is possible to choose material parameters such that $B_r = 0$, but only for $\theta_1 = \pi/2$ where $c_1/c_2 = \sqrt{2}$, for a Poisson ratio of 0. This is a specific case of an effect which will be discussed later.

To see the effect of the transmitted waves from the first boundary, now consider the second boundary. The sheet now has an incident wave of,

$$u_1^{(i)} = C_i e^{i[K_S x + kz\sin\theta_1 - \omega t]}, \tag{4.1.19}$$

and since this sheet can only support one type of wave (2.1.20), if there is a reflected wave it must be of the form,

$$u_1^{(r)} = C_r e^{-i[K_S x - kz\sin\theta_1 + \omega t]}, \tag{4.1.20}$$

where the overall vertical displacement in the bridge is,

$$u_1 = u_1^{(i)} + u_1^{(r)}. \tag{4.1.21}$$

As before take both a longitudinal and transverse wave in the elastic bulk, with transmitted waves,

$$\phi^{(t)} = C_t e^{i[k(x\cos\theta_1 + z\sin\theta_1) - \omega t]}, \tag{4.1.22}$$

$$\psi^{(t)} = D_t e^{i[k(x\frac{c_1}{c_2}\cos\theta_2 + z\sin\theta_1) - \omega t]}. \tag{4.1.23}$$

This leads to a horizontal displacement matching of,

$$ik\cos\theta_1(C_t) + ik\frac{c_1}{c_2}\cos\theta_2 D_t = A_i + A_r \tag{4.1.24}$$

and substituting the assumed wave forms into the boundary conditions (4.1.9) as before gives,

$$\sigma_{11} = \mu k\left(\left(2k\sin^2\theta_1 - k\frac{c_1^2}{c_2^2}\right)C_t + 2k\frac{c_1}{c_2}\cos\theta_2\sin\theta_1 D_t\right) = i\mu k\frac{c_1^2}{c_2^2}\gamma_S(C_i - C_r), \tag{4.1.25}$$

$$\sigma_{13} = \mu k\left(2k\cos\theta_1\sin\theta_1)C_t + \left(2k\sin^2\theta_1 - k\frac{c_1^2}{c_2^2}\right)D_t\right) = 0, \tag{4.1.26}$$

and in the same way as before, obtain the coefficients,

$$C_t = \frac{1}{ik}\,\frac{2\gamma_S\left(\frac{c_1^2}{c_2^2} - 2\sin^2\theta_1\right)}{\frac{c_1^2}{c_2^2}\left(\gamma_S\cos\theta_1 + 1\right) + 4\sin^2\theta_1\left(\frac{c_2^2}{c_1^2}\sin^2\theta_1 + \frac{c_2}{c_1}\cos\theta_1\cos\theta_2 - 1\right)}A_i, \tag{4.1.27}$$

$$C_r = \frac{\frac{c_1^2}{c_2^2}\left(\gamma_S\cos\theta_1 - 1\right) - 4\sin^2\theta_1\left(\frac{c_2^2}{c_1^2}\sin^2\theta_1 + \frac{c_2}{c_1}\cos\theta_1\cos\theta_2 - 1\right)}{\frac{c_1^2}{c_2^2}\left(\gamma_S\cos\theta_1 + 1\right) + 4\sin^2\theta_1\left(\frac{c_2^2}{c_1^2}\sin^2\theta_1 + \frac{c_2}{c_1}\cos\theta_1\cos\theta_2 - 1\right)}A_i, \tag{4.1.28}$$

$$D_t = \frac{1}{ik}\,\frac{4\gamma_S\cos\theta_1\sin\theta_1}{\frac{c_1^2}{c_2^2}\left(\gamma_S\cos\theta_1 + 1\right) + 4\sin^2\theta_1\left(\frac{c_2^2}{c_1^2}\sin^2\theta_1 + \frac{c_2}{c_1}\cos\theta_1\cos\theta_2 - 1\right)}A_i. \tag{4.1.29}$$

As with the first boundary, the system is identical to the membrane-string system coefficients (3.1.47) given normal incidence and replacing Γ for γ_S. Since all the considered waves in the bulk are right travelling, the reflection phase change seen at the first boundary does not occur at the second boundary.

Since the waves in this bridge have undergone wave conversion, it may also be useful to see if 'perfect conversion' is possible, where one wave type is converted entirely to

another with no reflection. For this purpose introduce the wave conversion metric,

$$WC = \frac{|\text{Amplitude 2}|}{|\text{Amplitude 1}| + |\text{Amplitude 2}|} \tag{4.1.30}$$

where "Amplitude 1" is the transmitted wave amplitude of the same type as the incident wave, and "Amplitude 2" is the transmitted wave amplitude of a different wave type. When the transmitted wave is entirely the same form as the incident wave WC will equal 0 and when the incident wave is entirely converted into a different wave form WC will equal 1. For this system these will be the transverse and longitudinal waves in the bulk respectively, which for this example gives

$$WC = \frac{|D_t|}{|C_t| + |D_t|}, \tag{4.1.31}$$

$$= \frac{|\sin(2\theta_1)|}{|\frac{c_1^2}{c_2^2} - 2\sin^2\theta_1| + |\sin(2\theta_1)|} \tag{4.1.32}$$

Interestingly, this does not depend on the properties of the bridge at all. Instead there is dependence only on the material properties of the bulk and of the angle of incidence. 'Perfect' wave transmission, where the incident wave is fully replicated on the other side of the bridge with no reflection, is only possible where $\sin(2\theta_1) = 0$. This requires either normal incidence or the limit of shallow incidence. However, from (4.1.15) there is no wave transmission at shallow incidence so perfect transmission only occurs for a single wave front at $\theta_1 = 0, \gamma_S = 1$. As with the membrane-string bridge system considered before, if there is more than one wave front the successive transmissions will superpose. Since for $\theta_1 = 0$ the coefficients at each boundary are identical to those obtained before, the coefficients obtained for repeated reflections (3.1.53, 3.1.54) will also be valid for this system at normal incidence.

Since there is only one incident angle and value of γ_S which results in perfect matching, it is useful to see how a bridge with $\gamma_S = 1$ will behave for other incident angles. If the longitudinal transmission remains close to 1 while the reflections and shear

transmission amplitudes remain small then this bridge, while not perfectly matching, will be adequate for reproducing incident wave patterns.

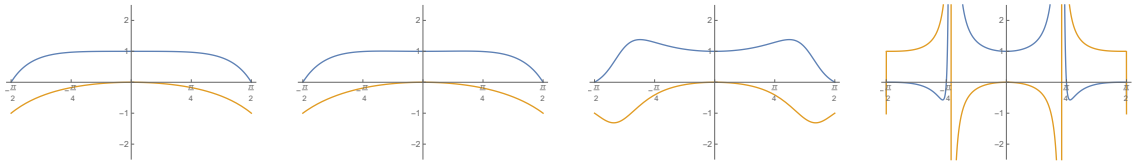

(a) $\frac{c_2}{c_1} = 0$ **(b)** $\frac{c_2}{c_1} = \frac{1}{3\sqrt{2}}$ **(c)** $\frac{c_2}{c_1} = \frac{2}{3\sqrt{2}}$ **(d)** $\frac{c_2}{c_1} = \frac{1}{\sqrt{2}}$

Figure 4.2: Coefficients for longitudinal transmission (blue) and reflection (orange) from a longitudinal oriented bridge with $\gamma_R = 1$ for a longitudinal incident wave with incident angle θ_1.

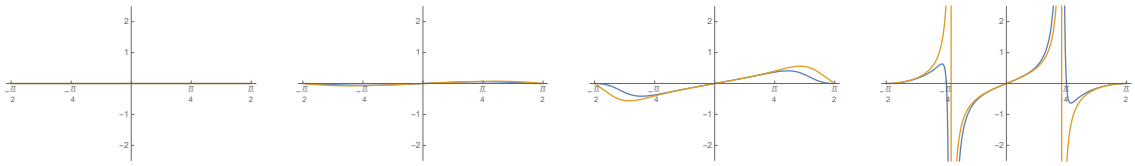

(a) $\frac{c_2}{c_1} = 0$ **(b)** $\frac{c_2}{c_1} = \frac{1}{3\sqrt{2}}$ **(c)** $\frac{c_2}{c_1} = \frac{2}{3\sqrt{2}}$ **(d)** $\frac{c_2}{c_1} = \frac{1}{\sqrt{2}}$

Figure 4.3: Coefficients for shear transmission (blue) and reflection (orange) from a longitudinal oriented bridge with $\gamma_R = 1$ for a longitudinal incident wave with incident angle θ_1.

Figs. 4.2 and 4.3 show the expected behaviour for normal incidence and shallow incidence, and for smaller ratios of c_2/c_1 bridge reasonably well for a wide range of incident angles. At higher values of c_2/c_1 however, the bridge has a resonance producing infinite amplitude shear and longitudinal reflections and transmissions.

To produce 'perfect conversion' where the entire incident wave is converted to another wave type with no reflection, then it is first required that $C_t = 0$. This gives the condition,

$$\frac{c_1^2}{c_2^2} = 2\sin^2\theta_1 \tag{4.1.33}$$

For all of the wave energy to be converted then it is necessary to have no reflections,

so also take $A_r = B_r = C_r = 0$. From inspection, if the conversion condition (4.1.33) is already true then B_r (4.1.17) is already 0. Then it is also required for A_r (4.1.16) and C_r (4.1.28) respectively that,

$$\frac{c_1^2}{c_2^2}\left(\gamma_S \cos\theta_1 - 1\right) + 2\frac{c_1^2}{c_2^2}\left(\frac{c_2^2}{c_1^2}\sin^2\theta_1 + \frac{c_2}{c_1}\cos\theta_1\cos\theta_2\right) = 0, \tag{4.1.34}$$

$$\frac{c_1^2}{c_2^2}\left(\gamma_S \cos\theta_1 - 1\right) - 2\frac{c_1^2}{c_2^2}\left(\frac{c_2^2}{c_1^2}\sin^2\theta_1 + \frac{c_2}{c_1}\cos\theta_1\cos\theta_2 - 1\right) = 0. \tag{4.1.35}$$

where manipulation yields the condition that regardless of γ_S, c_1/c_2 is either $\sqrt{2}$ or $\sqrt[6]{2}$, the latter of which is unobtainable by standard materials and the former is only obtainable as an ideal perfectly compressible material with Poisson ratio of 0. Substituting this into the conversion condition (4.1.33) yields that even for this material, the wave is only ideally converted for incidence of $\theta_1 = \pi/2$. The previous condition for no transmission (4.1.18) is a specific case of this where there is also no reflection and so all waves are trapped in the bridge.

Shear Wave Bridging

Next investigate an array of membranes oriented at bridging a shear wave. As before suppose that there is an array of bridges which occupy the domain $\infty < z < \infty,\ 0 \leq x \leq d,\ y = nl,\ n \in \mathbb{Z}$ and are connected to the bulk at $-\infty < z < \infty,\ x = 0,\ x = d,\ y = nl$. However, unlike the previous case these bridges will each be an elastic membrane (2.1.14). If there is no wave propagation in the y-axis then these membranes have governing equation,

$$\rho_M \frac{\partial^2 u_M}{\partial t^2} = T_M \frac{\partial^2 u_M}{\partial x^2}. \tag{4.1.36}$$

Begin with a shear incident wave (2.2.9),

$$\psi^{(i)} = B_i e^{i[k(x\frac{c_1}{c_2}\cos\theta_2 + z\sin\theta_1) - \omega t]}, \tag{4.1.37}$$

so that the reflected waves will have the same forms (4.1.5, 4.1.6) and from (2.1.16) the transmitted vertical displacement wave will have the form,

$$u_3^{(t)} = B_t e^{i[K_M x + k_1 z \sin\theta_1 - \omega t]}, \tag{4.1.38}$$

Conserving the stresses from the bridge (2.1.15) yields the boundary conditions,

$$\sigma_{11} = 0, \qquad \sigma_{13} = f_M T_M \frac{\partial u_3}{\partial x}\delta^{(l)}(y). \tag{4.1.39}$$

In the same way as before homogenise the stress and match the half plane vertical displacement (2.2.4) and stresses (2.2.7) at the boundary to obtain,

$$ik\sin\theta_1 A_r + ik\frac{c_1}{c_2}\cos\theta_2(B_i - B_r) = B_t \tag{4.1.40}$$

$$\left(2\sin^2\theta_1 - \frac{c_1^2}{c_2^2}\right)A_r + 2\frac{c_1}{c_2}\cos\theta_2\sin\theta_1(B_i - B_r) = 0, \tag{4.1.41}$$

$$-2k\cos\theta_1\sin\theta_1)A_r + \left(2k\sin^2\theta_1 - k\frac{c_1^2}{c_2^2}\right)(B_i + B_r) = i\frac{f_M}{l}T_M K_M A_t, \tag{4.1.42}$$

$$= i\frac{c_1}{c_2}\gamma_M B_t, \tag{4.1.43}$$

where γ_M is defined as,

$$\gamma_M = \frac{f_M}{l}\frac{c_2}{c_M}\frac{T_M}{\mu}. \tag{4.1.44}$$

This system of equations has solutions,

$$B_t = ik\frac{2\frac{c_1}{c_2}\cos\theta_2\left(1 - 2\sin^2\theta_2\right)}{\gamma_M\cos\theta_2 + 1 - 4\sin^2\theta_2\left(\frac{c_2}{c_1}\cos\theta_1\cos\theta_2 + \cos^2\theta_2\right)}B_i, \tag{4.1.45}$$

$$B_r = \frac{\gamma_M\cos\theta_2 - 1 - 4\sin^2\theta_1\left(\frac{c_2}{c_1}\cos\theta_1\cos\theta_2 - \cos^2\theta_2\right)}{\gamma_M\cos\theta_2 + 1 - 4\sin^2\theta_2\left(\frac{c_2}{c_1}\cos\theta_1\cos\theta_2 + \cos^2\theta_2\right)}B_i, \tag{4.1.46}$$

$$A_r = \frac{4\gamma_M\cos\theta_2\sin\theta_2\left(1 - 2\sin^2\theta_2\right)}{\gamma_M\cos\theta_2 + 1 - 4\sin^2\theta_2\left(\frac{c_2}{c_1}\cos\theta_1\cos\theta_2 + \cos^2\theta_2\right)}B_i. \tag{4.1.47}$$

from which it is again possible to immediately determine key behaviours of the system. Unlike for the longitudinal bridge, there are only two conditions for which there is no transmitted wave; the shallow incidence limit $\theta_2 \to \pi/2$ and a shear wave incidence

$\theta_2 = \pi/4$ both produce total reflection. As before normal incidence produces displacement wave amplitude ratios the same as given by the previous membrane-string bridge (3.1.46) with Γ replaced by γ_M.

At the second boundary now assume an incident and reflected displacement wave,

$$u_3^{(i)} = D_i e^{i[K_S x + k_1 z \sin\theta_1 - \omega t]}, \tag{4.1.48}$$

$$u_3^{(r)} = D_r e^{i[K_S x + k_1 z \sin\theta_1 - \omega t]}, \tag{4.1.49}$$

where,

$$u_3 = u_3^{(i)} + u_3^{(r)}, \tag{4.1.50}$$

and the same transmitted waves as from the longitudinal bridge (4.1.22, 4.1.23). Use the stress boundary conditions from the first boundary (2.2.7, 4.1.39) and match vertical displacements to obtain,

$$ik \sin\theta_1 C_t + ik\frac{c_1}{c_2}\cos\theta_2 D_t = D_i + D_r, \tag{4.1.51}$$

$$\left(2\sin^2\theta_1 - \frac{c_1^2}{c_2^2}\right) C_t + 2\frac{c_1}{c_2}\cos\theta_2 \sin\theta_1 D_t = 0, \tag{4.1.52}$$

$$2k_1 \cos\theta_1 \sin\theta_1 C_t + \left(2k_1 \sin^2\theta_1 - k_1\frac{c_1^2}{c_2^2}\right) D_t = i\frac{c_1}{c_2}\gamma_M (D_i - D_r). \tag{4.1.53}$$

which gives the solutions,

$$D_t = \frac{1}{ik}\frac{2\frac{c_2}{c_1}\gamma_M\left(1 - 2\sin^2\theta_2\right)}{\gamma_M\cos\theta_2 + 1 - 4\sin^2\theta_2\left(\frac{c_2}{c_1}\cos\theta_1\cos\theta_2 + \cos^2\theta_2\right)} D_i, \tag{4.1.54}$$

$$D_r = \frac{\gamma_M\cos\theta_2 - 1 + 4\sin^2\theta_1\left(\frac{c_2}{c_1}\cos\theta_1\cos\theta_2 + \cos^2\theta_2\right)}{\gamma_M\cos\theta_2 + 1 - 4\sin^2\theta_2\left(\frac{c_2}{c_1}\cos\theta_1\cos\theta_2 + \cos^2\theta_2\right)} D_i, \tag{4.1.55}$$

$$C_t = \frac{4\frac{c_2}{c_1}\gamma_M\cos\theta_2\sin\theta_2}{\gamma_M\cos\theta_2 + 1 - 4\sin^2\theta_2\left(\frac{c_2}{c_1}\cos\theta_1\cos\theta_2 + \cos^2\theta_2\right)} D_i, \tag{4.1.56}$$

which again produces identical coefficients for the displacement wave amplitudes as for the membrane-string bridge (3.1.47). Again make use of the previous wave conversion

metric (4.1.30) where,

$$WC = \frac{|C_t|}{|D_t| + |C_t|}, \tag{4.1.57}$$

$$= \frac{|\sin 2\theta_2|}{|1 - 2\sin^2\theta_2| + |\sin 2\theta_2|} \tag{4.1.58}$$

which, as before, does not depend on the properties of the bridge. Unlike before, however, there is also no dependence on the properties of the bulk. From this it is visible that the wave undergoes no conversion at $\theta_2 = 0,\ \pi/2$ and has total wave conversion at $\theta_2 = \pi/4$. As previously discussed however, at both $\theta_2 = \pi/2$ and $\theta_2 = \pi/4$ there is no transmission onto the bridge so the overall transmission in both cases would be 0. Hence perfect wave conversion is not possible and perfect wave transmission can only occur for normal incidence, which will follow the same conditions for perfect transmission for the membrane-string bridge (3.1.45, 3.1.54), replacing Γ for γ_M.

As with the longitudinal bridge previously, it may be useful to know how the system will behave for a wave arbitrary incidence on a bridge tuned for perfect bridging. Figs. 4.4 and 4.5] show the shear and longitudinal transmissions and reflections for a single incident shear wave on a bridge with $\gamma_M = 1$. As before these plots show that the overall bridge effect is better for materials with a lower value of c_2/c_1. However, unlike for the previous case, real transmissions and reflections do not occur for the full range of incident angles. Propagating waves only occur when $\sin\theta_1 < c_2/c_1$, with other waves decaying exponentially away from the boundary.

Also unlike the longitudinal waves, a more easily compressible bulk material does not produce vertical asymptotes and an infinite transmission or reflection for certain incident angles. The overall transmitted amplitude can, however, still be greater then the incident amplitude.

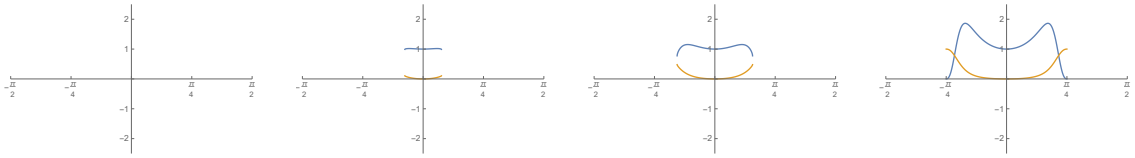

(a) $\frac{c_2}{c_1} = 0$ **(b)** $\frac{c_2}{c_1} = \frac{1}{3\sqrt{2}}$ **(c)** $\frac{c_2}{c_1} = \frac{2}{3\sqrt{2}}$ **(d)** $\frac{c_2}{c_1} = \frac{1}{\sqrt{2}}$

Figure 4.4: Coefficients for shear transmission (blue) and reflection (orange) from a transverse oriented bridge with $\gamma_M = 1$ for a shear incident wave with incident angle θ_2.

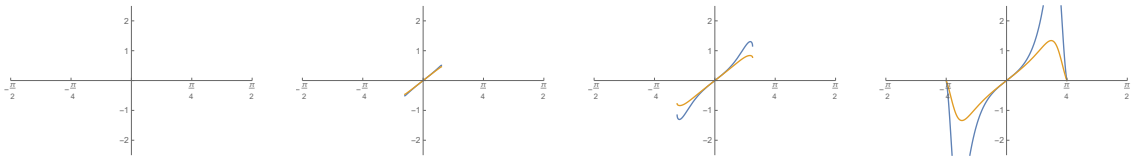

(a) $\frac{c_2}{c_1} = 0$ **(b)** $\frac{c_2}{c_1} = \frac{1}{3\sqrt{2}}$ **(c)** $\frac{c_2}{c_1} = \frac{2}{3\sqrt{2}}$ **(d)** $\frac{c_2}{c_1} = \frac{1}{\sqrt{2}}$

Figure 4.5: Coefficients for longitudinal transmission (blue) and reflection (orange) from a transverse oriented bridge with $\gamma_M = 1$ for a shear incident wave with incident angle θ_2.

4.1.2 Longitudinal and Transverse Bridging

Now consider attempting to bridge two different types of waves with a single bridge. Such a bridge will require both longitudinal and shear components, which will aim to have the added capability of being able to better carry waves at a non-normal incidence.

The new bridge will be a combination of the previous two bridges, with membranes with standard governing equations (2.1.14) equally spaced at $z = nl$ and sheets with standard governing equations (2.1.18) at $z = (n + 1/2)l$, $n \in \mathbb{Z}$. As such the previous two bridges are special cases of the new bridge.

Formulation of full bridging problem

Unlike for the previous cases consider both a longitudinal and shear incident wave (2.2.8, 2.2.9) with the same angular frequency ω,

$$\phi^{(i)} = A_i e^{i[k_1(x\cos\theta_1 + z\sin\theta_1) - \omega t]}, \tag{4.1.59}$$

$$\psi^{(i)} = B_i e^{i[k_2(x\cos\theta_2 + z\sin\theta_2) - \omega t]}, \tag{4.1.60}$$

using the same notation as before, where

$$c_1 = \frac{\omega}{k_1}, \quad c_2 = \frac{\omega}{k_2}. \tag{4.1.61}$$

Although ultimately these two systems will be considered independently, both systems can be solved simultaneously using the elastic bulk dispersion relation (2.2.14) and so for brevity the incident waves become,

$$\phi^{(i)} = A_i e^{i[k_1(x\cos\theta_1 + z\sin\theta_1) - \omega t]}, \tag{4.1.62}$$

$$\psi^{(i)} = B_i e^{i[k_1(x\frac{c_1}{c_2}\cos\theta_2 + z\sin\theta_1) - \omega t]}. \tag{4.1.63}$$

At the left boundary this leads to reflected waves of the form,

$$\phi^{(r)} = A_r e^{-i[k_1(x\cos\theta_1 - z\sin\theta_1) + \omega t]}, \tag{4.1.64}$$

$$\psi^{(r)} = B_r e^{-i[k_1(x\frac{c_1}{c_2}\cos\theta_2 - z\sin\theta_1) + \omega t]}, \tag{4.1.65}$$

and transmitted waves into sheet and membrane bridges respectively (2.1.16, 2.1.20),

$$u_1^{(t)} = A_t e^{i[K_M x + k_1 z\sin\theta_1 - \omega t]}, \tag{4.1.66}$$

$$u_3^{(t)} = B_t e^{i[K_S x + k_1 z\sin\theta_1 - \omega t]}, \tag{4.1.67}$$

where as before,

$$c_M = \frac{\omega}{K_M}, \quad c_S = \frac{\omega}{K_S}. \tag{4.1.68}$$

Conservation of vertical and horizontal displacements (2.2.4) at the boundary gives,

$$ik_1 \cos\theta_1(A_i - A_r) - ik_1 \sin\theta_1(B_i + B_r) = A_t \tag{4.1.69}$$

$$ik_1 \sin\theta_1(A_i + A_r) + ik_1 \frac{c_1}{c_2} \cos\theta_2(B_i - B_r) = B_t \tag{4.1.70}$$

and after homogenising, the two stresses from the bridges (2.1.15, 2.1.19) are conserved as,

$$\sigma_{11} = \frac{f_S}{l} E_S \frac{\partial u_1}{\partial x}, \qquad \sigma_{13} = \frac{f_M}{l} T_M \frac{\partial u_3}{\partial x}, \tag{4.1.71}$$

with horizontal and vertical stresses from the bulk (2.2.7) yielding,

$$\mu k_1 \left(\left(2k_1 \sin^2\theta_1 - k_1 \frac{c_1^2}{c_2^2} \right) (A_i + A_r) + 2k_1 \frac{c_1}{c_2} \cos\theta_2 \sin\theta_1 (B_i - B_r) \right) = i\mu k_1 \frac{c_1^2}{c_2^2} \gamma_S A_t, \tag{4.1.72}$$

$$\mu k_1 \left(2k_1 \cos\theta_1 \sin\theta_1)(A_i - A_r) + \left(2k_1 \sin^2\theta_1 - k_1 \frac{c_1^2}{c_2^2} \right) (B_i + B_r) \right) = i\mu k_1 \frac{c_1}{c_2} \gamma_M B_t, \tag{4.1.73}$$

where γ_S and γ_M are defined as before (4.1.14, 4.1.44). On repeating the process for the right boundary with incident waves,

$$u_1^{(i)} = C_i e^{i[K_M x + k_1 z \sin\theta_1 - \omega t]}, \tag{4.1.74}$$

$$u_3^{(i)} = D_i e^{i[K_S x + k_1 z \sin\theta_1 - \omega t]}, \tag{4.1.75}$$

this system will produce reflected waves,

$$u_1^{(r)} = C_r e^{i[-K_M x + k_1 \sin\theta_1 z - \omega t]}, \tag{4.1.76}$$

$$u_3^{(r)} = D_r e^{i[-K_S x + k_1 \sin\theta_1 z - \omega t]}, \tag{4.1.77}$$

and transmitted waves into the elastic region,

$$\phi^{(t)} = C_t e^{i[k_1(x\cos\theta_1 + z\sin\theta_1) - \omega t]}, \tag{4.1.78}$$

$$\psi^{(t)} = D_t e^{i[k_1(x\frac{c_1}{c_2}\cos\theta_2 + z\sin\theta_1) - \omega t]}. \tag{4.1.79}$$

Hence by matching the displacements at this boundary,

$$ik_1 \cos\theta_1(C_t) - ik_1 \sin\theta_1(D_t) = C_i + C_r \tag{4.1.80}$$

$$ik_1 \sin\theta_1(C_t) + ik_1 \frac{c_1}{c_2} \cos\theta_2(D_t) = D_i + D_r, \tag{4.1.81}$$

and similarly by matching stresses,

$$\mu k_1 \left(\left(2k_1 \sin^2\theta_1 - k_1 \frac{c_1^2}{c_2^2} \right) C_t + 2k_1 \frac{c_1}{c_2} \cos\theta_2 \sin\theta_1 D_t \right) = i\mu k_1 \frac{c_1^2}{c_2^2} \gamma_S (C_i - C_r), \tag{4.1.82}$$

$$\mu k_1 \left(2k_1 \cos\theta_1 \sin\theta_1) C_t + \left(2k_1 \sin^2\theta_1 - k_1 \frac{c_1^2}{c_2^2} \right) D_t \right) = i\mu k_1 \frac{c_1}{c_2} \gamma_M (D_i - D_r). \tag{4.1.83}$$

These two sets of boundary conditions can be expressed by the matrix equations,

$$ik_1 M \begin{pmatrix} A_i - A_r \\ \\ B_i + B_r \end{pmatrix} = ik_1 R \begin{pmatrix} A_i + A_r \\ \\ B_i - B_r \end{pmatrix} = \begin{pmatrix} A_t \\ \\ B_t \end{pmatrix}, \tag{4.1.84}$$

where,

$$M = \begin{pmatrix} \cos\theta_1 & -\sin\theta_1 \\ \\ -2\frac{c_2}{c_1} \frac{\cos\theta_1 \sin\theta_1}{\gamma_M} & \frac{c_1}{c_2} \left(\frac{1}{\gamma_M} - 2\frac{c_2^2}{c_1^2} \frac{\sin^2\theta_1}{\gamma_M} \right) \end{pmatrix}, \tag{4.1.85}$$

$$R = \begin{pmatrix} \frac{1}{\gamma_S} - 2\frac{c_2^2}{c_1^2} \frac{\sin^2\theta_1}{\gamma_S} & -2\frac{c_2}{c_1} \frac{\cos\theta_2 \sin\theta_1}{\gamma_S} \\ \\ \sin\theta_1 & \frac{c_1}{c_2} \cos\theta_2 \end{pmatrix} \tag{4.1.86}$$

and,

$$ik_1 D \begin{pmatrix} C_t \\ \\ D_t \end{pmatrix} = \begin{pmatrix} C_i + C_r \\ \\ D_i + D_r \end{pmatrix}, \quad ik_1 F \begin{pmatrix} C_t \\ \\ D_t \end{pmatrix} = \begin{pmatrix} C_i - C_r \\ \\ D_i - D_r \end{pmatrix} \tag{4.1.87}$$

where,

$$D = \begin{pmatrix} \cos\theta_1 & -\sin\theta_1 \\ \\ \sin\theta_1 & \frac{c_1}{c_2} \cos\theta_2 \end{pmatrix}, \quad F = \begin{pmatrix} \frac{1}{\gamma_S} - 2\frac{c_2^2}{c_1^2} \frac{\sin^2\theta_1}{\gamma_S} & -2\frac{c_2}{c_1} \frac{\cos\theta_2 \sin\theta_1}{\gamma_S} \\ \\ -2\frac{c_2}{c_1} \frac{\cos\theta_1 \sin\theta_1}{\gamma_M} & \frac{c_1}{c_2} \left(\frac{1}{\gamma_M} - 2\frac{c_2^2}{c_1^2} \frac{\sin^2\theta_1}{\gamma_M} \right) \end{pmatrix} \tag{4.1.88}$$

Define some incidence, reflection and transmission matrices,

$$\hat{i}_1 = \begin{pmatrix} A_i \\ \\ B_i \end{pmatrix}, \quad \hat{r}_1 = \begin{pmatrix} A_r \\ \\ B_r \end{pmatrix}, \quad \hat{t}_1 = \begin{pmatrix} A_t \\ \\ B_t \end{pmatrix}, \tag{4.1.89}$$

so that the left boundary is represented by,

$$ik_1 M \left(\hat{i}_1 - \begin{pmatrix} 1 & 0 \\ \\ 0 & -1 \end{pmatrix} \hat{r}_1 \right) = ik_1 R \left(\hat{i}_1 + \begin{pmatrix} 1 & 0 \\ \\ 0 & -1 \end{pmatrix} \hat{r}_1 \right) = \hat{t}_1. \tag{4.1.90}$$

Similarly at the right boundary define,

$$\hat{i}_2 = \begin{pmatrix} C_r \\ \\ D_r \end{pmatrix}, \quad \hat{r}_2 = \begin{pmatrix} C_r \\ \\ D_r \end{pmatrix}, \quad \hat{t}_2 = \begin{pmatrix} C_t \\ \\ D_t \end{pmatrix}, \tag{4.1.91}$$

so that,

$$ik_1 \hat{t}_2 = D^{-1}(\hat{i}_2 + \hat{r}_2) = F^{-1}(\hat{i}_2 - \hat{r}_2) \tag{4.1.92}$$

and from these it is clear that the transmissions are given by,

$$\hat{t}_1 = 2ik_1(M^{-1} + R^{-1})^{-1}\hat{i}_1, \qquad \hat{t}_2 = \frac{2}{ik_1}(D + F)^{-1}\hat{i}_2 \tag{4.1.93}$$

and the reflections are given by,

$$\hat{r}_1 = \begin{pmatrix} 1 & 0 \\ \\ 0 & -1 \end{pmatrix} (M + R)^{-1}(M - R)\hat{i}_1, \qquad \hat{r}_2 = (F^{-1} + D^{-1})^{-1}(F^{-1} - D^{-1})\hat{i}_2 \tag{4.1.94}$$

In a general case, $\hat{t}_1$ and $\hat{i}_2$ have the same amplitude but have some phase difference from the change in speed and so are related by,

$$\hat{i}_2 = \begin{pmatrix} e^{i\varphi_1} & 0 \\ \\ 0 & e^{i\varphi_2} \end{pmatrix} \hat{t}_1 = \boldsymbol{\varphi} \hat{t}_1 \tag{4.1.95}$$

where φ_1 and φ_2 are the phase difference from the membranes and sheets respectively,

$$\varphi_1 = \frac{\omega d}{c_s}, \qquad \varphi_2 = \frac{\omega d}{c_M}, \tag{4.1.96}$$

If and only if the angular frequency is given by,

$$\omega = \frac{2m\pi}{d}\frac{c_M c_S}{c_S - c_M}, \quad m \in \mathbb{Z} \tag{4.1.97}$$

then $\varphi_1 = \varphi_2$ and on disregarding the phase the wave pattern transmitted from the left boundary is identical to that incident on the right boundary.

For simplicity, consider only the case that $\varphi_1 = \varphi_2 = 0$ so $\boldsymbol{\varphi} = I_2$, where I_2 is the 2×2 identity matrix. It then follows from (4.1.95) that $\hat{t}_1 = \hat{i}_2$ and hence,

$$\hat{t}_2 = 4(D+F)^{-1}(M^{-1}+R^{-1})^{-1}\hat{i}_1. \tag{4.1.98}$$

The wave component re-incident upon a boundary undergoes two reflections and so is given by,

$$\hat{i}_{n+2} = \left((F^{-1}+D^{-1})^{-1}(F^{-1}-D^{-1})\right)^2 \hat{i}_n, \tag{4.1.99}$$

so as before successive reflection and transmission coefficients are obtained,

$$R_n = \begin{cases} \begin{pmatrix} 1 & 0 \\ 0 & -1 \end{pmatrix}(M+R)^{-1}(M-R) & n = 1 \\ 4(D+F)^{-1}\left((F^{-1}+D^{-1})^{-1}(F^{-1}-D^{-1})\right)^{2n-3}(M^{-1}+R^{-1})^{-1}, & n \geq 2 \end{cases} \tag{4.1.100}$$

$$T_n = 4(D+F)^{-1}\left((F^{-1}+D^{-1})^{-1}(F^{-1}-D^{-1})\right)^{2n-2}(M^{-1}+R^{-1})^{-1} \tag{4.1.101}$$

which are analogous to the similar coefficients from (3.1.51, 3.1.52). If the eigenvalues of the reflection matrix are both less than 1 then the total reflection and transmissions can be computed in the same way as the summation of the R_n and T_n terms. This

yields,

$$R_T = \begin{pmatrix} 1 & 0 \\ 0 & -1 \end{pmatrix} (M+R)^{-1}(M-R) + 4(D+F)^{-1}\left(\left(I_2 - (F^{-1}+D^{-1})^{-1}(F^{-1}-D^{-1})\right)^{-1} - I_2\right)(M^{-1}+R^{-1})^{-1} \tag{4.1.102}$$

$$T_T = 4(D+F)^{-1}\left(I_2 - \left((F^{-1}+D^{-1})^{-1}(F^{-1}-D^{-1})\right)^2\right)^{-1}(M^{-1}+R^{-1})^{-1} \tag{4.1.103}$$

Normal and Shallow wave incidence

To investigate the effectiveness of this bridge, start with the key cases from the single mode bridging: Normal incidence, shallow longitudinal incidence and shallow shear incidence. For normal incidence, $\theta_1 = \theta_2 = 0$ and so,

$$M = \begin{pmatrix} 1 & 0 \\ 0 & \frac{c_1}{c_2}\frac{1}{\gamma_M} \end{pmatrix}, \quad R = \begin{pmatrix} \frac{1}{\gamma_S} & 0 \\ 0 & \frac{c_1}{c_2} \end{pmatrix}, \quad D = \begin{pmatrix} 1 & 0 \\ 0 & \frac{c_1}{c_2} \end{pmatrix}, \quad F = \begin{pmatrix} \frac{1}{\gamma_S} & 0 \\ 0 & \frac{c_1}{c_2}\frac{1}{\gamma_M} \end{pmatrix}, \tag{4.1.104}$$

from which the transmissions are given by,

$$\hat{t}_1 = 2ik_1 \begin{pmatrix} \frac{1}{1+\gamma_S} & 0 \\ 0 & \frac{c_1}{c_2}\frac{1}{1+\gamma_M} \end{pmatrix} \hat{i}_1, \qquad \hat{t}_2 = \frac{2}{ik_1} \begin{pmatrix} \frac{\gamma_S}{1+\gamma_S} & 0 \\ 0 & \frac{c_2}{c_1}\frac{\gamma_M}{1+\gamma_M} \end{pmatrix} \hat{i}_2 \tag{4.1.105}$$

and similarly the reflections are,

$$\hat{r}_1 = \begin{pmatrix} \frac{\gamma_S-1}{\gamma_S+1} & 0 \\ 0 & \frac{\gamma_M-1}{\gamma_M+1} \end{pmatrix} \hat{i}_1, \qquad \hat{r}_2 = \begin{pmatrix} \frac{\gamma_S-1}{\gamma_S+1} & 0 \\ 0 & \frac{\gamma_M-1}{\gamma_M+1} \end{pmatrix} \hat{i}_2 \tag{4.1.106}$$

which describe the systems for normal incidence on single mode bridges in §4.1.1, indicating how for normal incidences each wave depends only on one bridge.

For shallow longitudinal incidences, $\theta_1 = \pi/2, \sin\theta_2 = c_2/c_1$ and so,

$$M = \begin{pmatrix} 0 & -1 \\ 0 & \frac{c_1}{c_2}\frac{1-2\frac{c_2^2}{c_1^2}}{\gamma_M} \end{pmatrix}, \quad R = \begin{pmatrix} \frac{1-2\frac{c_2^2}{c_1^2}}{\gamma_S} & -2\frac{c_2}{c_1}\frac{\cos\theta_2}{\gamma_S} \\ 0 & \frac{c_1}{c_2}\cos\theta_2 \end{pmatrix}. \tag{4.1.107}$$

Since M is singular, the transmission relation (4.1.93) can no longer be used to determine the transmission from the first boundary. Instead substitute the particular M and R into the first boundary condition (4.1.90) which results in no shear or longitudinal transmission from shallow longitudinal incidences. It is however possible to transmit a longitudinal wave front at this angle with an incident shear wave. This shear wave must have incidence such that $\sin\theta_2 = c_2/c_1$. Since standard materials have $c_2/c_1 \leq 1/\sqrt{2}$ then for any bulk material there exists a propagating wave which can meet this requirement.

For shallow shear incidences, $\theta_2 = \pi/2$, $\sin\theta_1 = c_1/c_2$ and so,

$$M = \begin{pmatrix} \cos\theta_1 & -\frac{c_1}{c_2} \\ -2\frac{c_1}{c_2}\cos\theta_1 & -\frac{c_1}{c_2}\frac{1}{\gamma_M} \end{pmatrix}, \quad R = \begin{pmatrix} -\frac{1}{\gamma_S} & 0 \\ \frac{c_1}{c_2} & 0 \end{pmatrix}, \tag{4.1.108}$$

for which R is clearly singular. As with the longitudinal case, the transmission matrix equation (4.1.93) cannot be valid and therefore instead substitute these M and R matrices directly into the first boundary condition (4.1.90). As before a shear shallow incidence cannot cause any transmission on the other side. However, unlike the previous case, it is not possible to produce a shear transmission parallel to the boundary since $\sin\theta_1 = c_1/c_2$ does not have a real solution for any possible Poisson ratio.

Perfect Bridging

To investigate whether perfect bridging is possible for both waves simultaneously then it is more convenient to put the overall transmission coefficient (4.1.98) in the form,

$$\hat{t}_2 = \frac{4}{|M|\,|M^{-1}+R^{-1}|}\left(I_2 + \frac{|M|^2 - |R|}{|R|}(M+R)^{-1}R\right)\hat{i}_1. \tag{4.1.109}$$

Then the condition for which there is no wave conversion in the transmitted wave is that the non diagonal components of the matrix $(M + R)^{-1}R$ are zero. Hence the longitudinal-to-shear coefficient is 0 when,

$$\sin\theta_1 \cos\theta_1 \left(1 - 4\frac{c_2^2}{c_1^2}\frac{\sin^2\theta_1}{\gamma_M\gamma_S}\right) = 0 \tag{4.1.110}$$

and the shear-to-longitudinal coefficient is 0 when,

$$\sin\theta_2 \cos\theta_2 \left(\frac{c_1}{c_2} - \frac{2}{\gamma_M\gamma_S}\cos^2\theta_2\right). \tag{4.1.111}$$

For both shear and longitudinal wave incidence this gives no wave conversion for normal incidence and shallow incidence. It also yields an extra set of solutions where γ_M and γ_S can be tuned to produce no wave conversion at an arbitrary incidence. To prevent conversion into shear waves there must be bridge parameters such that,

$$\gamma_M\gamma_S = 4\frac{c_2^2}{c_1^2}\sin^2\theta_1, \tag{4.1.112}$$

and to prevent conversion into longitudinal waves equally requires,

$$\gamma_M\gamma_S = 2\frac{c_2}{c_1}\cos^2\theta_2. \tag{4.1.113}$$

These two equations show that wave conversion can only be arbitrarily controlled for one incident wave; preventing wave conversion of one incident wave limits the other wave type to only one possible angle for which there is no conversion.

Next it will be considered whether it is possible to produce bridges in such a way that there is no wave conversion and no reflections for a single wave type. Begin by considering the first reflection coefficient for longitudinal waves. If it is assumed that the bridge already has parameters such that (4.1.112) is satisfied, the shear reflection is 0 if,

$$2\sqrt{\gamma_M\gamma_S}\left(4\frac{c_2^2}{c_1^2} - \gamma_M\gamma_S\right)\left(\frac{c_2}{c_1}(\gamma_M\gamma_S - 2) - \gamma_M\gamma_S\right) = 0 \tag{4.1.114}$$

which has solutions for normal incidence, shallow incidence and,

$$\gamma_M \gamma_S = \frac{2}{\frac{c_1}{c_2} - 1}, \tag{4.1.115}$$

which gives the angle requirement,

$$\sin\theta_1 = \sqrt{\frac{1}{2\frac{c_2^2}{c_1^2} - 2\frac{c_2}{c_1}}} \tag{4.1.116}$$

which has no real solutions. Hence it is not possible to use this bridge to perfectly match a longitudinal wave without inducing some shear wave reflection except for normal incidence.

Next consider the first reflection of a shear wave given that the bridge has been constructed in such a way that (4.1.113) is true. Then the longitudinal reflection caused by a shear incidence is 0 if,

$$\frac{c_1}{c_2}\gamma_M\gamma_S\left(2\frac{c_2}{c_1} - \gamma_M\gamma_S\right) = 0. \tag{4.1.117}$$

Like the longitudinal case, the only solutions are normal incidence and shallow incidence so as before 'perfect bridging' is only possible for normal incidence waves. Since the conditions for perfect bridging at normal incidence are already known, it will be useful to see how the $\gamma_S = \gamma_M = 1$ system behaves for a range of incident angles.

Normal Incidence Bridge Tuning

Since the only possible way to perfectly bridge waves in this system is for normally incident waves on bridges with $\gamma_S = \gamma_M = 1$, see how the transmission and reflection coefficients behave away from normal incidence. The main aim of the bridging is to replicate the wave pattern on the other side of the gap, and so first look at the overall transmission coefficients.

Below is plotted the transmission ratios for both longitudinal and shear waves resulting from a longitudinal or shear incident wave against the incidence angle of

the wave and the wave speed ratio c_2/c_1. While the longitudinal wave has a real transmission for all incidence angles, the shear wave only has wave transmission given that $\sin\theta_2 < c_2/c_1$; for other angles of incidence the right boundary only produces an evanescent wave which decays exponentially with distance from the bridge.

As expected the shear-shear and longitudinal-longitudinal coefficients are both 1 for normal incidence. It is visible from Figs. 4.6–4.9 that for small angles $\gamma_M = \gamma_S = 1$ still produces very little reflection or mode switching, especially for small values of c_2/c_1. This does come with limitations however; as mentioned above the shear wave only produces real transmissions and reflections when $\sin\theta < c_2/c_1$ and outside this range it is not possible to perfectly bridge the incident wave. Since $c_2/c_1 < 1/\sqrt{2}$ the largest range angles possible to transmit is only $-\pi/4 < \theta < \pi/4$, half of the range of possible incident angles. However for the majority of values of c_2/c_1, θ_1 and θ_2, the longitudinal-longitudinal and shear-shear transmissions remain close to 1 and the reflections and converted wave amplitudes remain small.

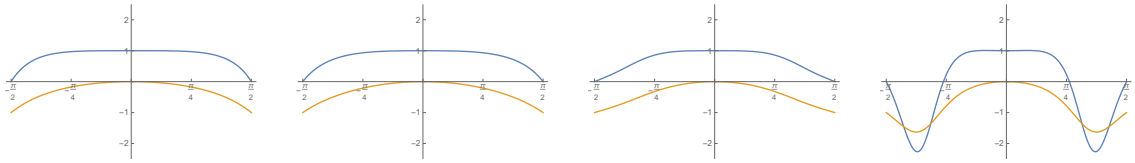

(a) $\frac{c_2}{c_1} = 0$ **(b)** $\frac{c_2}{c_1} = \frac{1}{3\sqrt{2}}$ **(c)** $\frac{c_2}{c_1} = \frac{2}{3\sqrt{2}}$ **(d)** $\frac{c_2}{c_1} = \frac{1}{\sqrt{2}}$

Figure 4.6: Coefficients for longitudinal transmission (blue) and reflection (orange) from a mixed mode bridge with $\gamma_R, \gamma_M = 1$ for a longitudinal incident wave with incident angle θ_1.

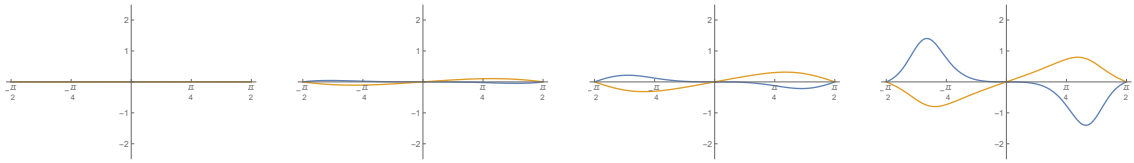

(a) $\frac{c_2}{c_1} = 0$ **(b)** $\frac{c_2}{c_1} = \frac{1}{3\sqrt{2}}$ **(c)** $\frac{c_2}{c_1} = \frac{2}{3\sqrt{2}}$ **(d)** $\frac{c_2}{c_1} = \frac{1}{\sqrt{2}}$

Figure 4.7: Coefficients for shear transmission (blue) and reflection (orange) from a mixed mode bridge with $\gamma_R, \gamma_M = 1$ for a longitudinal incident wave with incident angle θ_1.

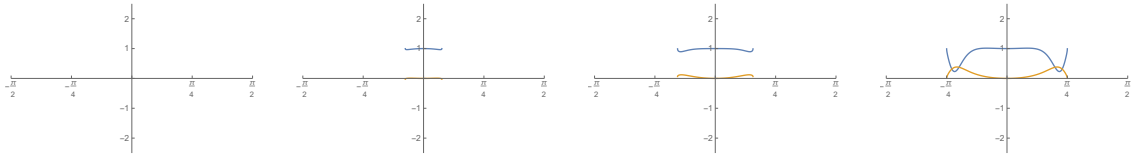

(a) $\frac{c_2}{c_1} = 0$ **(b)** $\frac{c_2}{c_1} = \frac{1}{3\sqrt{2}}$ **(c)** $\frac{c_2}{c_1} = \frac{2}{3\sqrt{2}}$ **(d)** $\frac{c_2}{c_1} = \frac{1}{\sqrt{2}}$

Figure 4.8: Coefficients for shear transmission (blue) and reflection (orange) from a mixed mode bridge with $\gamma_R, \gamma_M = 1$ for a shear incident wave with incident angle θ_2.

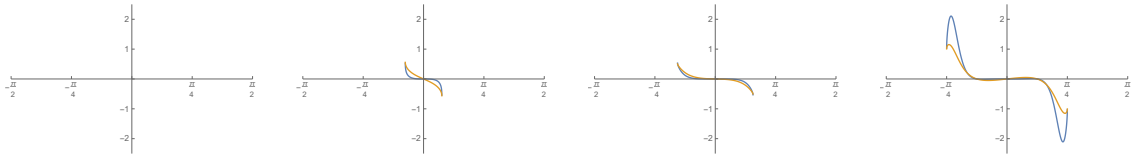

(a) $\frac{c_2}{c_1} = 0$ **(b)** $\frac{c_2}{c_1} = \frac{1}{3\sqrt{2}}$ **(c)** $\frac{c_2}{c_1} = \frac{2}{3\sqrt{2}}$ **(d)** $\frac{c_2}{c_1} = \frac{1}{\sqrt{2}}$

Figure 4.9: Coefficients for longitudinal transmission (blue) and reflection (orange) from a mixed mode bridge with $\gamma_R, \gamma_M = 1$ for a shear incident wave with incident angle θ_2.

If there is more than a single wave packet incident incident on the system then, with the assumption that the incident waves are kept in phase along the bridge, the successive reflection and transmission relations (4.1.102, 4.1.103) can be used to calculate the coefficients caused by reflected wave superposition. For these relations to be valid the eigenvalues of the internal reflection matrix (4.1.99) must be less than 1. For the values of c_2/c_1 considered in the figures above this is only relevant for $c_2/c_1 = 1/\sqrt{2}$. Physically, this can be interpreted as a resonance for which most of the energy is internally reflected back onto the bridge. This gives an increase in wave amplitude on the bridge for each additional incident wave, which for infinite incident waves will lead to an infinite wave amplitude in the bridge. Matching displacements at the boundary requires that the bridge will then transmit infinite amplitude waves. This will be visible in the plots by a vertical asymptote.

It is clear from the Figs. 4.10–4.13 that unlike the membrane bridge considered previously, an infinite number of incident waves do not superpose to produce a perfect transmission with no reflection. The infinite summation does produce several key differences between a single incident wave and infinite incident waves. First, there is in general an increase in the transmission and a decrease in reflection. This is most notable near normal incidence of the longitudinal waves where both the reflections and transmissions cancel to produce no overall wave pattern.

There is also a clear decrease in the amount of wave conversion in the system. Aside from the infinite reflections near the asymptotes, the wave conversion amplitudes from Figs. 4.11 and 4.13 are visibly less than the corresponding amplitudes in Figs. 4.7 and 4.9.

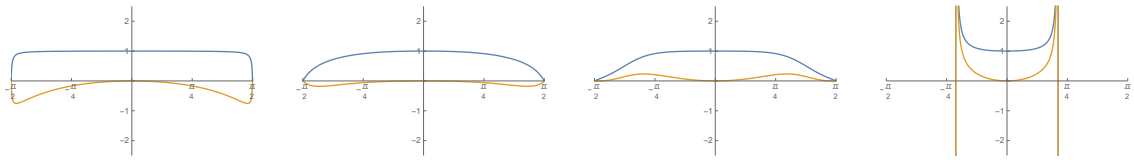

(a) $\frac{c_2}{c_1} = 0$ **(b)** $\frac{c_2}{c_1} = \frac{1}{3\sqrt{2}}$ **(c)** $\frac{c_2}{c_1} = \frac{2}{3\sqrt{2}}$ **(d)** $\frac{c_2}{c_1} = \frac{1}{\sqrt{2}}$

Figure 4.10: Coefficients for longitudinal transmission (blue) and reflection (orange) from a mixed mode bridge with $\gamma_R, \gamma_M = 1$ for infinite longitudinal incident waves with incident angle θ_1.

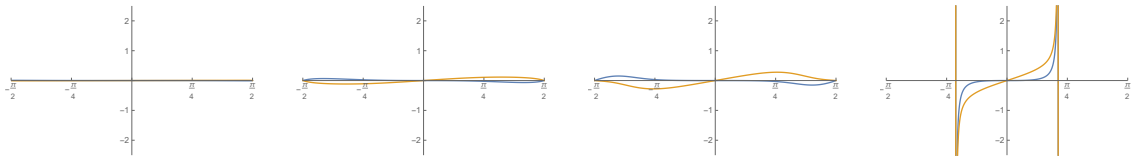

(a) $\frac{c_2}{c_1} = 0$ **(b)** $\frac{c_2}{c_1} = \frac{1}{3\sqrt{2}}$ **(c)** $\frac{c_2}{c_1} = \frac{2}{3\sqrt{2}}$ **(d)** $\frac{c_2}{c_1} = \frac{1}{\sqrt{2}}$

Figure 4.11: Coefficients for shear transmission (blue) and reflection (orange) from a mixed mode bridge with $\gamma_R, \gamma_M = 1$ for infinite longitudinal incident waves with incident angle θ_1.

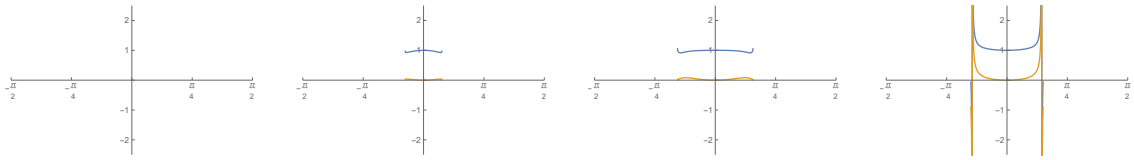

(a) $\frac{c_2}{c_1} = 0$ **(b)** $\frac{c_2}{c_1} = \frac{1}{3\sqrt{2}}$ **(c)** $\frac{c_2}{c_1} = \frac{2}{3\sqrt{2}}$ **(d)** $\frac{c_2}{c_1} = \frac{1}{\sqrt{2}}$

Figure 4.12: Coefficients for shear transmission (blue) and reflection (orange) from a mixed mode bridge with $\gamma_R, \gamma_M = 1$ for infinite shear incident waves with incident angle θ_2.

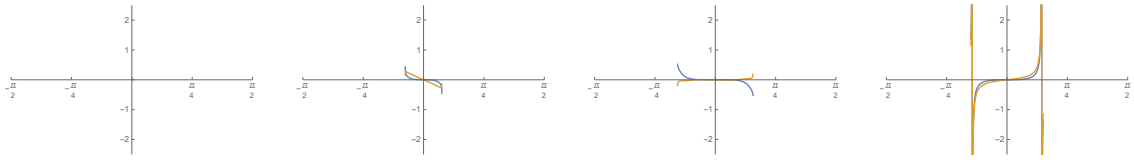

(a) $\frac{c_2}{c_1} = 0$ **(b)** $\frac{c_2}{c_1} = \frac{1}{3\sqrt{2}}$ **(c)** $\frac{c_2}{c_1} = \frac{2}{3\sqrt{2}}$ **(d)** $\frac{c_2}{c_1} = \frac{1}{\sqrt{2}}$

Figure 4.13: Coefficients for longitudinal transmission (blue) and reflection (orange) from a mixed mode bridge with $\gamma_R, \gamma_M = 1$ for infinite shear incident waves with incident angle θ_2.

4.1.3 Elastic Bulk Bridging Conclusion

In this section the effect of periodic insertions bridging the gap between two elastic half-planes has been investigated. Three different systems were considered; a longitudinal wave bridge, a shear wave bridge and a combination of the two.

All three systems only have perfect matching when the bridge parameters, γ_M and γ_S, both equal 1, and only for normally incident waves. Away from normal incidence any incident wave produces either a reflected wave or a wave conversion which changes the wave pattern in the system. The bridges are also not able to perfectly convert the wave. Any transmitted wave has some component which is the same form as the incident wave.

In general the bridges reproduce the wave pattern better for a less easily compressible bulk. Figs. 4.6–4.9 show that each system has less wave conversion and a higher transmission for low values of c_2/c_1 than higher values.

4.2 Elastic Surface Wave Bridging

Next consider a bridge oriented at bridging a linearly elastic structure as before, but instead designed to bridge waves which propagate along a surface. For this, suppose that there is an semi-infinite linearly elastic half plane with an infinitely deep gap. These two parts of the elastic half plane will occupy $0 \leq z < \infty, -\infty < y < \infty$, and $x \leq 0$ and $x \geq d$ respectively. Along the surface of the half plane will propagate a Rayleigh wave, a travelling wave solution which decays exponentially with depth away from the surface as detailed in §2.2.2. For an incident wave with angular frequency ω the wavenumber k is determined by the solution to the Rayleigh determinant (2.2.19).

The displacement potentials then have the standard 2D Rayleigh form (2.2.24),

$$\phi = \phi_0 e^{i[kx-\omega t]-k\alpha_R z}, \qquad \psi = \psi_0 e^{i[kx-\omega t]-k\beta_R z}, \tag{4.2.1}$$

with relations along the surface (2.2.22).

As before the aim is to construct a periodic bridge which can carry and reproduce the wave pattern incident on one side of the gap at the other side without causing any reflections. Since the wave amplitude will decay with depth it is simplest to start with periodic insertions connected uniformly at regular depth intervals. For convenience use the same bridge materials used for the bulk waves; thin membranes and stiff elastic sheets as detailed in §4.1.2.

4.2.1 Rayleigh Bridge Formulation

As before assume an incident and reflected wave in the bulk and a single transmitted wave in the bridges. Hence the incident and reflected wave potentials take the form,

$$\phi^{(i)} = A_i e^{i[kx-\omega t]-k\alpha_R z}, \qquad \phi^{(r)} = A_r e^{-i[kx+\omega t]-k\alpha_R z}, \tag{4.2.2}$$

$$\psi^{(i)} = B_i e^{i[kx-\omega t]-k\beta_R z}, \qquad \phi^{(r)} = B_r e^{-i[kx+\omega t]-k\beta_R z}, \tag{4.2.3}$$

with vertical and horizontal displacements from (2.2.4) and the displacements in the bridges are the same as for the bulk waves bridges (4.1.66, 4.1.67). This leads to displacement matching at the boundary of,

$$ik\left((A_i - A_r)e^{-k\alpha_R z} - i\beta_R(B_i + B_r)e^{-k\beta_R z}\right) = A_t, \tag{4.2.4}$$

$$ik\left(i\alpha_R(A_i + A_r)e^{-k\alpha_R z} + (B_i - B_r)e^{-k\beta_R z}\right) = B_t. \tag{4.2.5}$$

Similarly matching of stresses from the half plane (2.2.7) and the bridges (4.1.71) at the boundary yields,

$$\mu k^2\left((\beta_R^2-2\alpha_R^2-1)(A_i+A_r)e^{-k\alpha_R z}+2i\beta_R(B_i-B_r)e^{-k\beta_R z}\right)=i\mu k\frac{c_1^2}{c_2^2}\gamma_S A_t, \quad (4.2.6)$$

$$\mu k^2\left(-2i\alpha_R(A_i-A_r)e^{-k\alpha_R z}-(1+\beta_R^2)(B_i+B_r)e^{-k\beta_R z}\right)=i\mu k\frac{c_1}{c_2}\gamma_M B_t. \quad (4.2.7)$$

where γ_M and γ_S have the same definitions as the bulk case (4.1.14, 4.1.44). Unlike the previous boundaries there is now a dependence on depth. This removes some of the freedom of choosing parameters and since the aim is to perfectly bridge waves, in order to avoid any wave conversion the following formulation will differ from the previous methods. First, at the surface the wave potentials must satisfy the conditions arising from the free stress condition (2.2.22) and so,

$$i(B_i-B_r)=\frac{2\alpha_R}{1+\beta_R^2}(A_i+A_r), \quad -\beta_R(B_i+B_r)=i\frac{1+\beta_R^2}{2}(A_i-A_r). \quad (4.2.8)$$

Substituting into the boundary conditions gives the new relations,

$$ik\left(e^{-k\alpha_R z}-\frac{1+\beta_R^2}{2}e^{-k\beta_R z}\right)(A_i-A_r)=A_t, \quad (4.2.9)$$

$$ik\left(i\alpha_R e^{-k\alpha_R z}-i\frac{2\alpha_R}{1+\beta_R^2}e^{-k\beta_R z}\right)(A_i+A_r)=B_t, \quad (4.2.10)$$

$$ik\left((2\alpha_R^2+1-\beta_R^2)e^{-k\alpha_R z}-(1+\beta_R^2)e^{-k\beta_R z}\right)(A_i+A_r)=\frac{c_1^2}{c_2^2}\gamma_S A_t, \quad (4.2.11)$$

$$ik\left(2i\alpha_R e^{-k\alpha_R z}-2i\alpha_R e^{-k\beta_R z}\right)(A_i-A_r)=\frac{c_1}{c_2}\gamma_M B_t. \quad (4.2.12)$$

This set of equations has the solvability condition,

$$\frac{c_1^3}{c_2^3}\frac{e^{-k\alpha_R z}-\frac{1+\beta_R^2}{2}e^{-k\beta_R z}}{(2\alpha_R^2+1-\beta_R^2)e^{-k\alpha_R z}-(1+\beta_R^2)e^{-k\beta_R z}}\gamma_S=\frac{2e^{-k\alpha_R z}-2e^{-k\beta_R z}}{e^{-k\alpha_R z}-\frac{2}{1+\beta_R^2}e^{-k\beta_R z}}\frac{1}{\gamma_M} \quad (4.2.13)$$

which limits the freedom of choice in this system to a single parameter to preserve Rayleigh wave form for the reflected waves. Define a new parameter,γ_R to represent

this Rayleigh matching, such that

$$\gamma_R = \frac{c_1^2}{c_2^2}\frac{e^{-k\alpha_R z} - \frac{1+\beta_R^2}{2}e^{-k\beta_R z}}{(2\alpha_R^2 + 1 - \beta_R^2)e^{-k\alpha_R z} - (1+\beta_R^2)e^{-k\beta_R z}}\gamma_S = \frac{c_2}{c_1}\frac{2e^{-k\alpha_R z} - 2e^{-k\beta_R z}}{e^{-k\alpha_R z} - \frac{2}{1+\beta_R^2}e^{-k\beta_R z}}\frac{1}{\gamma_M}, \tag{4.2.14}$$

which gives the reflection coefficients,

$$\frac{A_r}{A_i} = \frac{\gamma_R - 1}{\gamma_R + 1}, \quad \frac{B_r}{B_i} = \frac{1 - \gamma_R}{1 + \gamma_R} \tag{4.2.15}$$

and transmission coefficients,

$$\frac{A_t}{A_i} = 2ik\frac{\left(e^{-k\alpha_R z} - \frac{1+\beta_R^2}{2}e^{-k\beta_R z}\right)}{1+\gamma_R}, \quad \frac{B_t}{B_i} = 2ik\frac{\left(e^{-k\beta_R z} - \frac{1+\beta_R^2}{2}e^{-k\alpha_R z}\right)}{1+\gamma_R}\gamma_R, \tag{4.2.16}$$

where the displacements along the bridge are related by,

$$\frac{B_t}{A_t} = -i\frac{2\alpha_R}{1+\beta_R^2}\frac{\left(e^{-k\beta_R z} - \frac{1+\beta_R^2}{2}e^{-k\alpha_R z}\right)}{\left(e^{-k\alpha_R z} - \frac{1+\beta_R^2}{2}e^{-k\beta_R z}\right)}\gamma_R. \tag{4.2.17}$$

From these relations, there is no initial reflection if $\gamma_R = 1$. However, substituting this into the bridge parameter equations (4.2.14) shows that as well as having a dependence on depth, the bridges are not independent of the wavenumber of the incident wave. Hence the bridge constructed in this way is not broadband, instead only working ideally for a single frequency.

From repeating this process at the right boundary for displacement potentials in the bulk,

$$\phi^{(t)} = C_t e^{i[kx-\omega t]-k\alpha_R z}, \tag{4.2.18}$$

$$\psi^{(t)} = D_t e^{i[kx-\omega t]-k\beta_R z}, \tag{4.2.19}$$

and in the bridges the displacements have the same transmitted forms (4.1.74, 4.1.75) and reflected forms, (4.1.76, 4.1.77) as for the bulk wave bridges. Then as before the

displacement and stress matching yields,

$$ik\left(C_t e^{-k\alpha_R z} - i\beta_R D_t e^{-k\beta_R z}\right) = C_i + C_r, \tag{4.2.20}$$

$$ik\left(i\alpha_R C_t e^{-k\alpha_R z} + D_t e^{-k\beta_R z}\right) = D_i + D_r, \tag{4.2.21}$$

$$\mu k^2\left((\beta_R^2 - 2\alpha_R^2 - 1)C_t e^{-k\alpha_R z} + 2i\beta_R D_t e^{-k\beta_R z}\right) = i\mu k\frac{c_1^2}{c_2^2}\gamma_S(C_i - C_r), \tag{4.2.22}$$

$$\mu k^2\left(-2i\alpha_R C_t e^{-k\alpha_R z} - (1+\beta_R^2)D_t e^{-k\beta_R z}\right) = i\mu k\frac{c_1}{c_2}\gamma_M(D_i - D_r). \tag{4.2.23}$$

which if the transmitted wave is a Rayleigh wave again allows the use of the classical surface relation for the displacement potentials (2.2.22). This leads to the relations,

$$ik\left(e^{-k\alpha_R z} - \frac{1+\beta_R^2}{2}e^{-k\beta_R z}\right)C_t = C_i + C_r, \tag{4.2.24}$$

$$ik\left(i\alpha_R e^{-k\alpha_R z} - i\frac{2\alpha_R}{1+\beta_R^2}e^{-k\beta_R z}\right)C_t = D_i + D_r, \tag{4.2.25}$$

$$ik\left((2\alpha_R^2 + 1 - \beta_R^2)e^{-k\alpha_R z} - (1+\beta_R^2)e^{-k\beta_R z}\right)C_t = \frac{c_1^2}{c_2^2}\gamma_S(C_i - C_r), \tag{4.2.26}$$

$$ik\left(2i\alpha_R e^{-k\alpha_R z} - 2i\alpha_R e^{-k\beta_R z}\right)C_t = \frac{c_1}{c_2}\gamma_M(D_i - D_r). \tag{4.2.27}$$

Again solve these to produce reflection coefficients,

$$\frac{C_r}{C_i} = \frac{\gamma_R - 1}{\gamma_R + 1}, \quad \frac{D_r}{D_i} = \frac{1-\gamma_R}{1+\gamma_R}, \tag{4.2.28}$$

and transmission coefficients,

$$\frac{C_t}{C_i} = \frac{2ik}{\left(e^{-k\alpha_R z} - \frac{1+\beta_R^2}{2}e^{-k\beta_R z}\right)}\frac{\gamma_R}{1+\gamma_R}, \quad \frac{D_t}{D_i} = \frac{2ik}{\left(e^{-k\beta_R z} - \frac{1+\beta_R^2}{2}e^{-k\alpha_R z}\right)}\frac{1}{1+\gamma_R}. \tag{4.2.29}$$

Since the aim is to not cause any wave conversion, there can be no phase difference between the two bridges. In this case the overall transmission from the right boundary will be of the form,

$$\frac{C_t}{A_i} = \frac{D_t}{B_i} = \frac{4\gamma_R}{(1+\gamma_R)^2}, \tag{4.2.30}$$

which is identical to the form studied previously for the membrane-string bridge (3.1.45). Importantly, both the ϕ and ψ have the same reduction in amplitude so the transmitted wave remains of Rayleigh form. Furthermore, on considering the displacements in the system the successive reflections and transmissions from the system become of the form studied previously (3.1.46, 3.1.47), with Γ replaced with γ_R.

4.2.2 Rayleigh Bridge Construction

Initially it may seem that despite the dependence on the wavenumber of the incident wave and depth of each bridge for the bridge parameters γ_M and γ_S, the construction of a bridge for this system is straightforward. However, on closer investigation of the requirements of the wave parameters it is evident that at certain depths it is not possible to construct bridges with the required parameters. In what follows, since perfect bridging is most desirable, consider only the case where γ_R=1.

From Fig. 4.14a there is a small range of depths for which γ_S values must be negative. Physically, however, γ_S must be positive and so it is not possible to construct bridges at these depths. This means that unlike all previous cases the bridge separation is not arbitrary.

First it must be determined whether the bridge at the surface of the half plane should consist of a membrane or sheet. In Fig. 4.14b the bridging requirement for a membrane at $z = 0$ is $\gamma_M = 0$, due to the free surface condition of the half plane. It is therefore not necessary to have a membrane at the surface for bridging to occur, so at $z = 0$ there will be a sheet with,

$$\gamma_S = 4\frac{c_2^2}{c_1^2}\left(1 - \frac{c_2^2}{c_1^2}\right). \tag{4.2.31}$$

As the depth of the bridges increase, the required values of the bridge parameters γ_M

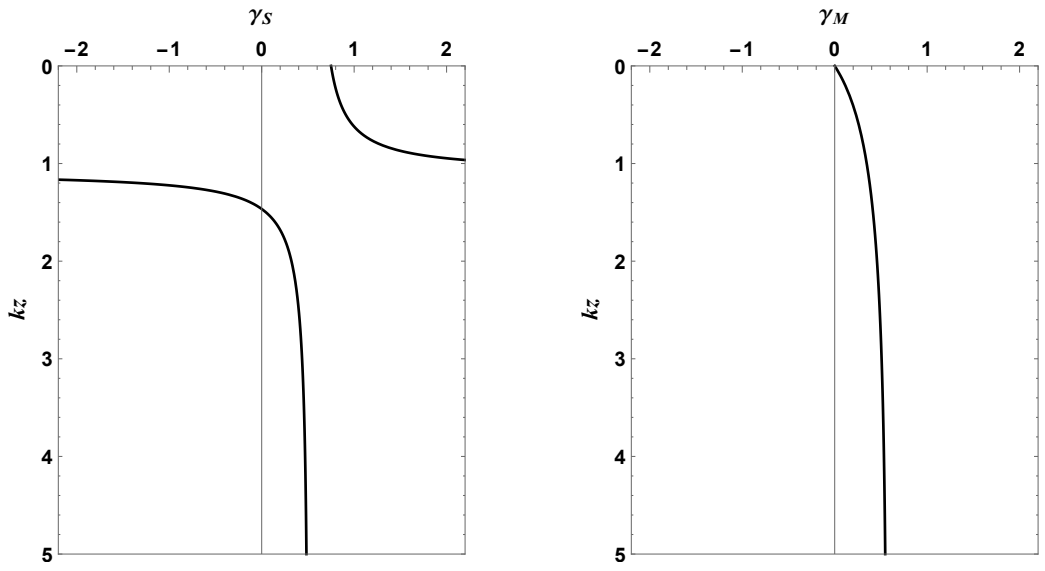

(a) Required γ_S value

(b) Required γ_M value

Figure 4.14: Required values of γ_M and γ_S for bridging a Rayleigh wave of wavenumber k at a depth of z for a bulk material with Poisson Ratio $\nu = 0.4$ and bridging parameter $\gamma_R = 1$.

and γ_S tend to fixed values. These are, as $kz \to \infty$,

$$\gamma_S \to 2\frac{c_2^2}{c_1^2}, \qquad \gamma_M \to \frac{c_2}{c_1}(1+\beta_R^2), \tag{4.2.32}$$

which are both positive for any choice of material parameters. Thus at an infinite depth of any bulk material it is possible to construct bridges. Therefore, the difficulty of constructing a bridge while avoiding negative parameters is strictly confined to the region visible in Fig. 4.14a. This can be seen more generally by considering the behaviour of γ_R (4.2.14). From this definition γ_M is positive for all positive values of z, regardless of material parameters, while $\gamma_S = 0$ when,

$$kz = \frac{1}{\alpha_R - \beta_R} \ln \left| 2\frac{1+\alpha_R^2}{1+\beta_R^2} - 1 \right|. \tag{4.2.33}$$

and has a singularity at,

$$kz = \frac{1}{\alpha_R - \beta_R} \ln \left| \frac{2}{1+\beta_R^2} \right|, \tag{4.2.34}$$

Between these two points γ_S must be negative and is positive at all other depths. The smallest value of l results from 'sandwiching' this negative region with two sheets. This gives an absolute limit on the size of l as,

$$l > \frac{\lambda}{2\pi}\frac{1}{\alpha_R - \beta_R}\ln\left|\alpha_R^2 + \frac{1-\beta_R^2}{2}\right|, \tag{4.2.35}$$

If the bridges are constructed such that the sheets are placed at depths of $z = nl$, and the membranes at $z = (n+1/2)l$, $n \in \mathbb{Z}$ then this condition gives inequalities for the location of the sheets either side of the negative region,

$$kn_l l < \frac{1}{\alpha_R - \beta_R}\ln\left|\frac{2}{1+\beta_R^2}\right| \tag{4.2.36}$$

$$k(n_l+1)l > \frac{1}{\alpha_R - \beta_R}\ln\left|2\frac{1+\alpha_R^2}{1+\beta_R^2} - 1\right| \tag{4.2.37}$$

where $n_l \in \mathbb{Z}$ is defined as being one greater than the number of sheets before the negative region. This can be solved to produce,

$$n_l \leq \frac{\ln\left|\frac{2}{1+\beta_R^2}\right|}{\ln\left|\alpha_R^2 + \frac{1-\beta_R^2}{2}\right|} \tag{4.2.38}$$

which is greater than 1 for all possible system parameters. To maximise the number of bridges take the above inequality (4.2.38) to be an equality. Then the smallest possible l is when,

$$\frac{l}{\lambda} = \frac{1}{2\pi(n_l+1)}\frac{1}{\alpha_R - \beta_R}\ln\left|2\frac{1+\alpha_R^2}{1+\beta_R^2} - 1\right|. \tag{4.2.39}$$

The homogenisation used to model the bridge is only valid when the separation between the layers of bridges is much less than the wavelength of the incident wave. To see if the homogenisation will remain valid the smallest possible value of l/λ is taken from (4.2.39) and plotted in Fig. 4.15 for the full possible range of Poisson ratios.

In Fig. 4.15 there is a discontinuous 'stepped' behaviour coming from n_l being strictly an integer. From the plot it is visible that $l/\lambda \lesssim 0.12$ and for smaller Poisson

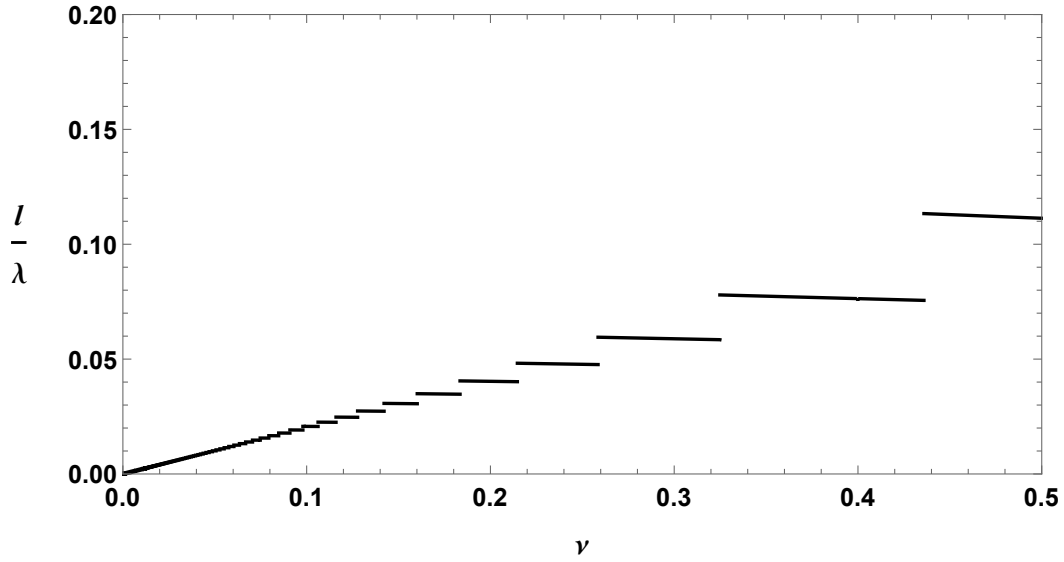

Figure 4.15: The smallest possible values of l/λ from (4.2.39) possible for a bridge for Rayleigh waves with $\gamma_R = 1$ in a bulk material with Poisson ratio ν

ratios decreases to 0. Therefore this method of bridging will be more valid for more easily compressible materials. However, the previous treatment for the membrane in §3.2.3 shows how a periodic forcing can be close to the homogenised result even for l/λ values of 0.1, which would make this bridge valid for all but the most incompressible Poisson ratios.

4.2.3 Rayleigh Bridge Conclusion

In this section the previous bridge construction for bulk waves has been used to bridge a propagating surface wave. While the formulation of the problem and the resulting coefficients for the bridge appear to have a similar form to those produced by the bulk systems, the presence of the surface and form of the wave makes the actual bridging significantly different.

Unlike the previous systems, since this system is restricted to Rayleigh waves only, there is only one wave type and one corresponding bridging parameter, γ_R. Like the

previous systems, when this parameter is equal to 1 the system will bridge perfectly and reproduce the incident wave pattern on the other side of the gap as a transmitted wave with no reflections.

However, this bridging parameter determines two other parameters, γ_M and γ_S, both of which correspond to one bridge type. These bridge parameters also have a dependence on the depth of the bridge and the wavelength of the incident wave. While it would be simple to tune bridges depending on their depth, the wavelength requirement means this bridge type cannot ever be broadband.

Also unlike the previous systems there is not an arbitrary choice in the spacing of the bridges. To ensure that the bridges can be constructed the individual bridge components must take the values which satisfy (4.2.13). However there is a range of γ_S values which must be negative. No bridge can be physically constructed with these values so the spacing must be set that all of the longitudinal bridges are at depths which correspond to a positive γ_S.

Finally then, it is possible to construct a periodic bridge which can perfectly transmit a normally incident Rayleigh wave across a gap. To satisfy the stress free surface, longitudinal bridges are constructed at nl and shear bridges at $(n + 1/2)l$, with l and the bridge material parameters specified by (4.2.39) and (4.2.14) respectively. Such a construction will lead to a sufficiently small l/λ so that the homogenisation procedure detailed earlier remains valid and to a high degree of accuracy the wave form will be transmitted.

4.3 Linear Elasticity Bridging Conclusion

In this chapter the same type of bridge construction has been used on two different types of waves, linearly elastic bulk waves and Rayleigh waves. Both of these wave types have conditions which lead to identical incidence and transmission, making it appear to an outside observer that there is no gap in the material. This has multiple real world uses.

The requirements for so called perfect bridging are very different for both bridge types. are however very different. To ideally bridge both types of bulk waves is only possible for normal incidence and requires bridging parameters of $\gamma_M = \gamma_S = 1$. However to bridge a Rayleigh wave requires both of these parameters to have a strict dependence on depth and wavelength meaning that the Rayleigh bridge is not broadband.

As the depth of the Rayleigh bridge increases the bridging parameters γ_M and γ_S tend to constant values which depend solely on the properties of the bulk. However to have both of these constant values tend to 1 as required for bulk bridging requires

$$2\frac{c_2^2}{c_1^2} = \frac{c_2}{c_1}(1 + \beta_R^2) = 1, \tag{4.3.1}$$

which no material can satisfy. To bridge shear waves only the requirement $\gamma_M = 1$ leads to a material with $c_2/c_1 \approx 0.364$, and equivalently the requirement $\gamma_S = 1$ for longitudinal waves leads to $c_2/c_1 = 1/\sqrt{2}$. While both of these are theoretically achievable by conventional materials, the longitudinal requirement is only possible in the limit of an ideal compressibility. As such it is possible to arbitrarily bridge either bulk waves or Rayleigh waves with this bridge but not both.

CHAPTER 5

Rod-Like Resonator Metasurface

In this chapter the behaviour of waves on the surface of a linearly elastic half plane with vertical rod-like resonators is considered. A full unimodal solution of this system has already been given by Colquitt et al. [25]. The aim of this chapter is to attempt to replicate these results, making use of the asymptotic model for Rayleigh waves [63] detailed in §2.2.3. While the results will not be a perfect match to those produced by full unimodal analysis it will be possible to produce an explicit dispersion relation and more easily characterise the key wave behaviours. Some of this work has been adapted and published [39] with additional discussion of similar structures.

This chapter will be organised as follows: First the asymptotic model for forcing at the surface of a half-plane will be applied to this system, leading to an approximate first mode dispersion relation. This dispersion relation will be compared with the full unimodal result from Colquitt et al. [25]. Then the same model will be used without homogenising the forcing at the boundary, producing a dispersion relation which accounts for higher order mode behaviour. This dispersion relation will then be used to investigate the effect different types of forcing profiles have on the overall behaviour of the system, which first mode analysis cannot account for.

5.1 Asymptotic Analysis

This section makes use of a linearly elastic half plane with vertical resonators at the surface. On making use of the asymptotic model introduced in §2.2.3 the half plane has propagating on it a travelling surface wave of angular frequency ω and wavenumber k with displacement potentials of the form (2.2.24),

$$\phi = A_\phi \, e^{i[kx-\omega t]-k\alpha_R z}, \qquad \psi = A_\psi \, e^{i[kx-\omega t]-k\beta_R z}, \tag{5.1.1}$$

where the vertical and horizontal displacements are defined by (2.2.4) and along the surface $z = 0$ have the relations (2.2.22). Hence the wave amplitudes are related by,

$$A_\psi = -i\frac{2\alpha_R}{1+\beta_R^2}A_\phi, \tag{5.1.2}$$

leading to displacements at the surface,

$$u_1 = ik\frac{1-\beta_R^2}{2}A_\phi, \qquad u_3 = k\alpha_R\frac{1-\beta_R^2}{1+\beta_R^2}A_\phi. \tag{5.1.3}$$

This wave is then incident upon a region where the surface of the half-space is coated with periodically arranged vertical resonators, with a uniform spacing l. Assume that these resonators are of uniform height L and diameter h_r, as shown in Fig. 5.1 where $h_r \ll l$. These resonators are modeled as rods such that they each have the governing equation (2.1.5), which if the resonators are arranged vertically becomes,

$$E_r\frac{\partial^2 u_r}{\partial z^2} = \rho_r\frac{\partial^2 u_r}{\partial t^2}, \tag{5.1.4}$$

and using the boundary condition (2.1.6), these rods have boundary conditions,

$$-\frac{\pi h_r^2}{4}E_r \, \frac{\partial u_3}{\partial z}|_{z=0} = V(x,y,t), \tag{5.1.5}$$

$$\frac{\partial u_3}{\partial z}|_{z=L} = 0, \tag{5.1.6}$$

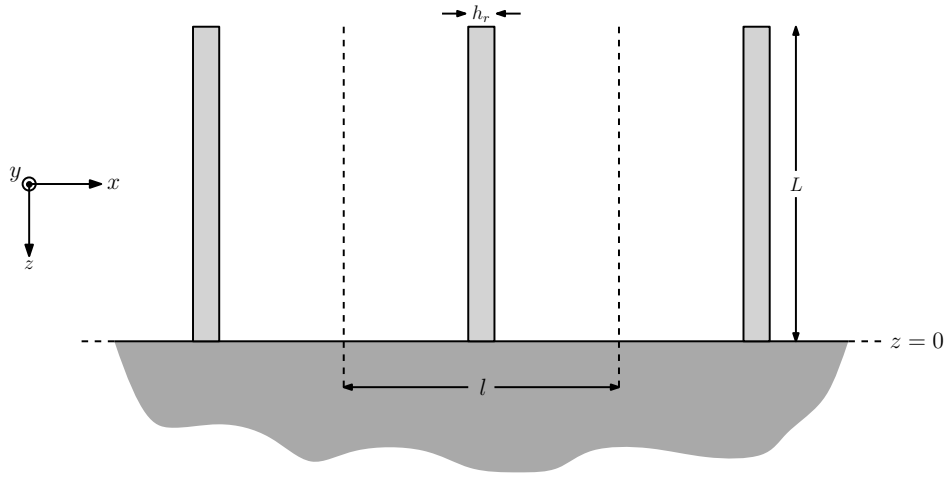

Figure 5.1: An array of rod-like resonators of length L and diameter h_r periodically attached with spacing l to the surface of a semi-infinite linearly elastic half space.

where $V(x, y, t)$ is the vertical force on the half plane caused by a single rod and h_r is the diameter of each rod, assuming that they are cylindrical. When surface waves are dominant, the governing equation for a surface wave on a half plane with vertical forcing is (2.2.23) subject to the surface boundary condition (2.2.26) at $z = 0$. In this system the forcing comes from an infinite number of periodically arranged rods, each with a point force taken from (5.1.5). Therefore the boundary condition (2.2.26) can be taken as,

$$\frac{\partial^2 \phi}{\partial x^2} - \frac{1}{c_R^2}\frac{\partial^2 \phi}{\partial t^2} = \frac{1+\beta_R^2}{2\mu B} V \delta^{(l)}(x)\delta^{(l)}(y). \tag{5.1.7}$$

It will be assumed that the solutions are time harmonic with fixed frequency ω. Then the solution for waves in the rod is given by,

$$u_r = A_r e^{i[Kz-\omega t]} + B_r e^{-i[Kz+\omega t]}, \tag{5.1.8}$$

where K is determined by the longitudinal dispersion relation (2.1.8) and A_r and B_r are constants. Substituting into the free boundary condition (5.1.6) gives the rod displacement as,

$$u_r = A_r e^{i[Kz-\omega t]} + A_r e^{i(2KL)} e^{-i[Kz+\omega t]}, \tag{5.1.9}$$

and on assuming that

$$V(x,y,t) = Ve^{i[kx-\omega t]}, \tag{5.1.10}$$

so use the boundary conditions at $z = 0$ to obtain,

$$A_r(1 + e^{i(2KL)}) = k\alpha_R \frac{1-\beta_R^2}{1+\beta_R^2} A_\phi, \tag{5.1.11}$$

$$-\frac{\pi h_r^2}{4} E_r A_r (1 - e^{i(2KL)}) = V. \tag{5.1.12}$$

On combining these,

$$V = \frac{\pi h_r^2}{4} E_r \frac{\omega}{c_r} k\alpha_R \frac{1-\beta_R^2}{1+\beta_R^2} \tan\left(\frac{\omega L}{c_r}\right) A_\phi. \tag{5.1.13}$$

Then, making use of the homogenisation scheme in §2.3 to remove the delta functions, the boundary condition becomes,

$$\frac{\partial^2 \phi}{\partial x^2} - \frac{1}{c_R^2}\frac{\partial^2 \phi}{\partial t^2} = \frac{1+\beta_R^2}{2l^2\mu B} V e^{i[kx-\omega t]}, \tag{5.1.14}$$

which gives on substitution of the assumed wave solution,

$$\left(k^2 - \frac{\omega^2}{c_R^2}\right) = -\frac{1-\beta_R^2}{2l^2\mu B}\frac{\pi h_r^2}{4} E_r \frac{\omega}{c_r} k\alpha_R \tan\left(\frac{\omega L}{c_r}\right). \tag{5.1.15}$$

Then, define a resonator variable Υ by,

$$\Upsilon(\omega) = -\alpha_R \frac{1-\beta_R^2}{2l^2\mu B}\frac{\pi h_r^2}{4} E_r \frac{\omega}{c_r} \tan\left(\frac{\omega L}{c_r}\right), \tag{5.1.16}$$

so on substitution the explicit dispersion relation becomes,

$$k = \frac{\Upsilon(\omega)}{2} \pm \sqrt{\left(\frac{\Upsilon(\omega)}{2}\right)^2 + \frac{\omega^2}{c_R^2}}, \tag{5.1.17}$$

which is plotted in Fig. 5.2 using the material parameters detailed in Table 5.1 alongside the full unimodal solution for the dispersion relation from Colquitt et al. which is given by,

$$4\frac{k^2c_2^2}{\omega^2}\sqrt{\frac{k^2c_2^2}{\omega^2} - \frac{c_2^2}{c_1^2}}\sqrt{\frac{k^2c_2^2}{\omega^2} - 1} - \left(2\frac{k^2c_2^2}{\omega^2} - 1\right)^2 = \sqrt{\frac{k^2c_2^2}{\omega^2} - \frac{c_2^2}{c_1^2}}\frac{\pi h_r^2 E_r\ c_2}{4l^2\mu\ c_r}\tan\left(\frac{\omega L}{c_r}\right). \tag{5.1.18}$$

Table 5.1: The numerical system parameter values for the rod resonators and half-space used to produce the dispersion relation curves of Figs. 5.2 and 5.3.

Symbol	Definition	Value
l	Lattice spacing	2 m
ρ	Half-plane density	13000 kg m^{-3}
μ	Half-plane shear modulus	325 MPa
λ	Half-plane first Lamè parameter	702 MPa
L	Resonator length	14 m
h_r	Resonator diameter	0.3m
ρ_r	Resonator density	450 kg m^{-3}
E_r	Resonator Young Modulus	1.70 GPa

In the plot in Fig. 5.2, it is difficult to tell where the full unimodal and asymptotic solutions differ demonstrating that the asymptotics are an excellent approximation for the full unimodal solution. To show the small divergences, more closely examine the region of the plot around the asymptotes of the graph, where the difference between the full unimodal solution and the asymptotic solution should be greatest.

The regions of greatest divergence from Fig. 5.3 show a measurable error in k of 0.04 m^{-1} at the first asymptote and 0.06 m^{-1} at the second leading to relative errors of around 2.5% and 1.4% respectively. These errors are less than it would be expected that even an ideal physical system would replicate the dispersion relation. Furthermore, due to the shallow gradient near the asymptotes, the differences between k values are much greater than the differences between the predicted values of wave frequency or speed. As such the asymptotic model used can produce an accurate approximation for the physical system described.

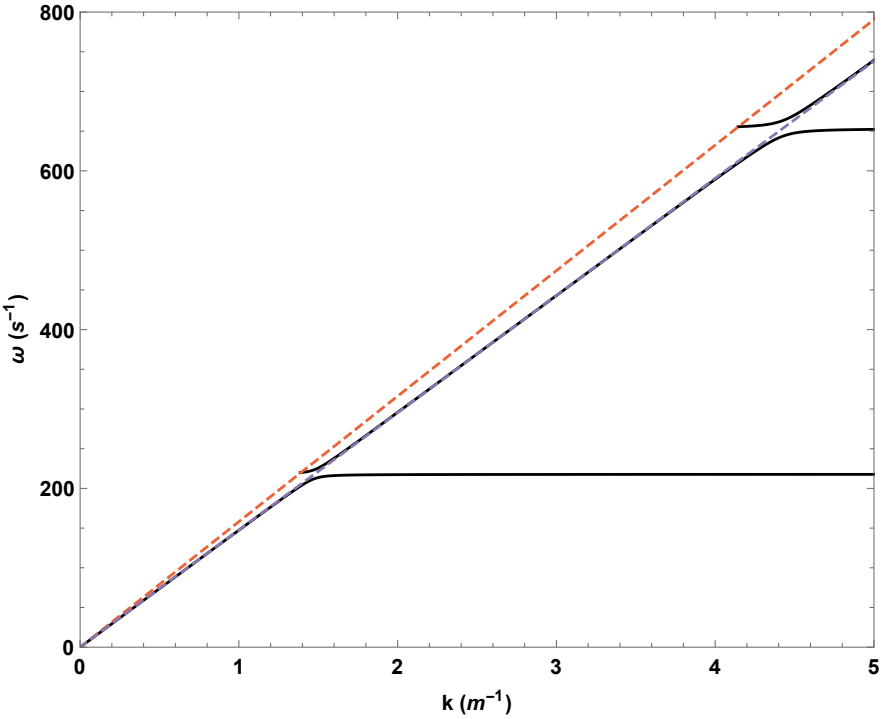

Figure 5.2: The dispersion curves for surface waves on the half plane coated with rod-like resonators, using physical parameters from Table 5.1. The solid blue lines show the dispersion curve of the full unimodal solution from (5.1.18) and the solid black lines the dispersion curve of the asymptotic solution from (5.1.17). The dashed orange and purple lines correspond to the shear and Rayleigh wave lines respectively.

5.2 Fourier Series Solutions

To verify the use of the homogenisation scheme in both the full unimodal and asymptotic cases, make use of the asymptotic formulation again but instead solve for the full boundary conditions without using the homogenisation procedure.

5.2.1 Delta Function Fourier Series

To solve the same system but with full boundary conditions, substitute the Fourier series representation of the delta function (2.3.5) into the asymptotic boundary condition

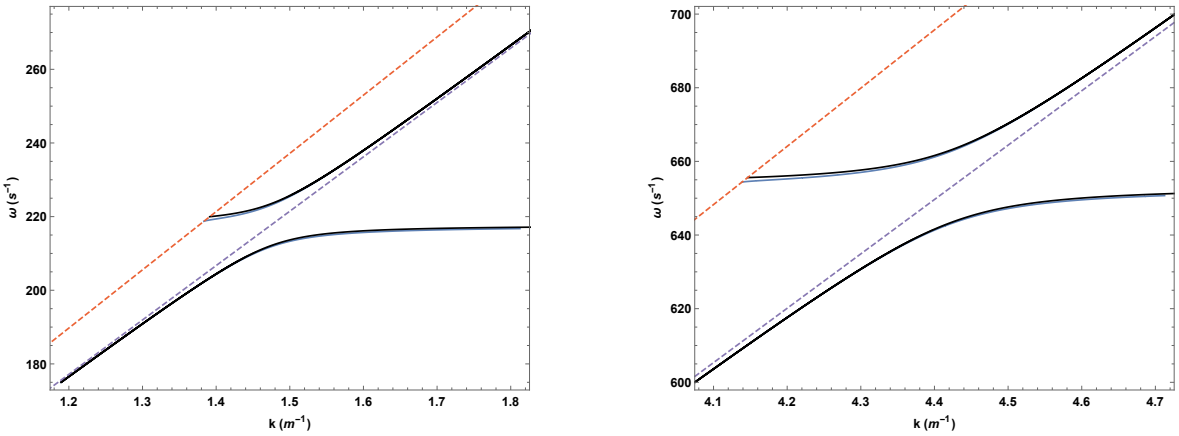

(a) First asymptote. **(b)** Second asymptote.

Figure 5.3: The dispersion curves near the asymptotes for surface waves on the half plane coated with rod-like resonators, using physical parameters from Table 5.1. The solid blue lines show the dispersion curve of the full unimodal solution from (5.1.18) and the solid black lines the dispersion curve of the asymptotic solution from (5.1.17). The dashed orange and purple lines correspond to the shear and Rayleigh wave lines respectively.

(5.1.7),

$$\frac{\partial^2\phi}{\partial x^2}+\frac{\partial^2\phi}{\partial y^2}-\frac{1}{c_R^2}\frac{\partial^2\phi}{\partial t^2}=\frac{1+\beta_R^2}{2\mu Bl^2}V\sum_{m,n=-\infty}^{\infty}e^{i\left(\frac{n\pi x}{l}+\frac{m\pi y}{l}\right)}. \tag{5.2.1}$$

Since the surface is no longer being homogenised, the dispersion relation may depend on the orientation of the waves. Assume that the form of ϕ along the surface is given by,

$$\phi=e^{i[k(x\cos\theta+y\sin\theta)-\omega t]}\sum_{m,n=-\infty}^{\infty}A_{mn}e^{i\left(\frac{n\pi x}{l}+\frac{m\pi y}{l}\right)} \tag{5.2.2}$$

Assume also that since these are both Fourier series, and a Fourier series has a unique representation, each term in the summation of ϕ directly corresponds to a term in the delta series summations. Thus, define each mn^{th} term as,

$$\phi_{mn}=A_{mn}e^{i[k(x\cos\theta+y\sin\theta)-\omega t]}e^{i\left(\frac{n\pi x}{l}+\frac{m\pi y}{l}\right)}, \tag{5.2.3}$$

where $m, n \in \mathbb{Z}$. Then on substituting into the original equation,

$$\left(\frac{\omega^2}{c_R^2} - \left(\left(k\cos\theta + \frac{n\pi}{l}\right)^2 + \left(k\sin\theta + \frac{m\pi}{l}\right)^2\right)\right) A_{mn} e^{i[kx-\omega t]} = \frac{1+\beta_R^2}{2\mu B l^2} V, \tag{5.2.4}$$

and making use of the previously obtained solution for waves in the rods (5.1.12),

$$V(x,y,t) = -\frac{\pi h_r^2}{4} E_r \frac{\omega}{c_r} u_3 \tan\left(\frac{\omega L}{c_r}\right) e^{i[k(x\cos\theta + y\sin\theta) - \omega t]}, \tag{5.2.5}$$

and so by taking the 0^{th} term in the summation, an expression for A_{mn} can be obtained in terms of A_{00},

$$A_{mn} = A_{00} \frac{\frac{\omega^2}{c_R^2} - k^2}{\frac{\omega^2}{c_R^2} - \left(k\cos\theta + \frac{n\pi}{l}\right)^2 - \left(k\sin\theta + \frac{m\pi}{l}\right)^2}. \tag{5.2.6}$$

Suppose also that derivatives are taken in the direction of wave propagation (denoted by $\hat{x}_{mn}$) for each individual component of the summation, so that the relation for how the waves decay in the bulk is given by,

$$\frac{\partial^2 \phi_{mn}}{\partial z^2} + \alpha_R^2 \frac{\partial^2 \phi^2}{\partial \hat{x}_{mn}^2} = 0 \tag{5.2.7}$$

and the surface relation between potentials at $z = 0$ given as,

$$\frac{\partial \psi_{mn}}{\partial \hat{x}_{mn}} = -\frac{2}{1+\beta_R^2} \frac{\partial \phi_{mn}}{\partial z}, \tag{5.2.8}$$

From this it follows that the full form of the ϕ_{mn} terms are,

$$\phi_{mn} = A_{mn} e^{i[k_{mn}\hat{x} - \omega t] - k_{mn}\alpha_R z}, \tag{5.2.9}$$

where,

$$k_{mn} = \sqrt{\left(k\cos\theta + \frac{n\pi}{l}\right)^2 + \left(k\sin\theta + \frac{m\pi}{l}\right)^2}. \tag{5.2.10}$$

Along the surface, using the displacement potential relations (2.2.22) then,

$$\psi_{mn} = -i \frac{2\alpha_R}{1+\beta_R^2} \phi_{mn}. \tag{5.2.11}$$

The vertical displacement at the base of each rod is given by,

$$u_3 = \sum_{m,n=-\infty}^{\infty} \frac{\partial \phi_{mn}}{\partial z} + \frac{\partial \psi_{mn}}{\partial \hat{x}_{mn}}, \tag{5.2.12}$$

$$= \sum_{m,n=-\infty}^{\infty} -k_{mn}\alpha_R \phi_{mn} + ik_{mn}\psi_{mn}, \tag{5.2.13}$$

$$= \sum_{m,n=-\infty}^{\infty} k_{mn}\alpha_R \left(\frac{1-\beta_R^2}{1+\beta_R^2}\right) A_{mn}, \tag{5.2.14}$$

and using the expression for A_{mn} from above,

$$u_3 = \alpha_R \left(\frac{1-\beta_R^2}{1+\beta_R^2}\right) A_{00} \sum_{m,n=-\infty}^{\infty} \frac{\left(\frac{\omega^2}{c_R^2} - k^2\right)\sqrt{\left(k\cos\theta + \frac{n\pi}{l}\right)^2 + \left(k\sin\theta + \frac{m\pi}{l}\right)^2}}{\frac{\omega^2}{c_R^2} - \left(k\cos\theta + \frac{n\pi}{l}\right)^2 - \left(k\sin\theta + \frac{m\pi}{l}\right)^2}, \tag{5.2.15}$$

and so substituting this into the 0^{th} term,

$$\left(\frac{\omega^2}{c_R^2} - k^2\right) A_{00} = \frac{\beta_R^2 - 1}{2\mu B l^2}\frac{\pi h_r^2}{4} E_r \frac{\omega}{c_r} \tan\left(\frac{\omega L}{c_r}\right) \alpha_R A_{00} \sum_{m,n=-\infty}^{\infty} \frac{\left(\frac{\omega^2}{c_R^2} - k^2\right)\sqrt{\left(k\cos\theta + \frac{n\pi}{l}\right)^2 + \left(k\sin\theta + \frac{m\pi}{l}\right)^2}}{\frac{\omega^2}{c_R^2} - \left(k\cos\theta + \frac{n\pi}{l}\right)^2 - \left(k\sin\theta + \frac{m\pi}{l}\right)^2}, \tag{5.2.16}$$

from which the asymptotic dispersion relation accounting for the surface structure is,

$$\frac{8\mu B l^2 c_r}{\omega E_r (1-\beta_R^2)\pi h_r^2} \cot\left(\frac{\omega L}{c_r}\right) = \sum_{m,n=-\infty}^{\infty} \frac{\sqrt{\left(k\cos\theta + \frac{n\pi}{l}\right)^2 + \left(k\sin\theta + \frac{m\pi}{l}\right)^2}}{\frac{\omega^2}{c_R^2} - \left(k\cos\theta + \frac{n\pi}{l}\right)^2 - \left(k\sin\theta + \frac{m\pi}{l}\right)^2}. \tag{5.2.17}$$

Similarly, if the first Fourier coefficient is finite then the vertical displacement is also finite, or conversely, using the dispersion relation to obtain the wave number for a given frequency the Fourier series can be obtained from using the value of the vertical displacement as a boundary condition,

$$A_{00} = \left(k^2 - \frac{\omega^2}{c_R^2}\right)^{-1} \frac{1+\beta_R^2}{2\mu B l^2}\frac{\pi h_r^2}{4} E_r \frac{\omega}{c_r} \tan\left(\frac{\omega L}{c_r}\right)\ u_3. \tag{5.2.18}$$

If the wave speed is close to the Rayleigh speed and the wavelength of the system is much greater than l then it is clear that the terms in the summation will quickly

become negligible. Then, if the new surface wave has speed $c = \omega/k$ and wavelength $\lambda = 2\pi/k$,

$$\frac{\sqrt{\left(k\cos\theta + \frac{n\pi}{l}\right)^2 + \left(k\sin\theta + \frac{m\pi}{l}\right)^2}}{\frac{\omega^2}{c_R^2} - \left(k\cos\theta + \frac{n\pi}{l}\right)^2 - \left(k\sin\theta + \frac{m\pi}{l}\right)^2} = -\frac{l}{\pi}\frac{\sqrt{\left(\frac{2l}{\lambda}\cos\theta + n\right)^2 + \left(\frac{2l}{\lambda}\sin\theta + m\right)^2}}{\left(\frac{2l}{\lambda}\cos\theta + n\right)^2 + \left(\frac{2l}{\lambda}\sin\theta + m\right)^2 - \left(\frac{2l}{\lambda}\right)^2\frac{c^2}{c_R^2}}, \quad (5.2.19)$$

and making use of the long wave assumption $\lambda \gg l$,

$$\frac{\sqrt{\left(k\cos\theta + \frac{n\pi}{l}\right)^2 + \left(k\sin\theta + \frac{m\pi}{l}\right)^2}}{\frac{\omega^2}{c_R^2} - \left(k\cos\theta + \frac{n\pi}{l}\right)^2 - \left(k\sin\theta + \frac{m\pi}{l}\right)^2} \simeq -\frac{l}{\pi\sqrt{m^2+n^2}}, \ m \text{ or } n \neq 0. \quad (5.2.20)$$

On contrasting this with the result for when m and n both equal 0,

$$\frac{\sqrt{\left(k\cos\theta + \frac{n\pi}{l}\right)^2 + \left(k\sin\theta + \frac{m\pi}{l}\right)^2}}{\frac{\omega^2}{c_R^2} - \left(k\cos\theta + \frac{n\pi}{l}\right)^2 - \left(k\sin\theta + \frac{m\pi}{l}\right)^2} = -\frac{\lambda}{2\pi\left(1 - \frac{c}{c_R}\right)}, \ m, n = 0 \quad (5.2.21)$$

it is clear that the first term is much greater than the lower order terms due to the multiplication of $\frac{\lambda}{l}$. Therefore for any finite number of terms in this dispersion relation, the lower order terms will act as a small correction to the homogenised solution. To demonstrate this, the table below shows the numerical solution to the dispersion relation for an example given ω and different amounts of terms kept in the summation.

n	0	$[-1, 1]$	$[-5, 5]$	$[-10, 10]$
k	0.679858	0.679830	0.679827	0.679827

Table 5.2: The solutions to partial evaluations of (5.2.17) for given intervals of n with $m = 0$, $\omega = 100$, for system parameters from Table 5.1.

In this table, the values of k seem accurate from taking just the first term up to 4 decimal places. This demonstrates how accurate the homogenisation is in this case and how few additional terms need to be accounted for to produce values with high degrees of precision.

However, elementary analysis of the dispersion relation shows that by adding in the lower order terms, the system cannot have a solution. This is because if ω and k are finite then when n tends to infinity the series tends to the harmonic series, which diverges slowly. Since this is due to the behaviour of the delta function, using another function will most likely remove the divergence from the lower order terms. This will also have the added advantage of making the system more physically realisable as the delta function is an ideal modelling of a point force and cannot exist in a physical system where all objects have a finite thickness to distribute the force over.

If it is assumed that whatever forcing used is also periodic on the same scale as the resonators then reuse the Fourier series method but instead use arbitrary coefficients. To model a more realistic forcing than that of the periodic delta functions, suppose that the periodic rods impart a more realistic 'smooth' forcing, represented by a combined Fourier series of,

$$\sum_{m,n=-\infty}^{\infty} \frac{E_{mn}}{l^2} e^{i\left(\frac{n\pi x}{l}+\frac{m\pi y}{l}\right)}. \tag{5.2.22}$$

Then the surface boundary condition can be represented as,

$$\frac{\partial^2\phi}{\partial x^2}+\frac{\partial^2\phi}{\partial y^2}-\frac{1}{c_R^2}\frac{\partial^2\phi}{\partial t^2}=\frac{1+\beta_R^2}{2\mu B l^2}V\sum_{m,n=-\infty}^{\infty} E_{mn}e^{i\left(\frac{n\pi x}{l}+\frac{m\pi y}{l}\right)}. \tag{5.2.23}$$

Assuming the same form of ϕ as before (5.2.3) and taking the 0^{th} term again yields the relation between the summation constants as,

$$A_{mn}=A_{00}\frac{E_{mn}}{E_{00}}\frac{\frac{\omega^2}{c_R^2}-k^2}{\frac{\omega^2}{c_R^2}-\left(k\cos\theta+\frac{n\pi}{l}\right)^2-\left(k\sin\theta+\frac{m\pi}{l}\right)^2}. \tag{5.2.24}$$

which, using the same relation between the displacement potentials along the surface (5.2.11) then leads to the expression for the displacement along the surface as,

$$u_3=\alpha_R\left(\frac{1-\beta_R^2}{1+\beta_R^2}\right)A_{00}\sum_{m,n=-\infty}^{\infty}\frac{E_{mn}}{E_{00}}\frac{\left(\frac{\omega^2}{c_R^2}-k^2\right)\sqrt{\left(k+\frac{n\pi}{l}\right)^2+\left(\frac{m\pi}{l}\right)^2}}{\frac{\omega^2}{c_R^2}-\left(k+\frac{n\pi}{l}\right)^2-\left(\frac{m\pi}{l}\right)^2}. \tag{5.2.25}$$

Then on repeating the same process as for the delta function Fourier series substitute this displacement into the surface boundary condition (5.1.7) and rearrange to produce the dispersion relation,

$$\frac{8\mu B l^2 c_r}{\omega E_r(1-\beta_R^2)\pi h_r^2}\cot\left(\frac{\omega L}{c_r}\right)=\sum_{m,n=-\infty}^{\infty}\frac{E_{mn}}{E_{00}}\frac{\sqrt{\left(k\cos\theta+\frac{n\pi}{l}\right)^2+\left(k\sin\theta+\frac{m\pi}{l}\right)^2}}{\frac{\omega^2}{c_R^2}-\left(k\cos\theta+\frac{n\pi}{l}\right)^2-\left(k\sin\theta+\frac{m\pi}{l}\right)^2}. \tag{5.2.26}$$

If the chosen Fourier series converges to a 'smooth' function, where the forcing and all derivatives are continuous then each term in the summation for the dispersion relation will have a reduced magnitude and so in general this series will converge.

5.3 Vertical Rod Metasurface Conclusion

Previous efforts in treating a system of vertical rod-like resonators along the surface of an elastic half plane have been based on an full unimodal formulation. There have however been recent developments in an asymptotic method to more easily treat surface waves by producing a direct wave equation. This method relies on applied stresses or displacements along the surface and allows complicated systems that produce surface waves to be solved from a system of equations much simpler than that produced by the full unimodal method.

Applying the asymptotic method to the system of surface resonators has successfully produced a more complete solution than that produced by full unimodal analysis. Using this method two solutions were obtained, using two different approaches of treating the effect of the surface resonators. The first of these solutions used homogenisation of the forcing of the rods into the half plane to obtain a long wave solution. This produced a quadratic equation in terms of the wave number, k, which could then be simply solved to produce a simple closed form explicit dispersion relation for wave number in

terms of angular frequency, ω. It has been shown that graphically the solution obtained is very close to the full unimodal solution obtained previously.

The second approach treated the forcing as a Fourier series, for which the previous approach is a specific case where only the first term of the Fourier series is considered. This approach allows for a full solution of the system much simpler than that produced by a unimodal formulation, making term by term analysis of the solution possible. Taking the solution term by term yields a powerful insight into the system, provides a justification for the previous homogenisation assumption by showing that if the wavelength is greater than the distance between resonators then the first term dominates, and also shows effects arising from the geometry of the periodic arrangement, rather than just the resonators. Since the delta function is non analytic the use of it in the forcing leads to a divergence in the summation. Making the Fourier series arbitrary allows this method to be applied to any 'thin' periodic forcing. Hence this result can be easily changed to be guided by experimental results to refine the model.

Also importantly, by showing that this simple model can be closely approximated by a Helmholtz equation, it has been shown that it is possible to construct a representative experimental setup for elastic surface waves using a thin elastic membrane. This is also a significant improvement on a fully elastic half plane experimental setup and so complicated systems can now be analysed experimentally without needing an experiment which is expensive and difficult to build and manage.

CHAPTER 6

Beam-Like Resonator Metasurface

Following the successful treatment of the rod resonator system, again make use of the asymptotic model to treat a more sophisticated resonator array. Instead of considering stiff rod-like resonators instead use flexural beams. These more accurately model the motion of real world arrays along surfaces such as trees under low frequency seismic excitation.

In this chapter the effect that a periodic array of flexural resonators embedded into the surface of an elastic half-space has on propagating surface waves is discussed. In order to better see the effect of the flexural motion, and because in the frequency ranges considered flexural waves dominate, the longitudinal motion of the resonators is neglected. The problem being considered in this chapter concerns the effect on a travelling Rayleigh wave with stresses caused by resonators applied at the surface and so the asymptotic model from §2.2.3 should be ideal for the investigation which follows. For completeness, however, the exact solution will also be computed numerically and used as a comparison to the asymptotic solution as verification. Special attention is devoted to the effect of various junction conditions joining the beams to the elastic half-space which arise from considering flexural motion and are not present for the case of purely compressional resonators.

This discussion will be organised as follows: The problem formulation is given in Section 6.1 and sections which follow then each detail the treatment of a different boundary condition between the resonators and the half-space. Section 6.2 considers the resonators as simply supported, with the resonators able to freely rotate but conserve displacements and horizontal stresses. In Section 6.3 the resonators are considered as ideally attached at the base to rails which can move freely but matches the bending moment and the gradient at the surface. For the boundary considered in Section 6.4 the resonators are considered as ideally attached to the half-space and so all variables between the resonator and half-space are fully matched. In each section, the solution obtained from the asymptotic formulation is compared with the full unimodal solution.

This work has been published in [111] with added computational work demonstrating the behaviour of the resonances of the system.

6.1 Problem Statement

To start, consider linearly elastic motion on a 3D half-space $-\infty < x_1 < \infty$, $-\infty < x_2 < \infty$, $0 \leq x_3 < \infty$ and make use of both the exact formulation and asymptotic model for Rayleigh waves detailed in §2.2.3. Consider also the motion of a regular infinite array of identical flexural resonators of length L and cylindrical cross section with diameter h_b that are ideally attached to the surface at $z = 0$, as shown in Fig. 6.1. Treating these resonators as classical Euler-Bernoulli beams yields the governing equations for flexural motion of each beam from (2.1.9) as,

$$B_b \frac{\pi h_b^4}{64} \frac{\partial^4 u_1}{\partial z^4} = -M_b \frac{\partial^2 u_1}{\partial t^2}, \tag{6.1.1}$$

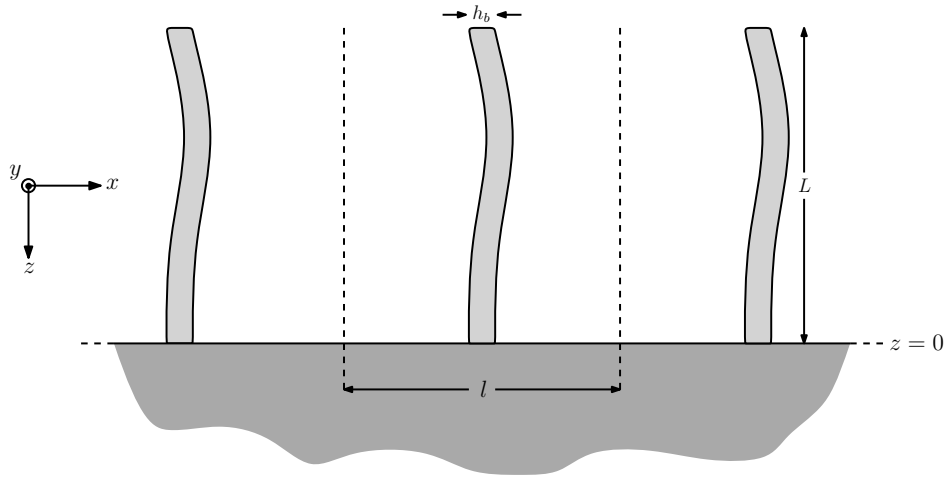

Figure 6.1: An array of beam-like resonators of length L and diameter h_b periodically attached with spacing l to the surface of a semi-infinite linearly elastic half space.

with boundary conditions (2.1.12). Suppose also that the ends of the beams at $x_3 = -L$ are not subject to any additional forcing. Then, the boundary conditions at the free end of the beam are,

$$\frac{\partial^3 u_i}{\partial x_3^3} = 0, \qquad \frac{\partial^2 u_i}{\partial x_3^2} = 0, \quad i = 1, 2, \tag{6.1.2}$$

and the solution of the above system will depend on the specific boundary condition chosen for the interface between the half-space and the resonators. In what follows, adapt and study a range of different boundary conditions, which will be defined and studied in the sections which follow.

It is also assumed that the beams' diameter is much less than the separation between them so approximate each as a point loading, represented by the periodic Dirac delta function (2.3.1). If it is also assumed that the wavelength of the travelling surface wave is much greater than the separation between the beams, then the homogenisation procedure in §2.3 can be used to a reasonable approximation. Therefore at the surface the load can be distributed as,

$$\sum_{n,m=-\infty}^{\infty} \sigma_{ij}\delta^{(l)}(x)\delta^{(l)}(y) \approx \frac{1}{l^2}\sigma_{i3}, \quad i = 1, 3. \tag{6.1.3}$$

Each type of boundary condition treated in this paper will result from the matching of variables between the resonators and the surface of the half-space at $x_3 = 0$. These junction conditions are summarised in §A.1.

For sufficiently thin resonators the resistance to bending motion is, typically, much smaller than the resistance to compression and therefore, in the linear regime, the flexural and compressional deformations are decoupled at leading order (see, for example, [65]). Moreover [25] suggests that, for the case of resonant arrays on thin plates, the effects of flexural and compressional resonances can be considered independently. Therefore, in the present paper, we focus on the flexural motion of the resonators and consider pure bending only such that vertical motion on the surface of the half-space does not couple to compressional deformation of the resonators. It is however emphasised that vertical tractions may arise at the surface of the half-space as a result of rotations in the flexural resonators [65] and these are taken into account.

6.2 Simply Supported Beams

Begin by considering the resonators as simply supported at the surface of the half-space. In this system, there is no need to conserve bending angle and there is no overall bending moment at the coupling. Instead only the horizontal displacement and the transverse force require matching. The boundary conditions (2.1.12) at the end of the beam fixed into the half-space are therefore,

$$\begin{aligned} u_1|_{z=0} &= u_H, \\ \frac{\partial^2 u_1}{\partial z^2}|_{z=0} &= 0, \end{aligned} \tag{6.2.1}$$

and the stress at the end of the beam is,

$$H(x, y, t) = \frac{\pi h_b^4}{64} B_b \, \frac{\partial^3 u_1}{\partial z^3}|_{z=0}, \tag{6.2.2}$$

where u_H is the horizontal displacement at the surface under the beam and $H(x, y, t)$ is the horizontal force at the surface of the half-space caused by the resonators.

Solving the beam equation (6.1.1) with these boundary conditions and the free end conditions (6.1.2) in the usual way yields the relation for horizontal force,

$$H(x, y, t) = B_b \frac{\pi h_b^4}{64} K^3 u_H \frac{\cos(KL)\cosh(KL) - 1}{\cosh(KL)\sin(KL) - \cos(KL)\sinh(KL)}, \tag{6.2.3}$$

where from (2.1.13), K is given by,

$$K = \left(\frac{64 M_R}{B_b \pi h_b^4}\right)^{\frac{1}{4}} \sqrt{\omega}. \tag{6.2.4}$$

This force is applied as a point force in a regular array. If the size of the overall array and wavelength of the wave are assumed to be large in comparison with the distance between the point forces then homogenise these point forces into a continuous surface stress using the distribution (6.1.3). This stress is given by,

$$\sigma_{31} = H(x, y, t)\delta^{(l)}(x)\delta^{(l)}(y) \tag{6.2.5}$$

$$= \frac{H(x, y, t)}{l^2}, \tag{6.2.6}$$

where l is the distance between two beams.

Start with the full unimodal formulation for the system. Taking the surface stresses in terms of displacement potentials from (2.2.7),

$$-2i\ \mu k^2 \alpha \phi - \mu k^2 (1 + \beta^2)\psi = \frac{H(x, y, t)}{l^2}, \tag{6.2.7}$$

$$\left((\lambda + 2\mu)k^2\alpha^2 - \lambda k^2\right)\phi - 2i\mu k^2 \beta \psi = 0, \tag{6.2.8}$$

then for ease of manipulation let the surface stress from the beams be expressed by,

$$\sigma_{31} = K^3 \hat{H} u_H, \tag{6.2.9}$$

and using (2.2.4) and substituting along the surface to find u_H,

$$u_H = k(i\phi + \beta\psi). \tag{6.2.10}$$

By substituting from (6.2.3) and solving simultaneously the full unimodal dispersion relation for this system is given by,

$$\left((\lambda+2\mu)k^2\alpha^2-\lambda k^2\right)\left(-\mu k^2\left(1+\beta^2\right)-kK^3\hat{H}\beta\right)=\left(2\ \mu k^2\alpha+kK^3\hat{H}\right)\left(-2\mu k^2\beta\right). \tag{6.2.11}$$

It is clear that in this form this expression will be difficult to manipulate. If the asymptotic model produces a close approximation which can be used to investigate the behaviour of the dispersion relation, then this will allow this system to be easily understood on a more fundamental level than the full unimodal solution can.

Begin by applying the asymptotic model to this system. From (2.2.25) along the surface,

$$\frac{\partial^2\psi}{\partial x^2}-\frac{1}{c_R^2}\frac{\partial^2\psi}{\partial t^2}=-\frac{1+\beta_R^2}{2\mu Bl^2}H(x,y,t), \tag{6.2.12}$$

and by combining (2.2.22) and (6.2.10), u_H is given by,

$$u_H=-k\beta_R\frac{1-\beta_R^2}{1+\beta_R^2}\psi. \tag{6.2.13}$$

As in (6.2.9) let $H(x,y,t)$ be denoted by,

$$\frac{H(x,y,t)}{l^2}=K^3\hat{H}u_H \tag{6.2.14}$$

$$=-kK^3\hat{H}\beta_R\frac{1-\beta_R^2}{1+\beta_R^2}\psi, \tag{6.2.15}$$

and so the dispersion relation is given by,

$$\left(-k^2+\frac{\omega^2}{c_R^2}\right)\psi=kK^3\hat{H}\ \beta_R\frac{1-\beta_R^2}{2\mu B}\ \psi. \tag{6.2.16}$$

From the above it follows that the dispersion relation can be given explicitly by the solution to the quadratic equation,

$$k^2+kK^3\hat{H}\ \beta_R\frac{1-\beta_R^2}{2\mu B}\ -\frac{\omega^2}{c_R^2}=0. \tag{6.2.17}$$

This asymptotic solution can also be obtained directly from the full unimodal dispersion relation obtained earlier by expanding around the Rayleigh solution. If the Rayleigh condition (2.2.19) is taken in the form $R(r) = 0$ where,

$$r = \frac{\omega^2}{c_2^2 k^2}, \tag{6.2.18}$$

and

$$R(r) = (2-r)^2 - 4\sqrt{1-r}\sqrt{1-\frac{c_2^2}{c_1^2}r}, \tag{6.2.19}$$

the one term Taylor expansion of this around the Rayleigh line can then be written,

$$R(r) \approx \left(\frac{\omega^2}{c_2^2 k^2} - \frac{c_R^2}{c_2^2}\right) R'\left(\frac{c_R^2}{c_2^2}\right) = -2\left(1 - \frac{\omega^2}{c_R^2 k^2}\right) B. \tag{6.2.20}$$

By expanding the full unimodal dispersion relation, (6.2.11), it can be shown that for the simply supported beams,

$$R(r) = \frac{K^3 \hat{H}}{\mu k}\beta(1-\beta^2), \tag{6.2.21}$$

and so,

$$k^2 - \frac{\omega^2}{c_R^2} = -k\frac{K^3\hat{H}}{2\mu B}\beta(1-\beta^2), \tag{6.2.22}$$

which is identical to the asymptotic dispersion relation (6.2.17) given that $\beta = \beta_R$.

It is clear that the asymptotic dispersion relation (6.2.17) is much simpler than the full unimodal one obtained previously (6.2.11). Most importantly, the dispersion relation can be given for k as an explicit function of ω and, therefore, manipulated with greater ease. To see if this dispersion relation is useful, compare it with the exact relation and see how the two sets of results compare. This is shown in Fig. 6.2 using the parameter values in Table 6.1.

Due to the choice of system parameters, for each of the demonstration figures, Figs. 6.2–6.5, the homogenisation from (6.1.3) is only valid when the wavelength is

Table 6.1: The numerical system parameters for the beam resonator and half-space used to produce the dispersion curves shown in Figs. 6.2– 6.5.

Symbol	Definition	Value
l	Lattice spacing	2 m
ρ	Half-plane density	13000 kg m^{-3}
μ	Half-plane shear modulus	325 MPa
λ	Half-plane first Lamè parameter	702 MPa
L	Resonator length	14 m
h_b	Resonator diameter	0.3m
ρ_b	Resonator density	450 kg m^{-3}
B_b	Resonator Bending Stiffness	1.70 GPa

much greater than 2 metres, or alternately when $k \ll \pi m^{-1}$. Also, while the asymptotic method gives a solution which is valid for all k, in the full unimodal system β will become purely imaginary when $\frac{\omega}{k} > c_2$ and so no propagating solution can exist in this region of the plot.

This plot shows how closely the asymptotic method matches with the full unimodal result, particularly near the Rayleigh line and for lower frequency waves. Due to the asymptotes, this plot also shows that the asymptotic model can be used to model a dispersion relation and remain accurate even for large stresses. The regions around the asymptotes also produce an effective band gap, which are ranges of frequencies for which a wave cannot propagate through the system. Such band gaps have many practical real-world applications, as they can filter a wide range of wave frequencies.

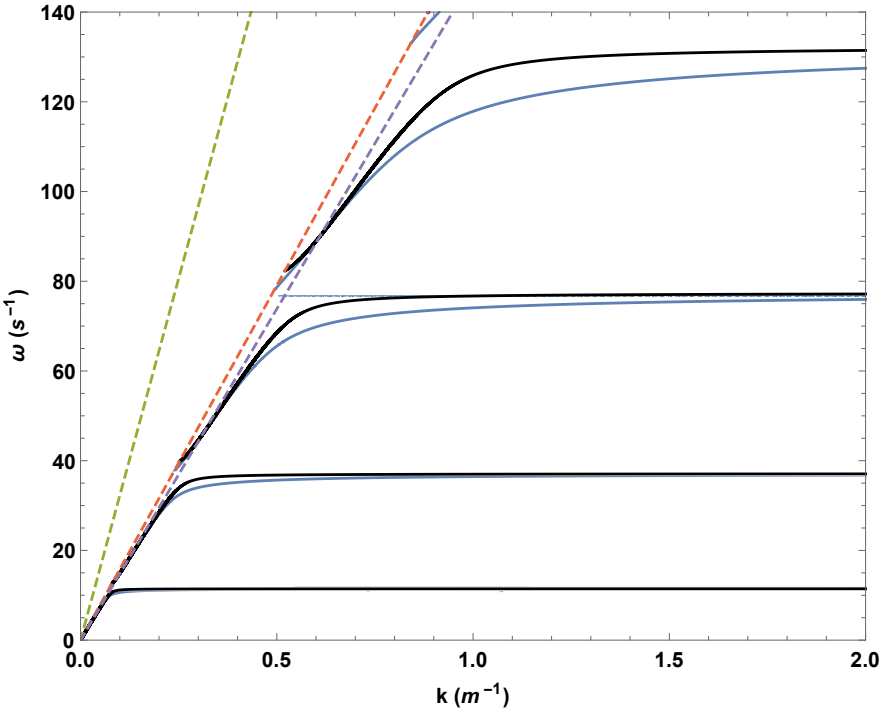

Figure 6.2: The dispersion curves for surface waves on the half-space coated with simply supported beam-like resonators, using physical parameters from Table 6.1. The solid blue lines show the dispersion curve of the full unimodal solution from (6.2.11) and the solid black lines the dispersion curve of the asymptotic solution from (6.2.17). The dashed green, orange and purple lines correspond to the longitudinal, shear and Rayleigh wave lines respectively.

6.3 Beams on a Rail

Suppose that the resonators are held at $z = 0$ to a rail parallel to the surface of the half-space, which allows the base of the beam to move freely but changes the bending angle of the beam depending on the gradient of the surface. This allows the beam to impart a bending moment on the half-space but no horizontal forcing. There is therefore no need to conserve displacements and the horizontal stress must equal zero.

This then leads to the boundary conditions (2.1.12) becoming,

$$\begin{aligned} \frac{\partial u_1}{\partial z}|_{z=0} &= u_{V,x}, \\ B_b \frac{\pi h_b^4}{64} \frac{\partial^2 u_1}{\partial z^2}|_{z=0} &= -\frac{\pi h_b^4}{64} \frac{\partial \sigma_{33}}{\partial x}|_{z=0}, \\ \frac{\partial^3 u_1}{\partial z^3}|_{z=0} &= 0, \end{aligned} \tag{6.3.1}$$

and the vertical stress at the end of the beam is given by,

$$V(x,y,t) = \frac{\pi h_b^2}{4} \sigma_{33}|_{z=0}, \tag{6.3.2}$$

where $V(x,y,t)$ is the vertical force from the beams into the half-space and $u_{V,x}$ is the gradient of the vertical displacement along the surface. Whilst this junction condition may initially appear somewhat counter-intuitive, it can be understood in terms of so-called 'gyroscopic hinges' [86].

Solving these in the usual way along with the free end conditions (6.1.2) and the beam equation (6.1.1) gives the vertical force,

$$V(x,y,t) = i\frac{K}{k}\frac{\pi h_b^2}{4} B_b \; u_{V,x} \frac{1 - \cos(KL)\cosh(KL)}{\cosh(KL)\sin(KL) + \cos(KL)\sinh(KL)} \tag{6.3.3}$$

Again start with the full unimodal treatment. As with $H(x,y,t)$ previously, use the force distribution (6.1.3) and define $\hat{V}$ such that,

$$\frac{V(x,y,t)}{l^2} = i\frac{K}{k}\hat{V} u_{V,x}, \tag{6.3.4}$$

where $u_{V,x}$ be expressed in displacement potentials from (2.2.4) as,

$$u_{V,x} = -ik^2\alpha\phi - k^2\psi. \tag{6.3.5}$$

Then, from (2.2.7) the surface stresses on the half-space are,

$$-2i\;\mu k^2 \alpha\phi - \mu k^2(1+\beta^2)\psi = 0, \tag{6.3.6}$$

$$\left((\lambda + 2\mu)k^2\alpha^2 - \lambda k^2\right)\phi - 2i\;\mu k^2 \beta\psi = -K\hat{V}(-k\alpha\phi + ik\psi), \tag{6.3.7}$$

for which, rearranging and solving simultaneously leads to the full unimodal dispersion relation,

$$\left((\lambda+2\mu)k^2\alpha^2-\lambda k^2-kK\hat{V}\alpha\right)\left(-\mu k^2\left(1+\beta^2\right)\right) \;=\; \left(2\;\mu k^2\alpha\right)\left(-2\mu k^2\beta+kK\hat{V}\right) \tag{6.3.8}$$

As could be expected, this dispersion relation is very similar to the one obtained for the simply supported case. As before, it is difficult to manipulate and interpret so, to understand the system on a more fundamental level, again use the asymptotic model to obtain a simpler approximate system solution.

To apply the asymptotic model to this system, where there is only a vertical stress, apply (2.2.26) along the surface of the half-space,

$$\frac{\partial^2\phi}{\partial x^2}-\frac{1}{c_R^2}\frac{\partial^2\phi}{\partial t^2}=\frac{1+\beta_R^2}{2\mu B}V(x,y,t), \tag{6.3.9}$$

or equivalently, using the surface potential relation (2.2.22) and making the assumption of a harmonic wave to make this in terms of ψ,

$$\frac{\partial^2\psi}{\partial x^2}-\frac{1}{c_R^2}\frac{\partial^2\psi}{\partial t^2}=-i\frac{\alpha_R}{\mu B}V(x,y,t). \tag{6.3.10}$$

Combining (2.2.22) with (6.3.5), $u_{V,x}$ is given by,

$$u_{V,x}=-k^2\frac{1-\beta_R^2}{2}\psi. \tag{6.3.11}$$

Then by taking $\hat{V}$ from (6.3.4) and substituting into the surface boundary condition,

$$\left(-k^2+\frac{\omega}{c_R^2}\right)\psi=-k\;\frac{\alpha_R}{\mu B}K\hat{V}\frac{1-\beta_R^2}{2}\psi, \tag{6.3.12}$$

leading to the asymptotic dispersion relation,

$$k^2-k\;\frac{\alpha_R}{\mu B}K\hat{V}\frac{1-\beta_R^2}{2}-\frac{\omega^2}{c_R^2}=0. \tag{6.3.13}$$

In the same way as before that the asymptotic dispersion relation can be obtained by expressing the full unimodal dispersion relation (6.3.8) in terms of $R(r)$

$$R(r) = -\frac{K\hat{V}}{\mu k}\alpha(1-\beta^2), \tag{6.3.14}$$

and using the single term Taylor expansion of $R(r)$ around the Rayleigh solution, for a near-Rayleigh wave speed,

$$k^2 - \frac{\omega^2}{c_R^2} = k\frac{K\hat{V}}{2\mu B}\alpha(1-\beta^2), \tag{6.3.15}$$

which as with the simply supported case gives the asymptotic dispersion relation (6.3.13) if $\alpha = \alpha_R$ and $\beta = \beta_R$.

As with the simply supported case, the dispersion relation from the asymptotic model is much simpler than the one produced by the full unimodal analysis. It is again quadratic and so can be expressed to explicitly give k in terms of ω. To examine how well the asymptotic model approximates the full unimodal solution, plot the two solutions in Fig. 6.3, using the system parameters from Table 6.1.

This plot shows how again the asymptotic model reproduces the main features of the full unimodal solution, particularly near the Rayleigh line. For all of the modes the asymptotic model predicts the asymptote, the overall shape of the dispersion relation and the existence of a large band gap for each mode.

6.4 Fully Matched Beams

Full matching of the beams is a more complete coupling between the half-space and the resonators, ensuring that all relevant displacements, gradients, moments and stresses at the coupling between the two media are conserved. Predictably this also leads to a more involved solution for both the beam motion solution and the surface wave

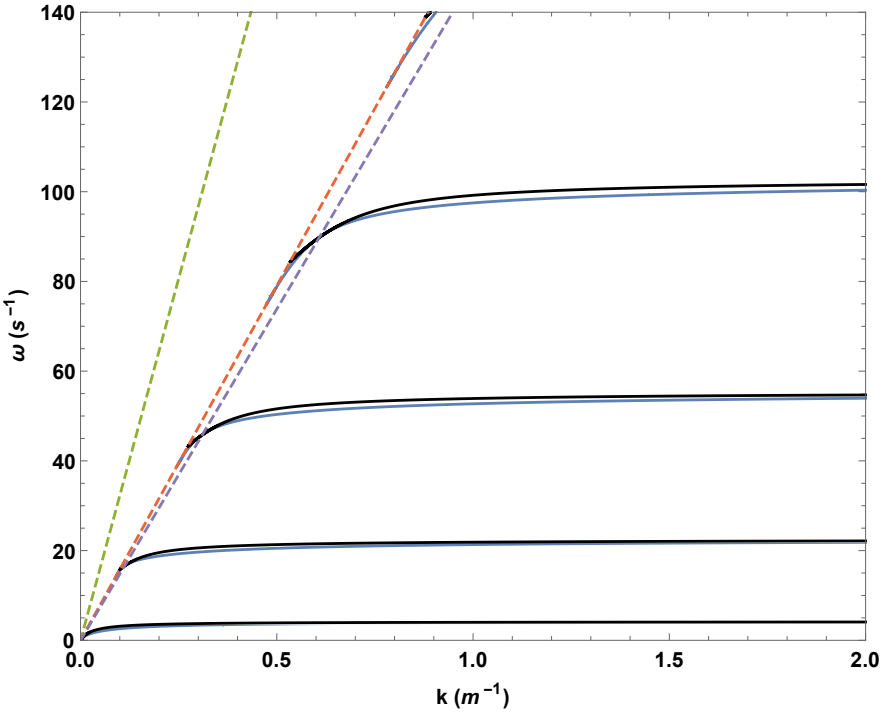

Figure 6.3: The dispersion curves for surface waves on the half-space coated with beam-like resonators supported by rails, using physical parameters from Table 6.1. The solid blue lines show the dispersion curve of the full unimodal solution from (6.3.8) and the solid black lines the dispersion curve of the asymptotic solution from (6.3.13). The dashed green, orange and purple lines correspond to the longitudinal, shear and Rayleigh wave lines respectively.

dispersion relation. For simplicity, we also assume an ideal contact between the beams and half-space, neglecting any local contact strain effects.

Since the beam itself is unchanged, the governing equation for the bulk of the beam from (6.1.1) and the boundary conditions for the free end from (6.1.2) are the same as those for the previous two cases. Matching at $z = 0$ gives the boundary conditions (2.1.12) for the fully matched beams as,

$$\begin{aligned} u_1|_{z=0} &= u_H, \\ \frac{\partial u_1}{\partial z}|_{z=0} &= u_{V,x}, \\ B_b \frac{\pi h_b^4}{64} \frac{\partial^2 u_1}{\partial z^2}|_{z=0} &= -\frac{\pi h_b^4}{64} \frac{\partial \sigma_{33}}{\partial x}|_{z=0}, \end{aligned} \tag{6.4.1}$$

and the stresses at the base of the beam as given by,

$$\begin{aligned} H(x,y,t) &= \frac{\pi h_b^4}{64} B_b \ \frac{\partial^3 u_1}{\partial z^3}|_{z=0}, \\ V(x,y,t) &= \frac{\pi h_b^2}{4} \sigma_{33}|_{z=0}. \end{aligned} \tag{6.4.2}$$

Solving these conditions in the usual way along with (6.1.1,6.1.2) gives,

$$\begin{aligned} H(x,y,t) &= \frac{\pi h_b^4}{64} B_b K^2 (\xi u_{V,x} + K\eta u_H), \\ V(x,y,t) &= i\frac{\pi h_b^2}{4} B_b \frac{K}{k} (\zeta u_{V,x} + K\xi u_H), \end{aligned} \tag{6.4.3}$$

where,

$$\xi = \frac{\sin(KL)\sinh(KL)}{\cos(KL)\cosh(KL)+1}, \tag{6.4.4}$$

$$\eta = \frac{\cosh(KL)\sin(KL)+\cos(KL)\sinh(KL)}{\cos(KL)\cosh(KL)+1}, \tag{6.4.5}$$

$$\zeta = \frac{\cosh(KL)\sin(KL)-\cos(KL)\sinh(KL)}{\cos(KL)\cosh(KL)+1}. \tag{6.4.6}$$

As in the previous sections, begin with the full unimodal treatment and then use the asymptotic model for comparison.

Unlike the cases discussed previously, the full unimodal solution will not intersect with the asymptotic solution at the Rayleigh line. To do so, the beam must behave

as though the coupled end with the half-space is free. This imposes requirements for the displacement and gradient at the base of the beam but these do not match with the required displacement and gradient for the half-space. This will not affect the full unimodal solution but will affect the accuracy of the asymptotic solution since the assumption that stresses tend to zero at the Rayleigh line is no longer valid.

In the same approach as before begin with the full unimodal treatment. From (2.2.7) and using the distribution (6.1.3), in terms of the two displacement potentials, the surface stresses on the half-space are,

$$\begin{aligned} -2i\ \mu k^2\alpha\phi - \mu k^2(1+\beta^2)\psi &= \frac{H(x,y,t)}{l^2}, \\ \left((\lambda+2\mu)k^2\alpha^2 - \lambda k^2\right)\phi - 2i\ \mu k^2\beta\psi &= \frac{V(x,y,t)}{l^2}. \end{aligned} \tag{6.4.7}$$

Let u_H be expressed in displacement potentials as from (6.2.10) and $u_{V,x}$ as from (6.3.5). Then by substituting in the stresses from (6.4.3),

$$\left(2\mu k^2\alpha + \frac{\pi h_b^4}{64l^2}B_b k\left(K^3\eta - K^2 k\alpha\xi\right)\right)\left(2\mu k^2\beta + \frac{\pi h_b^2}{4l^2}B_b\left(K^2\beta\xi - Kk\zeta\right)\right) =$$

$$\left(\mu k^2\left(1+\beta^2\right) + \frac{\pi h_b^4}{64l^2}B_b k\left(K^3\beta\eta - K^2 k\xi\right)\right)$$
$$\left((\lambda+2\mu)k^2\alpha^2 - \lambda k^2 + \frac{\pi h_b^2}{4l^2}B_b\left(K^2\xi - Kk\alpha\zeta\right)\right) \tag{6.4.8}$$

As expected, this dispersion relation is significantly longer and more complicated than those obtained for the previous systems, and correspondingly more difficult to interpret. Again then, attempt to produce an accurate approximation using the asymptotic model.

The asymptotic model in Kaplunov and Prikazchikov [63] consists of two relations which each use a single surface stress to produce a wave. Since this system has two stresses, one of which is perpendicular and the other of which is parallel to the surface, the two relations must be combined to produce one wave from two stresses.

To do this, assume that each stress produces a wave and that these waves have the same wavelength and frequency, effectively behaving as one wave. These waves will each have a pair of displacement potentials, ψ_1 and ϕ_1, and ψ_2 and ϕ_2 such that the overall displacement potentials ϕ and ψ are given by,

$$\begin{aligned} \phi &= \phi_1 + \phi_2, \\ \psi &= \psi_1 + \psi_2. \end{aligned} \tag{6.4.9}$$

Each pair of potentials then corresponds to one of the surface relations from (2.2.25, 6.3.10),

$$\frac{\partial^2 \psi_1}{\partial z^2} - \frac{1}{c_R^2}\frac{\partial^2 \psi_1}{\partial t^2} = -\frac{1+\beta_R^2}{2\mu B l^2} H(x,y,t), \tag{6.4.10}$$

$$\frac{\partial^2 \psi_2}{\partial z^2} - \frac{1}{c_R^2}\frac{\partial^2 \psi_2}{\partial t^2} = -i\frac{\alpha_R}{\mu B l^2} V(x,y,t), \tag{6.4.11}$$

On assuming that the wave potentials are harmonic functions in the form (2.2.24), this manipulation can lead to a general expression for a multi stress system,

$$\frac{\partial^2 \psi}{\partial z^2} - \frac{1}{c_R^2}\frac{\partial^2 \psi}{\partial t^2} = -\frac{1+\beta_R^2}{2\mu B}\sigma_{31} - i\frac{\alpha_R}{\mu B}\sigma_{33}. \tag{6.4.12}$$

Taking u_H from (6.2.13) and $u_{V,x}$ from (6.3.11) then on substitution of the stresses from (6.4.3),

$$\begin{aligned} k^2 - \frac{\omega^2}{c_R^2} =& \frac{\alpha_R}{\mu B l^2}\frac{\pi h_b^2}{4} B_b \frac{K}{k}\left(k^2 \frac{1-\beta_R^2}{2}\,\zeta + Kk\beta_R \frac{1-\beta_R^2}{1+\beta_R^2}\,\xi\right) \\ & - \frac{1+\beta_R^2}{2\mu B l^2}\frac{\pi h_b^4}{64} B_b K^2 \left(k^2 \frac{1-\beta_R^2}{2}\,\xi + Kk\beta_R \frac{1-\beta_R^2}{1+\beta_R^2}\,\eta\right), \end{aligned} \tag{6.4.13}$$

which can be written as a quadratic equation in terms of k,

$$\begin{aligned} 0 =& k^2\left(1 + \frac{1+\beta_R^2}{2\mu B l^2}\frac{\pi h_b^4}{64} B_b K^2 \frac{1-\beta_R^2}{2}\,\xi\right) \\ & - k\left(\frac{\alpha_R}{\mu B l^2}\frac{\pi h_b^2}{4} B_b K \frac{1-\beta_R^2}{2}\,\zeta - \frac{1+\beta_R^2}{2\mu B l^2}\frac{\pi h_b^4}{64} B_b K^3 \beta_R \frac{1-\beta_R^2}{1+\beta_R^2}\,\eta\right) \\ & - \left(\frac{\omega^2}{c_R^2} + \frac{\alpha_R}{\mu B l^2}\frac{\pi h_b^2}{4} B_b K^2 \beta_R \frac{1-\beta_R^2}{1+\beta_R^2}\,\xi\right). \end{aligned} \tag{6.4.14}$$

As with the previous cases, this is a quadratic equation so the dispersion relation can be expressed explicitly in terms of k. While more difficult to interpret than the

simply supported asymptotic solution, it is still a great improvement on the full unimodal dispersion relation. To determine if this solution is valid, again compare the asymptotic and full unimodal solutions.

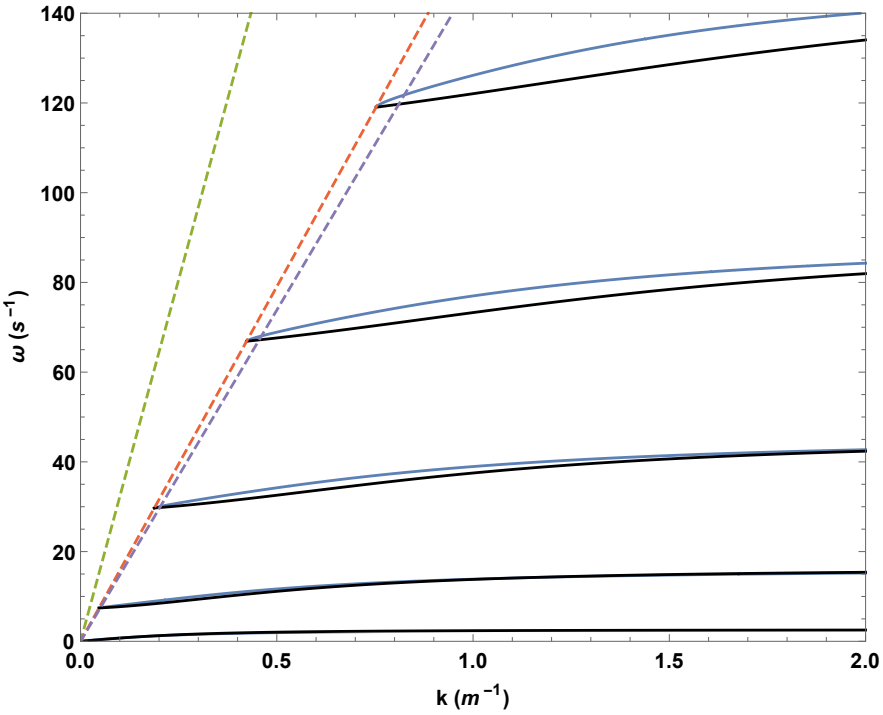

Figure 6.4: The dispersion curves for surface waves on the half-space coated with fully matched beam-like resonators, using physical parameters from Table 6.1. The solid blue lines show the dispersion curve of the full unimodal solution from (6.4.8) and the solid black lines the dispersion curve of the asymptotic solution from (6.4.13). The dashed green, orange and purple lines correspond to the longitudinal, shear and Rayleigh wave lines respectively.

From Fig. 6.4 the asymptotic model predicts the main features of the dispersion curves, including predicting the existence and general shape of the solution branch for each quasi periodic mode and also giving a close approximation of the intersections with the Rayleigh line. The key feature of the plot, and one present in both the asymptotic and full unimodal results, is the band gaps. This system is notable for the large range of frequencies which do not have a corresponding real wave number solution and will,

therefore, not propagate through the system. While it is difficult to locate where the band gaps are from the full unimodal dispersion relation, they can be approximated by the intersections between the asymptotic model and the shear wave line.

This system also highlights some of the limitations of this model. As previously mentioned and shown on Fig. 6.4, unlike for a single stress the asymptotics and the full unimodal solution are not guaranteed to intersect at the Rayleigh line. This is due to the way the stresses are treated in the two methods. In the asymptotic model there is no interaction between the two stresses and there will be Rayleigh line intersections only at,

$$(1+\beta_R^2)\sigma_{31} = 2i\ \alpha_R\ \sigma_{33}, \tag{6.4.15}$$

whereas for the full unimodal dispersion relation there is a cross multiplication of the two stress terms. This leads to a much more complicated condition for the stresses to cancel and for the solution to correspond with the Rayleigh solution. This can be shown by assuming that the two stresses have the form,

$$\begin{aligned} \sigma_{31} &= H_\phi\phi + H_\psi\psi, \\ \sigma_{33} &= V_\phi\phi + V_\psi\psi. \end{aligned} \tag{6.4.16}$$

Expanding these stresses as before yields,

$$-R(r) = i\frac{2\beta}{\mu k^2}H_\phi + \frac{1+\beta^2}{\mu k^2}H_\psi - \frac{1+\beta^2}{\mu k^2}V_\phi + i\frac{2\alpha}{\mu k^2}V_\psi + \frac{H_\phi V_\psi - V_\phi H_\psi}{\mu^2 k^4}. \tag{6.4.17}$$

If it is assumed that there will be a coincidence at the Rayleigh line, then at this point replace α and β with α_R and β_R and use the surface relation (2.2.22) to obtain,

$$-\left(k^2 - \frac{\omega^2}{c_R^2}\right)\psi = -\frac{1+\beta_R^2}{2\mu B}\sigma_{31} - i\frac{\alpha_R}{\mu B}\sigma_{33} + \frac{V_\phi H_\psi - H_\phi V_\psi}{2\mu^2 B k^2}\psi. \tag{6.4.18}$$

Clearly this equation is equivalent to the multi stress boundary condition (6.4.12) but with an added stress interaction term which the previous asymptotic model does not

predict. For this example take the surface stresses (6.4.3) and put them into the required form which yields,

$$\begin{aligned} H_\phi &= i\frac{\pi h_b^4}{64l^2}B_b K^2 k(K\eta - k\alpha\zeta), \qquad & H_\psi &= \frac{\pi h_b^4}{64l^2}B_b K^2 k(\beta K\eta - k\xi), \\ V_\phi &= \frac{\pi h_b^2}{4l^2}B_b K(k\alpha\zeta - K\xi), & V_\psi &= i\frac{\pi h_b^2}{4l^2}(\beta K\xi - k\zeta). \end{aligned} \tag{6.4.19}$$

Letting $\alpha = \alpha_R$ and $\beta = \beta_R$ and substituting these into the expansion (6.4.18) leads to the dispersion relation,

$$\begin{aligned} k^2 - \frac{\omega^2}{c_R^2} =& \frac{\alpha_R}{\mu B l^2}\frac{\pi h_b^2}{4}B_b\frac{K}{k}\left(k^2\frac{1-\beta_R^2}{2}\,\zeta + Kk\beta_R\frac{1-\beta_R^2}{1+\beta_R^2}\,\xi\right) \\ &- \frac{1+\beta_R^2}{2\mu B l^2}\frac{\pi h_b^4}{64}B_b K^2\left(k^2\frac{1-\beta_R^2}{2}\,\xi + Kk\beta_R\frac{1-\beta_R^2}{1+\beta_R^2}\,\eta\right) \\ &- \frac{\pi h^6}{256l^4}\frac{B_b^2K^3}{2\mu^2 k}\left((k\alpha_R\zeta - K\xi)(\beta_R K\eta - k\xi) + (\beta_R K\xi - k\zeta)(K\eta - k\alpha_R\zeta)\right), \end{aligned} \tag{6.4.20}$$

which is the same as (6.4.13) but with an added term from the stress interaction. Due to cancellation in the stress interaction term this dispersion relation is also a quadratic, but even for simple stresses in a general case this new equation could be up to a 4th order polynomial. This can be plotted against the full unimodal solution to determine if the stress interaction makes a significant difference to the solution. As predicted Fig. 6.5 shows that accounting for the stress interaction forces the model to coincide with the full unimodal dispersion relation at the Rayleigh line. However a comparison with the asymptotic dispersion relation in Fig. 6.2 does not show a significant improvement for the rest of the plot over the standard asymptotic model. This indicates that for this system the stress interaction does not have a significant effect on the overall behaviour of the waves.

The stress interaction problem also indicates a more fundamental and significant possible limitation with using this model on a multi stress system. The asymptotic model requires both stresses to be small for the combined result to be an accurate

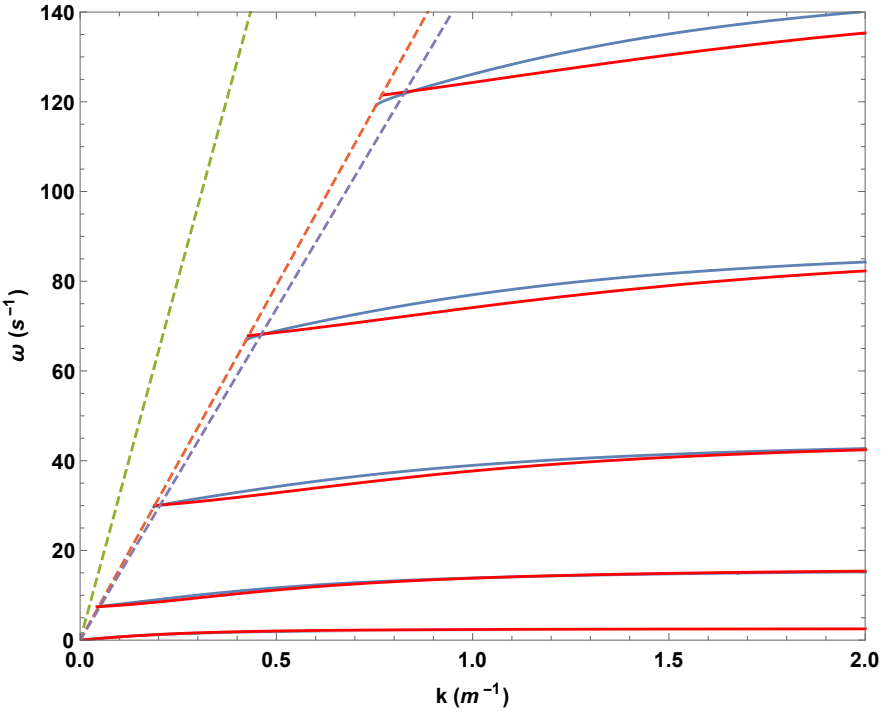

Figure 6.5: The dispersion curves for surface waves on the half-space coated with fully matched beam-like resonators, using physical parameters from Table 6.1. The solid blue lines show the dispersion curve of the full unimodal solution from (6.4.8) and the solid red lines the dispersion curve of the asymptotic solution with stress interaction term from (6.4.20). The dashed green, orange and purple lines correspond to the longitudinal, shear and Rayleigh wave lines respectively.

approximation. If one stress is always large while the other is small then the asymptotic model cannot be valid, even if the result crosses the Rayleigh line.

Finally, much of the behaviour of the dispersion curve is away from the Rayleigh line, where the asymptotic model cannot accurately predict. For example, instead of predicting asymptotes at,

$$\cos(KL)\cosh(KL) + 1 = 0, \tag{6.4.21}$$

the asymptotic model instead produces asymptotes at,

$$-\frac{1+\beta_R^2}{2\mu B l^2}\frac{\pi h_b^4}{64}B_b K^2\frac{1-\beta_R^2}{2}\ \sin(KL)\sinh(KL) = \cos(KL)\cosh(KL) + 1. \tag{6.4.22}$$

This is notable as the asymptotes for a simply supported beam and a beam on a rail were predicted by the asymptotic model. This led to the asymptotic model for that system remaining accurate to a good degree even while away from the Rayleigh line. For the fully matched system however, at some point away from the Rayleigh line the full unimodal solution and the asymptotics must significantly diverge.

Therefore, while this is a powerful technique for when both stresses are small the results cannot be relied upon away from this condition.

6.5 Vertical Beam Metasurface Conclusions

An array of flexural resonators attached to the surface of an elastic half-space is analysed using an explicit model for the Rayleigh wave. This chapter generalises previous considerations using both full unimodal and asymptotic solutions for an elastic half-space in the case of a longitudinal array of resonating rods [25]. The considered bending array appears to be a better model for a number of applications including, but not limited to, modelling of forests.

Three types of boundary conditions are considered, and for each the asymptotic solution is verified using full unimodal solutions for the half-space. The first boundary condition to be considered treats the resonators as simply supported at the surface of the half-space. Matching of the beam equation yields a horizontal stress only. The second considered boundary condition treats the resonators as being supported by a freely moving rail at the surface of the half-space. In contrast to the previous system this yields a vertical stress only.

For both of these boundary conditions the asymptotic formulation closely matches with the full unimodal solution. The asymptotic solution obtained predicts both a

coincidence with the full unimodal solution at the Rayleigh line, and also quasi-periodic resonances arising from the solution to the beam equation.

The final boundary condition considered in this paper fully matches all variables at the boundary. Unlike the previous two cases this results in both a vertical stress and a horizontal stress, requiring an alteration to the existing asymptotic formulation to account for both stresses. While this asymptotic solution closely matches with the full unimodal solution it does not accurately predict the coincidence with the Rayleigh line or the location of the system resonances. A further addition to the asymptotic model produces a solution which does accurately predict coincidence with the full unimodal solution with the Rayleigh line, but still does not accurately predict resonances.

All of the systems considered produce band gaps in the region around the beam resonances, with the largest band gaps produced by the beam on a rail and fully matched boundary conditions. This demonstrates the potential for such systems to be utilised in controlling the propagation of surface waves.

The explicit asymptotic formulation has the potential to be applied in more sophisticated systems where an exact solution may be difficult or impossible to obtain since it reduces the vector problem in full linear elasticity to a scalar problem along the surface. It has been shown that for the systems in this paper the asymptotic formulation easily produces simple explicit solutions which match closely with the full unimodal solution.

The formulation discussed involves a surface scalar problem identical to the equation for transverse forces applied to an elastic membrane. Currently, experimental setups to model elastic half-spaces can be large and expensive and this formulation gives scope for simpler experiments on membranes which model the behaviour at the surface of an elastic half-space.

CHAPTER 7

Second Order Rayleigh Wave Asymptotics

Previous chapters have made extensive use of a leading order asymptotic model for the surface of an elastic half plane, from Kaplunov and Prikazchikov [63] detailed in §2.2.3. While this model has been used effectively in multiple situations, the treatment of flexural resonators in Chapter 5 shows that this model does have limitations. To ensure that this asymptotic model remains valid as the complexity of problems increases it is necessary to consider further development of the model. In this chapter the same method used to produce the leading order asymptotic model is used to add a second order term and introduce a new combined model.

This chapter shall be arranged as follows: First the results of the leading order expansion for surface waves on an elastic half plane from Kaplunov and Prikazchikov [63] will be described, followed by the derivation for a second order model which will add an additional term to the existing model. This new model will then be applied to a variety of simple problems on which the leading order asymptotic model has already been applied. The results from our new model will be compared directly with both the solution from the leading order asymptotic model and with either an exact or full unimodal solution. The first problem considered will be a simple 2D harmonic forcing. This will be followed by considering a moving point load along the surface. Finally a

system consisting of vertical rod-like resonators periodically embedded into the surface of the half plane originally from Colquitt et al. [25] will be considered, followed by a final conclusion and discussion of the results.

7.1 Perturbed Governing Equations

First, follow the approach from Kaplunov and Prikazchikov [63] to find perturbed Rayleigh wave solutions. For generality, adopt 3D Cartesian coordinates of the form (x_1, x_2, x_3) where the surface of the half plane is at $x_3 = 0$. For ease of use, use the standard subscript notation for derivatives such that the standard equations of elasticity (2.2.5) take the form,

$$\begin{aligned} \phi_{,11} + \phi_{,33} - \frac{1}{c_1^2}\phi_{,tt} = 0, \\ \psi_{,11} + \psi_{,33} - \frac{1}{c_2^2}\psi_{,tt} = 0 \end{aligned} \tag{7.1.1}$$

with surface conditions (2.2.7) at $x_3 = 0$ in the form,

$$\begin{aligned} 2\phi_{,13} + \psi_{,11} - \psi_{,33} = \frac{Q}{\mu}, \\ (\kappa^{-2} - 2)\phi_{,11} + \kappa^{-2}\phi_{,33} + 2\psi_{,13} = \frac{P}{\mu}. \end{aligned} \tag{7.1.2}$$

where $\kappa = c_2/c_1$ and Q and P represent some horizontal and vertical surface loading respectively. Suppose that ϕ and ψ can be asymptotically expanded into the infinite series,

$$\phi = \epsilon^{-1}\phi_0 + \phi_1 + \epsilon\phi_2 + \epsilon^2\phi_3 + ..., \quad \psi = \epsilon^{-1}\psi_0 + \psi_1 + \epsilon\psi_2 + \epsilon^2\psi_3 + ..., \tag{7.1.3}$$

where the small parameter $0 < \epsilon \ll 1$ is given by,

$$c = c_R(1 \pm \epsilon). \tag{7.1.4}$$

where c is the phase velocity of the perturbed wave solution. Using a multiple scales approach in the usual way, define new fast time and slow time variables, τ_f and τ_s

respectively such that,

$$\tau_f = t, \qquad \tau_s = \epsilon t, \tag{7.1.5}$$

leading to the operator identity,

$$\frac{\partial}{\partial t} = \frac{\partial}{\partial \tau_f} + \epsilon \frac{\partial}{\partial \tau_s}. \tag{7.1.6}$$

Using this operator relation to perturb the bulk equations (7.1.1) yields,

$$\begin{aligned} \phi_{,33} + \alpha_R^2 \phi_{,11} - 2\frac{\epsilon}{c_1^2}\phi_{,\tau_f\tau_s} - \frac{\epsilon^2}{c_1^2}\phi_{,\tau_s\tau_s} = 0, \\ \psi_{,33} + \beta_R^2 \psi_{,11} - 2\frac{\epsilon}{c_2^2}\psi_{,\tau_f\tau_s} - \frac{\epsilon^2}{c_2^2}\psi_{,\tau_s\tau_s} = 0. \end{aligned} \tag{7.1.7}$$

The derivation for the leading order term of this asymptotic expansion is given in §A.2.

7.2 Second Order Asymptotic Model

We now intend to use the same method to produce a higher order asymptotic model. Suppose that ϕ and ψ have the three term asymptotic expansions,

$$\phi = \epsilon^{-1}\phi_0 + \phi_1 + \epsilon\phi_2, \quad \psi = \epsilon^{-1}\psi_0 + \psi_1 + \epsilon\psi_2, \tag{7.2.1}$$

We shall first complete the asymptotic treatment for a vertical stress only so let $Q = 0$, $P = O(1)$. Assume the solution for ϕ_0 (A.2.20) and relations for the first order non-homogeneous ϕ and ψ terms (A.2.15) from §A.2. Also assume that ϕ and ψ are related as a single plane harmonic function [14]. Taking the perturbed bulk equations (7.1.7) at $O(\epsilon)$,

$$\begin{aligned} \phi_{2,33} + \alpha_R^2 \phi_{2,11} - \frac{2}{c_1^2}\phi_{1,\tau_f\tau_s} - \frac{1}{c_1^2}\phi_{0,\tau_s\tau_s} = 0, \\ \psi_{2,33} + \beta_R^2 \psi_{2,11} - \frac{2}{c_2^2}\psi_{1,\tau_f\tau_s} - \frac{1}{c_2^2}\psi_{0,\tau_s\tau_s} = 0. \end{aligned} \tag{7.2.2}$$

Supposing that the second order term solutions have the form,

$$\begin{aligned} \phi_2 = \phi_{20} + x_3\phi_{21} + x_3^2\phi_{22}, \\ \psi_2 = \psi_{20} + x_3\psi_{21} + x_3^2\psi_{22}, \end{aligned} \tag{7.2.3}$$

where ϕ_{20} and ψ_{20} are the complementary solution and $x_3\phi_{21} + x_3^2\phi_{22},\ x_3\psi_{21} + x_3^2\psi_{22}$ are the particular integrals. Then it follows by substitution that,

$$2\phi_{21,3} + 2\phi_{22} + 4x_3\phi_{22,3} = \frac{2}{c_1^2}(\phi_{01,\tau_f\tau_s} + x_3\phi_{11,\tau_f\tau_s}) + \frac{1}{c_1^2}\phi_{0,\tau_s\tau_s}, \tag{7.2.4}$$

$$2\psi_{21,3} + 2\psi_{22} + 4x_3\psi_{22,3} = \frac{2}{c_2^2}(\psi_{01,\tau_f\tau_s} + x_3\psi_{11,\tau_f\tau_s}) + \frac{1}{c_2^2}\psi_{0,\tau_s\tau_s}, \tag{7.2.5}$$

Matching coefficients in the usual way,

$$2\phi_{22,311} = \frac{1}{c_1^2}\phi_{11,11\tau_f\tau_s}, \qquad 2\phi_{21,3} + 2\phi_{22} = \frac{2}{c_1^2}\phi_{10,\tau_f\tau_s} + \frac{1}{c_1^2}\phi_{0,\tau_s\tau_s}, \tag{7.2.6}$$

$$2\psi_{22,311} = \frac{1}{c_2^2}\psi_{11,11\tau_f\tau_s}, \qquad 2\psi_{21,3} + 2\psi_{22} = \frac{2}{c_2^2}\psi_{10,\tau_f\tau_s} + \frac{1}{c_2^2}\psi_{0,\tau_s\tau_s}. \tag{7.2.7}$$

Using the relations (A.2.15) from above yields,

$$2\phi_{22,311} = -\frac{1}{\alpha_R^2 c_1^4}\phi_{0,3\tau_f\tau_f\tau_s\tau_s}, \qquad 2\psi_{22,311} = -\frac{1}{\beta_R^2 c_2^4}\psi_{0,3\tau_f\tau_f\tau_s\tau_s}. \tag{7.2.8}$$

If it is assumed that the forcing produces a near-Rayleigh travelling surface wave then the fast time variable must correspond to the Rayleigh wave speed with the slow time acting as an $O(\epsilon)$ correction. Hence, introduce the travelling wave ansatz,

$$\frac{\partial^2}{\partial\tau_f^2} = c_R^2\frac{\partial^2}{\partial x_1^2}, \tag{7.2.9}$$

which gives on substitution,

$$2\phi_{22} = -\frac{c_R^2}{\alpha_R^2 c_1^4}\phi_{0,\tau_s\tau_s}, \qquad 2\psi_{22} = -\frac{c_R^2}{\beta_R^2 c_2^4}\psi_{0,\tau_s\tau_s}, \tag{7.2.10}$$

and so,

$$2\phi_{21,3} = \frac{2}{c_1^2}\phi_{10,\tau_f\tau_s} + \frac{1}{\alpha_R^2 c_1^2}\phi_{0,\tau_s\tau_s}, \tag{7.2.11}$$

$$2\psi_{21,3} = \frac{2}{c_2^2}\psi_{10,\tau_f\tau_s} + \frac{1}{\beta_R^2 c_2^2}\psi_{0,\tau_s\tau_s}. \tag{7.2.12}$$

Then by using the relations for harmonic functions,

$$2\phi_{21,1} = \frac{2}{\alpha_R c_1^2}\phi^*_{10,\tau_f\tau_s} + \frac{1}{\alpha_R^3 c_1^2}\phi^*_{0,\tau_s\tau_s}, \tag{7.2.13}$$

$$2\psi_{21,1} = \frac{2}{\beta_R c_2^2}\psi^*_{10,\tau_f\tau_s} + \frac{1}{\beta_R^3 c_2^2}\psi^*_{0,\tau_s\tau_s}. \tag{7.2.14}$$

Substituting the second order expansions for ϕ and ψ into the boundary conditions and setting $x_3 = 0$ gives,

$$\begin{aligned} 2\phi_{20,13} + (1+\beta_R^2)\psi_{20,11} &= -2\phi_{21,1} + 2\psi_{21,3} + 2\psi_{22}, \\ -(1+\beta_R^2)\phi_{20,11} + 2\psi_{20,13} &= -2\frac{1-\beta_R^2}{1-\alpha_R^2}(\phi_{21,3} + \phi_{22}) - 2\psi_{21,1}. \end{aligned} \tag{7.2.15}$$

On substituting the above relations for harmonic functions, these yield,

$$2\phi_{20,13} + (1+\beta_R^2)\psi_{20,11} = \frac{2}{c_2^2}\psi_{10,\tau_f\tau_s} + \frac{1}{c_2^2}\psi_{0,\tau_s\tau_s} - \frac{2}{\alpha_R c_1^2}\phi^*_{10,\tau_f\tau_s} - \frac{1}{\alpha_R^3 c_1^2}\phi^*_{0,\tau_s\tau_s}, \tag{7.2.16}$$

$$2\phi^*_{20,13} + (1+\beta_R^2)\psi^*_{20,11} = \frac{2}{c_2^2}\psi^*_{10,\tau_f\tau_s} + \frac{1}{c_2^2}\psi^*_{0,\tau_s\tau_s} + \frac{2}{\alpha_R c_1^2}\phi_{10,\tau_f\tau_s} + \frac{1}{\alpha_R^3 c_1^2}\phi_{0,\tau_s\tau_s}, \tag{7.2.17}$$

and,

$$-(1+\beta_R^2)\phi_{20,11} + 2\psi_{20,13} = -\frac{1-\beta_R^2}{1-\alpha_R^2}\left(\frac{2}{c_1^2}\phi_{10,\tau_f\tau_s} + \frac{1}{c_1^2}\phi_{0,\tau_s\tau_s}\right) - \frac{2}{\beta_R c_2^2}\psi^*_{10,\tau_f\tau_s} - \frac{1}{\beta_R^3 c_2^2}\psi^*_{0,\tau_s\tau_s}. \tag{7.2.18}$$

Then use the leading order relations (A.2.18) to find a relation for ψ^*_{10} in terms of ϕ_0 and ϕ_{10},

$$\psi^*_{10,11} = -\frac{2\alpha_R}{1+\beta_R^2}\phi_{10,11} + \left(\frac{2}{(1+\beta_R^2)\alpha_R c_1^2} - \frac{1}{\beta_R c_2^2}\right)\phi_{0,\tau_f\tau_s}, \tag{7.2.19}$$

and using the travelling wave ansatz (7.2.9) this becomes,

$$\psi^*_{10,\tau_f\tau_s} = -\frac{2\alpha_R}{1+\beta_R^2}\phi_{10,\tau_f\tau_s} + \left(\frac{2c_R^2}{(1+\beta_R^2)\alpha_R c_1^2} - \frac{c_R^2}{\beta_R c_2^2}\right)\phi_{0,\tau_s\tau_s}, \tag{7.2.20}$$

Then by taking advantage of relations between harmonic functions,

$$\begin{aligned} 2\alpha_R\phi_{20,11} + (1+\beta_R^2)\psi^*_{20,11} = &\left(\frac{2\alpha_R}{1+\beta_R^2}\right)\left(\frac{1+\beta_R^2}{\alpha_R^2 c_1^2} - \frac{2}{c_2^2}\right)\phi_{10,\tau_f\tau_s} \\ &+ \left(\frac{2\alpha_R}{1+\beta_R^2}\right)\left(\left(\frac{1+\beta_R^2}{2\alpha_R^4} + \frac{1-\beta_R^2}{\alpha_R^2}\right)\frac{1}{c_1^2} - \left(4\frac{1-\beta_R^2}{1+\beta_R^2} + 1\right)\frac{1}{c_2^2}\right)\phi_{0,\tau_s\tau_s} \end{aligned} \tag{7.2.21}$$

$$\begin{aligned} -(1+\beta_R^2)\phi_{20,11} + 2\psi_{20,13} = &-\left(\frac{2}{c_2^2} - \frac{1+\beta_R^2}{\beta_R^2 c_2^2}\right)\phi_{10,\tau_f\tau_s} \\ &- \left(\frac{1}{c_2^2} + 4\frac{1-\alpha_R^2}{(1+\beta_R^2)\alpha_R\beta_R c_2^2} - 2\frac{1-\beta_R^2}{\beta_R^2 c_2^2} - \frac{1+\beta_R^2}{2\beta_R^4 c_2^2}\right)\phi_{0,\tau_s\tau_s} \end{aligned} \tag{7.2.22}$$

This system of equations can be expressed as,

$$\begin{aligned} 2\alpha_R\phi_{20,11} + (1+\beta_R^2)\psi^*_{20,11} &= \left(\frac{2\alpha_R}{1+\beta_R^2}\right)\left(a\phi_{0,\tau_s\tau_s} + b\phi_{10,\tau_f\tau_s}\right), \\ -(1+\beta_R^2)\phi_{20,11} - 2\beta_R\psi^*_{20,11} &= -\left(c\phi_{0,\tau_s\tau_s} + d\phi_{10,\tau_f\tau_s}\right), \end{aligned} \tag{7.2.23}$$

where,

$$\begin{aligned} a &= \left(\frac{1+\beta_R^2}{2\alpha_R^4} + \frac{1-\beta_R^2}{\alpha_R^2}\right)\frac{1}{c_1^2} - \left(4\frac{1-\beta_R^2}{1+\beta_R^2} + 1\right)\frac{1}{c_2^2}, \qquad b = \frac{1+\beta_R^2}{\alpha_R^2 c_1^2} - \frac{2}{c_2^2}, \\ c &= \frac{1}{c_2^2} + 4\frac{1-\alpha_R^2}{(1+\beta_R^2)\alpha_R\beta_R c_2^2} - 2\frac{1-\beta_R^2}{\beta_R^2 c_2^2} - \frac{1+\beta_R^2}{2\beta_R^4 c_2^2}, \qquad d = \frac{2}{c_2^2} - \frac{1+\beta_R^2}{\beta_R^2 c_2^2}. \end{aligned} \tag{7.2.24}$$

Using the Rayleigh identity, this system of equations can then be simplified to,

$$c\phi_{0,\tau_s\tau_s} + d\phi_{10,\tau_f\tau_s} = a\phi_{0,\tau_s\tau_s} + b\phi_{10,\tau_f\tau_s} \tag{7.2.25}$$

which leads to the relation for the second order component of ϕ,

$$\phi_{10,\tau_f\tau_s} = \frac{a-c}{d-b}\phi_{0,\tau_s\tau_s}, \tag{7.2.26}$$

$$= \Gamma_R\ \phi_{0,\tau_s\tau_s}, \tag{7.2.27}$$

where Γ_R can be significantly simplified as,

$$\Gamma_R = 2\frac{1-\beta_R^2}{1+\beta_R^2} - \frac{1}{2} + \frac{1}{2B}\left(2(1-\beta_R^2)^2 + \frac{(\alpha_R^2-\beta_R^2)^2}{\alpha_R^3\beta_R^3}\right), \tag{7.2.28}$$

which is plotted in Fig [7.1] for varying values of the Poisson ratio, ν.

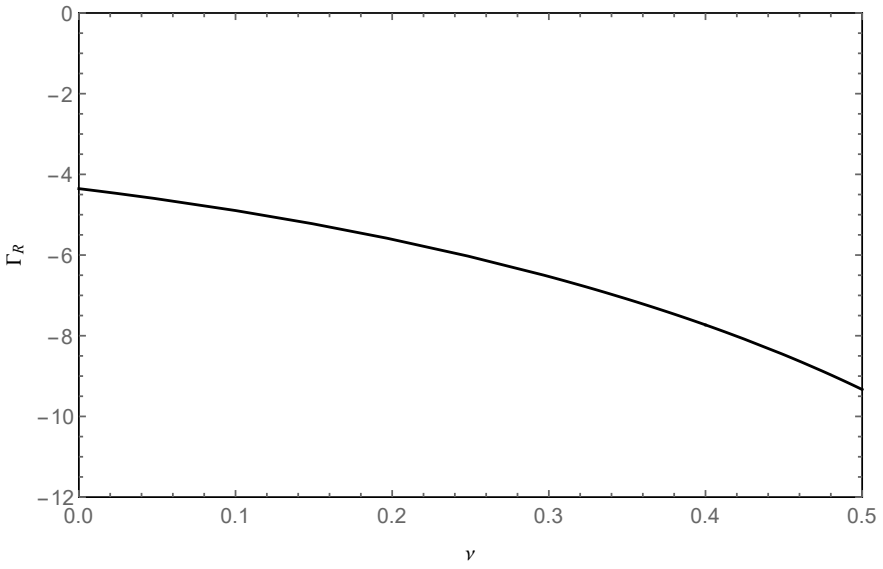

Figure 7.1: The values for Γ_R (7.2.28) for varying Poisson ratio ν.

To obtain a general relation for ϕ, combine the second order relation (7.2.27) and the leading order relation (A.2.20) to produce,

$$2\epsilon\phi_{,\tau_f\tau_f\tau_f\tau_s} = -c_R^2\frac{1+\beta_R^2}{2\mu B}\left(P_{,\tau_f\tau_f} + \epsilon\Gamma_R P_{\tau_f\tau_s}\right). \tag{7.2.29}$$

Then it follows from the operator relationship (7.1.6) that,

$$2\epsilon\frac{\partial^2}{\partial\tau_f\partial\tau_s} = \frac{\partial^2}{\partial t^2} - \frac{\partial^2}{\partial\tau_f^2} - \epsilon^2\frac{\partial^2}{\partial\tau_s^2}, \tag{7.2.30}$$

$$= \frac{\partial^2}{\partial t^2} - c_R^2\frac{\partial^2}{\partial x_1^2} - \epsilon^2\frac{\partial^2}{\partial\tau_s^2}, \tag{7.2.31}$$

$$= -c_R^2\Box - \epsilon^2\frac{\partial^2}{\partial\tau_s^2}. \tag{7.2.32}$$

where the D'Alambertian operator, $\Box$, is defined as

$$\Box = \frac{\partial^2}{\partial x_1^2} - \frac{1}{c_R^2}\frac{\partial^2}{\partial t^2}. \tag{7.2.33}$$

This gives,

$$\Box\phi = \frac{1+\beta_R^2}{2\mu B}P - \frac{\epsilon^2}{c_R^2}(2\Gamma_R+1)\phi_{,\tau_s\tau_s} + 2\frac{\epsilon^3}{c_R^2}\Gamma_R\phi_{10,\tau_s\tau_s}, \tag{7.2.34}$$

$$\Box\phi_{,\tau_f\tau_f} = \frac{1+\beta_R^2}{2\mu B}P_{,\tau_f\tau_f} - \frac{\epsilon^2}{c_R^2}(2\Gamma_R+1)\phi_{,\tau_f\tau_f\tau_s\tau_s} + 2\frac{\epsilon^3}{c_R^2}\Gamma_R\phi_{10,\tau_f\tau_f\tau_s\tau_s}, \tag{7.2.35}$$

and the $O(\epsilon^2)$ term can be expanded using the operator relation,

$$\frac{\epsilon^2}{c_R^4}\phi_{\tau_f\tau_f\tau_s\tau_s} = \frac{\epsilon}{2}\left(\frac{2\epsilon}{c_R^2}\phi_{0,\tau_f\tau_f\tau_s\tau_s}\right) + O(\epsilon^3) \tag{7.2.36}$$

$$= \frac{1+\beta_R^2}{8\mu B}\left(c_R^2\Box P + \epsilon^2 P_{,\tau_s\tau_s}\right) + O(\epsilon^3) \tag{7.2.37}$$

so on neglecting the remaining $O(\epsilon^2)$ terms, these can be combined using the travelling wave ansatz (7.2.9) to give,

$$\Box\phi_{,11} = \frac{1+\beta_R^2}{2\mu B}P_{,11} + \frac{\Gamma_R}{2}\frac{1+\beta_R^2}{2\mu B}\Box P \tag{7.2.38}$$

$$= \frac{1+\beta_R^2}{2\mu B}\left(P_{,11} + \frac{2\Gamma_R+1}{4}\Box P\right) \tag{7.2.39}$$

and on repeating the process in a similar fashion for a horizontal load,

$$\Box\psi_{,11} = -\frac{1+\beta_R^2}{2\mu B}\left(Q_{,11} + \frac{2\Gamma_R+1}{4}\Box Q\right). \tag{7.2.40}$$

From the definition of Γ_R (7.2.28),

$$\frac{2\Gamma_R+1}{4} = \frac{1-\beta_R^2}{1+\beta_R^2} + \frac{1}{4B}\left(2(1-\beta_R^2)^2 + \frac{(\alpha_R^2-\beta_R^2)^2}{\alpha_R^3\beta_R^3}\right). \tag{7.2.41}$$

We can verify this using a Taylor expansion around the Rayleigh solution. If the Rayleigh determinant is expressed as a function of $r = c^2/c_2^2$,

$$R(r) = (2-r)^2 - 4\sqrt{1-r}\sqrt{1-\kappa^2 r} \tag{7.2.42}$$

which has Taylor expansion around the Rayleigh solution $r_0 = c_R^2/c_2^2$,

$$R(r) \approx R(r_0) + R'(r_0)(r-r_0) + \frac{1}{2}R''(r_0)(r-r_0)^2 + ... \tag{7.2.43}$$

These derivatives are,

$$R'(r) = 2(r-2) + 2\frac{\kappa^2(1-r)+(1-\kappa^2 r)}{\sqrt{1-r}\sqrt{1-\kappa^2 r}}, \tag{7.2.44}$$

$$R''(r) = 2 + \frac{(1-\kappa^2)^2}{(\sqrt{1-r}\sqrt{1-\kappa^2 r})^3} \tag{7.2.45}$$

and it is clear that,

$$(r-r_0) = -r_0\left(1-\frac{r}{r_0}\right) = -(1-\beta_R^2)\left(1-\frac{c^2}{c_R^2}\right). \tag{7.2.46}$$

so for each term of the Taylor series. By definition the leading order term is given by,

$$R(r_0) = 0, \tag{7.2.47}$$

which as expected represents a solution $R(r) = 0$ at $c = c_R$. The next order term is given by,

$$R'(r_0)(r-r_0) = \left(2(2-r_0) - 2\frac{\kappa^2 r_0(1-r_0)+(1-\kappa^2 r_0)r_0}{\sqrt{1-r_0}\sqrt{1-\kappa^2 r_0}}\right)\left(1-\frac{c^2}{c_R^2}\right), \tag{7.2.48}$$

$$= -2B\left(1-\frac{c^2}{c_R^2}\right), \tag{7.2.49}$$

which is the same behaviour as the leading order model. The second order term then takes the form,

$$\frac{1}{2}R''(r_0)(r-r_0)^2 = \left(r_0^2 + \frac{(r_0-\kappa^2 r_0)^2}{2(\sqrt{1-r_0}\sqrt{1-\kappa^2 r_0})^3}\right)\left(1-\frac{c^2}{c_R^2}\right)^2, \tag{7.2.50}$$

$$= \left((1-\beta_R^2)^2 + \frac{(\alpha_R^2-\beta_R^2)^2}{2\alpha_R^3\beta_R^3}\right)\left(1-\frac{c^2}{c_R^2}\right)^2. \tag{7.2.51}$$

On combining these expressions we produce the Taylor series,

$$R(r) \approx -2B\left(1-\frac{c^2}{c_R^2}\right)\left(1-\frac{1}{4B}\left(2(1-\beta_R^2)^2 + \frac{(\alpha_R^2-\beta_R^2)^2}{\alpha_R^3\beta_R^3}\right)\left(1-\frac{c^2}{c_R^2}\right)\right), \tag{7.2.52}$$

which can then be substituted into the previous boundary conditions along the surface. In the case of a vertical stress only,

$$R(r) = -\frac{1+\beta^2}{\mu k^2}P, \tag{7.2.53}$$

$$1-\frac{c^2}{c_R^2} \approx \frac{1+\beta^2}{2\mu B k^2}\left(1-\frac{1}{4B}\left(2(1-\beta_R^2)^2 + \frac{(\alpha_R^2-\beta_R^2)^2}{\alpha_R^3\beta_R^3}\right)\left(1-\frac{c^2}{c_R^2}\right)\right)^{-1}P, \tag{7.2.54}$$

$$\approx \frac{1+\beta_R^2}{2\mu B k^2}\left(1+\left(\frac{1-\beta_R^2}{1+\beta_R^2}+\frac{1}{4B}\left(2(1-\beta_R^2)^2 + \frac{(\alpha_R^2-\beta_R^2)^2}{\alpha_R^3\beta_R^3}\right)\right)\left(1-\frac{c^2}{c_R^2}\right)\right)P. \tag{7.2.55}$$

This clearly has the same form as the boundary condition obtained above (7.2.39), and by rearranging, the coefficient from the Taylor series matches exactly with the coefficient from the asymptotic expansion (7.2.41).

7.3 Example Problems

In order to verify that this second order model is valid, we shall next consider three different fundamental types of forcing along the surface and see how the solution obtained from the newly obtained model compares with the result from the previous leading order model and the exact solution. For each, it is expected that the second order model will closely match the exact solution in the vicinity of wave speeds close

to the Rayleigh solution and will, in general, be more accurate than the leading order solution.

7.3.1 2D Harmonic Forcing

As in Kaplunov et al. [63], introduce a vertical load of constant amplitude,

$$P = P_0 e^{ik[x_1 - ct]}, \tag{7.3.1}$$

where k is the wave number and as before c is the wave speed. For this forcing the exact solution for ϕ is given by,

$$\phi = \frac{P_0(1+\beta^2)}{\mu k^2 R(c)} e^{ik[x_1 - ct] - k\alpha x_3}, \tag{7.3.2}$$

with

$$R(c) = (1+\beta^2)^2 - 4\alpha\beta. \tag{7.3.3}$$

If we define the wave speed by $c = (1+\varepsilon)c_R$ then $c^2 - c_R^2 = 2\varepsilon c_R^2 + \varepsilon^2$ and the leading order asymptotic solution is hence given by,

$$\phi = \frac{P_0(1+\beta_R^2)}{2(2\varepsilon+\varepsilon^2)\mu B k^2} e^{ik[x_1 - ct] - k\alpha_R x_3}. \tag{7.3.4}$$

We shall repeat the same procedure but use our newly derived second order model (7.2.39), which yields,

$$\phi = \frac{P_0(1+\beta_R^2)}{2(2\varepsilon+\varepsilon^2)\mu B k^2} \left(1 + \frac{2\Gamma_R + 1}{2}\epsilon\right) e^{i[kx_1 - ct] - k\alpha_R x_3}. \tag{7.3.5}$$

It is clear to see that this result is the same as that obtained with the leading order mode l but with an $O(\varepsilon)$ correction term. To compare the previously obtained results from Kaplunov et al. with that of our new second order model, introduce the scaled potential,

$$\phi_s = \frac{(2\varepsilon+\varepsilon^2)\mu k^2}{2P_0} e^{-ik[x_1 - ct]} \phi(x_1, 0, t). \tag{7.3.6}$$

where Fig. 7.2 shows the plots of ϕ_s for both asymptotic models and the exact solution near the Rayleigh speed

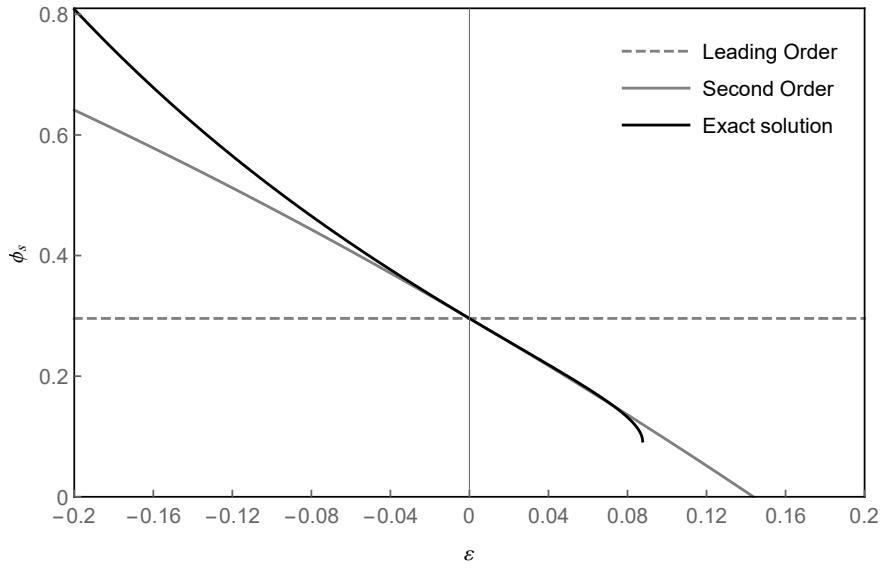

Figure 7.2: A comparison of the leading and second order asymptotic models with the exact solution for the scaled potential ϕ_s near the Rayleigh speed. Here the leading order and second order asymptotic solutions correspond to the dashed grey and solid grey lines respectively and the exact solution is denoted by the solid black line.

From this figure the improvement of the second order model is clear; while both asymptotic models match exactly with the exact solution at $\varepsilon = 0$, the second order model stays close to the exact solution for a remarkably wide range of wave speeds. It does not however model the mode conversion of the exact solution, where the travelling surface wave solution becomes evanescent and begins to decay along the surface. This is due to treating α and β as fixed constants. In the exact solution as c increases α and β become purely imaginary and the wave propagates into the bulk, a behaviour the asymptotic model cannot replicate.

7.3.2 Plane Strain Steady-State Problem

Since we have shown that the above model is valid for a static harmonic load, we shall next move to modelling the effects of a moving load. As with before we will make use of a system given by Kaplunov et al. [63], in this instance considering a point vertical load moving at constant speed, c. Using the delta function to represent the point forcing, this load is given by $P = P_0\delta(x_1 - ct)$ along $x_3 = 0$. From Kaplunov et al., introduce a moving coordinate system $s = x_1 - ct$ such that

$$\frac{\partial^2}{\partial x_1^2} = \frac{\partial^2}{\partial s^2}, \qquad \Box = (1 - c^2)\frac{\partial^2}{\partial s^2}, \tag{7.3.7}$$

for which the leading order asymptotics yields,

$$\phi_{,ss}(s, 0) = \frac{1 + \beta_R^2}{2\mu B}\frac{c_R^2}{c_R^2 - c^2}P_0\delta(s), \tag{7.3.8}$$

and so instead at second order,

$$\phi_{,ss}(s, 0) = \frac{1 + \beta_R^2}{2\mu B}\left(\frac{c_R^2}{c_R^2 - c^2} + \frac{2\Gamma_R + 1}{4}\right)P_0\delta(s). \tag{7.3.9}$$

This retains the key properties of the leading order solution, most notably the resonance at $c = c_R$. This form makes the change from the leading order to the second order model solution relatively straightforward as for constant c, the second order correction acts as a constant multiplicative factor. For instance, where in Kaplunov et al., the leading order displacement potentials were found to be,

$$\phi_{,s}(s, x_3) = \frac{1 + \beta_R^2}{2\pi\mu B}\frac{c_R^2}{c_R^2 - c^2}P_0 \tan^{-1}\left(\frac{s}{\alpha_R x_3}\right), \tag{7.3.10}$$

$$\psi_{,s}(s, x_3) = -\frac{\alpha_R}{4\pi\mu B}\frac{c_R^2}{c_R^2 - c^2}P_0 \ln\,(s^2 + \beta_R^2 x_3^2), \tag{7.3.11}$$

from the second order model we instead yield,

$$\phi_{,s}(s, x_3) = \frac{1 + \beta_R^2}{2\pi\mu B}\left(\frac{c_R^2}{c_R^2 - c^2} - \frac{2\Gamma_R + 1}{4}\right)P_0 \tan^{-1}\left(\frac{s}{\alpha_R x_3}\right), \tag{7.3.12}$$

$$\psi_{,s}(s, x_3) = -\frac{\alpha_R}{4\pi\mu B}\left(\frac{c_R^2}{c_R^2 - c^2} - \frac{2\Gamma_R + 1}{4}\right)P_0 \ln\,(s^2 + \beta_R^2 x_3^2). \tag{7.3.13}$$

Using the dimensionless variables v, v_R and ξ such that,

$$\xi = \frac{s}{x_3}, \quad v = \frac{c}{c_2}, \quad v_R = \frac{c_R}{c_2}, \tag{7.3.14}$$

in the same way we can also produce the second order solution for the steady-state displacements,

$$u_1^{st} = \frac{1+\beta_R^2}{2\pi\mu B}\left(\frac{v_R^2}{v_R^2-v^2} - \frac{2\Gamma_R+1}{4}\right) P_0\left(\tan^{-1}\left(\frac{\xi}{\alpha_R}\right) - \frac{1+\beta_R^2}{2}\tan^{-1}\left(\frac{\xi}{\beta_R}\right)\right), \tag{7.3.15}$$

$$u_2^{st} = -\frac{(1+\beta_R^2)\alpha_R}{4\pi\mu B}\left(\frac{v_R^2}{v_R^2-v^2} - \frac{2\Gamma_R+1}{4}\right) P_0\left(\ln\left(\xi^2+\alpha_R^2\right) - \frac{2}{1+\beta_R^2}\ln\left(\xi^2+\beta_R^2\right)\right). \tag{7.3.16}$$

As in Kaplunov et al., introduce a scaled stress S_{33} such that,

$$S_{33} = \pi\frac{\sigma_{33}x_3}{P_0}, \tag{7.3.17}$$

for which the exact solution of the system gives,

$$S_{33} = \frac{\alpha}{R(c)}\left(\frac{(1+\beta^2)^2}{\xi^2+\alpha^2} - \frac{4\beta^2}{\xi^2+\beta^2}\right). \tag{7.3.18}$$

The leading order asymptotic solution then gives,

$$S_{33} = \frac{2\alpha_R\beta_R}{B}\frac{v_R^2}{v_R^2-v^2}\left(-\frac{\alpha_R}{\xi^2+\alpha_R^2} + \frac{\beta_R}{\xi^2+\beta_R^2}\right) \tag{7.3.19}$$

and hence it is straightforward to obtain S_{33} from the second order asymptotic solution,

$$S_{33} = \frac{2\alpha_R\beta_R}{B}\left(\frac{v_R^2}{v_R^2-v^2} - \frac{2\Gamma_R+1}{4}\right)\left(-\frac{\alpha_R}{\xi^2+\alpha_R^2} + \frac{\beta_R}{\xi^2+\beta_R^2}\right). \tag{7.3.20}$$

We shall again compare the leading order solution with the solution obtained from the second order model. This comparison is given in Fig 7.3 for a Poisson ratio of $\nu = 0.25$, with $v_R \approx 0.9194$, at $\xi = 0.2$.

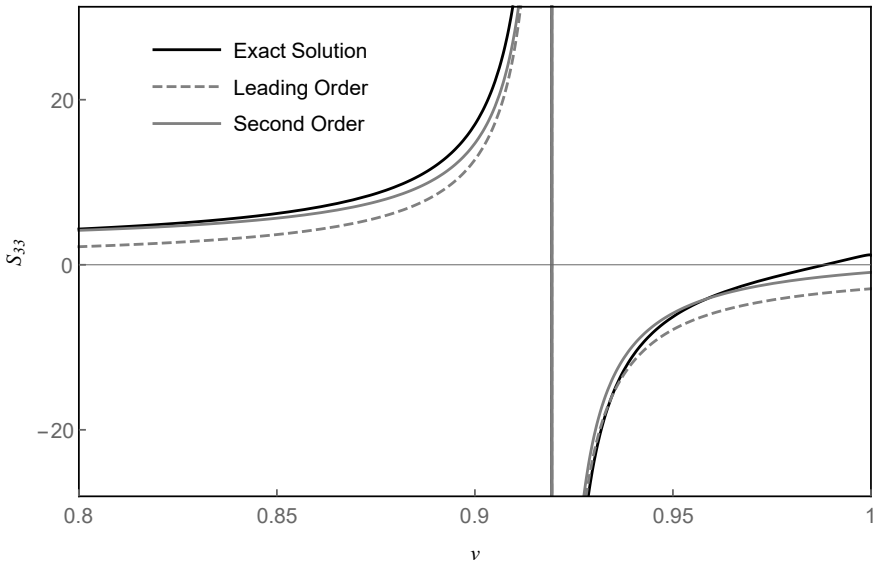

Figure 7.3: A comparison of the leading and second order asymptotic models with the exact solution for the scaled stress S_{33} near the Rayleigh speed for $\xi = 0.2$. Here the leading order and second order asymptotic solutions correspond to the dashed grey and solid grey lines respectively and the exact solution is denoted by the solid black line.

This again shows a significant improvement between the leading order and the exact solution, with the second order model being a consistent improvement for a wide range of speeds, even those far away from the resonance at the Rayleigh speed. The plot shows that for forcing speeds less than the Rayleigh speed in particular, the second order model approximates the exact solution remarkably well.

Furthermore, the second order model in this instance only introduces a constant multiplying factor to the leading order model. This is a feature of having a forcing of the form $P = P(x_1 - ct)$ and so for any similar moving load problems the second order model will be more accurate than the leading order model but no more difficult to apply.

It is however important to note that this model is only valid near the surface of a

near-resonant load, ie. for $c \approx c_R$, and $s \ll x_3$. While when both of these conditions are met the model is shown to be highly accurate, the asymptotic solution cannot predict far-field behaviour or the effect of non-resonant moving loads.

7.3.3 Vertical Rod-like Resonators

We will now attempt to replicate and improve on the results produced by the leading order asymptotic model for a more involved system. As discussed in Chapter 5, and in Ege et al. [39] the asymptotic model was used to accurately interpret the behaviour of a system consiting of an array of identical vertical rod like resonators along the surface of a half plane, originally proposed by Colquitt et al. [25].

If the spacing between each rod is l then we can introduce the dimensionless variables,

$$K = kl, \quad \Omega = \frac{\omega l}{c_R}, \tag{7.3.21}$$

where ω is the angular frequency of the wave. Hence the full unimodal dispersion relation for this system from Colquitt et al. [25] can be expressed in dimensionless form as,

$$R\left(\frac{c_R\Omega}{c_2 K}\right) = 2B\frac{\alpha}{\alpha_R}\left(\frac{\Omega}{K}\right)^3 \Upsilon, \tag{7.3.22}$$

where,

$$\Upsilon = \frac{h}{l}E_R\frac{c_R}{c_V}\alpha_R\frac{\beta_R^2 - 1}{2\mu B}\tan\left(\Omega\frac{c_R}{c_V}\right), \tag{7.3.23}$$

and h, E_R and c_V are respectively the width, Young Modulus and compressional wave speed of the resonators. The leading order asymptotic dispersion relation for wave number k and angular frequency ω produced for this system can be expressed,

$$K^2 + K\Upsilon\Omega - \Omega^2 = 0. \tag{7.3.24}$$

Using the second order model introduced above, we instead produce the dispersion relation,

$$K^3 - K^2\left(\frac{2\Gamma_R - 3}{4}\right)\Upsilon\Omega - K\Omega^2 + \left(\frac{2\Gamma_R + 1}{4}\right)\Upsilon\Omega^3 = 0. \tag{7.3.25}$$

This dispersion relation is plotted in Fig 7.4. For simplicity, use the same system parameters as used in the previous treatments of the problem, from Table 5.1. Although not immediately clear, it is possible to show that this is the same as the leading order dispersion relation with an $O(\epsilon)$ correction.

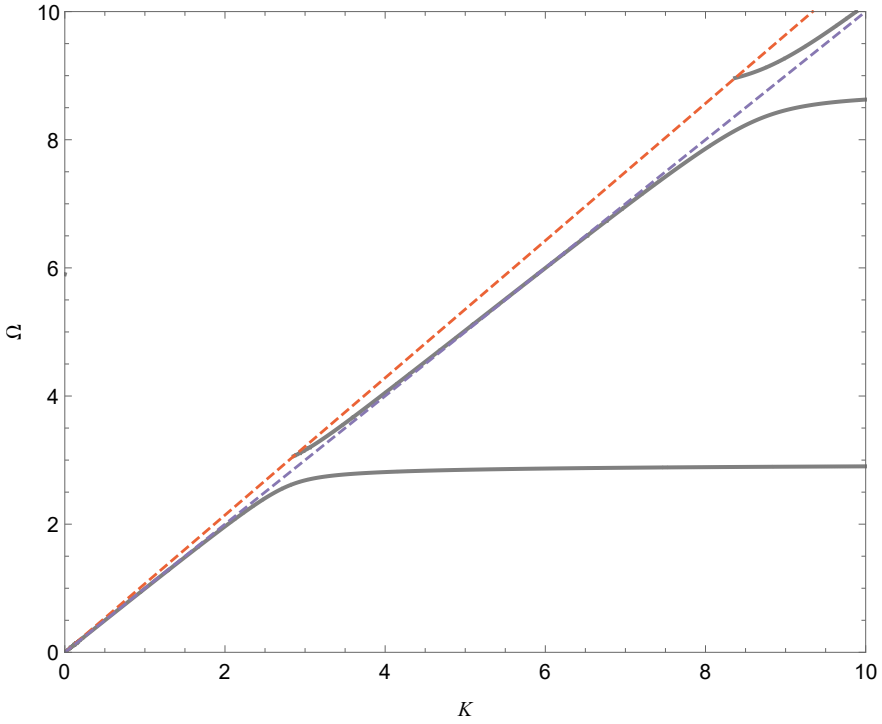

Figure 7.4: The second order asymptotic solution (7.3.25), denoted by the grey curve, for a 2D system of rod like resonators. The Rayleigh line is plotted in dashed purple and the shear wave line in dashed orange.

This shows the main behaviours of the full unimodal solution, specifically the resonances at the rod resonant frequency, as well as anti-resonances which intersect the Rayleigh line. To see if this is an improvement on the leading order model, we will compare the results of the leading order and second order model to the full unimodal

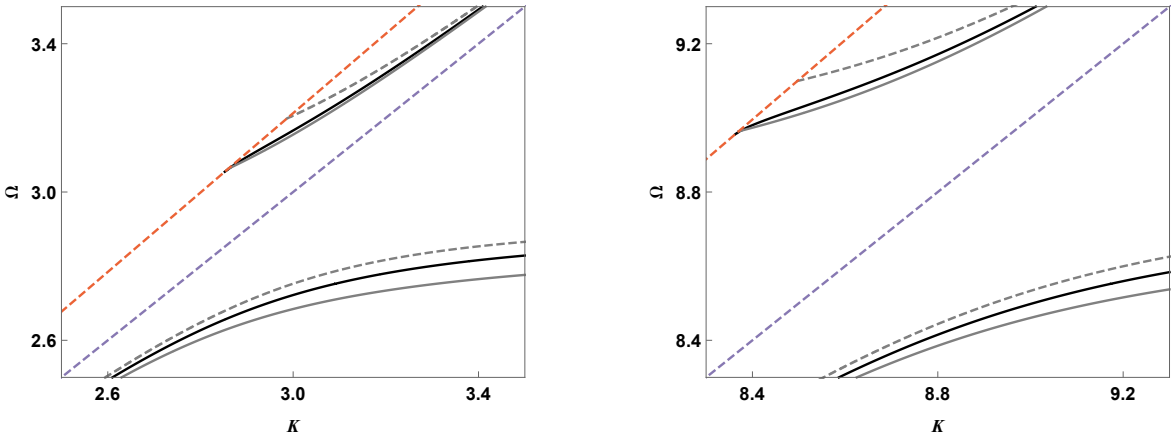

(a) First Asymptote

(b) Second Asymptote

Figure 7.5: The dispersion relation near the first two resonances for a 2D system of rod like resonators. The second order asymptotic solution (7.3.25) is denoted by the solid grey curve, the full unimodal solution (7.3.22) by the solid black curve, and the first order asymptotic solution (7.3.24) by the dashed grey curve. The Rayleigh line is plotted in dashed purple and the shear wave line in dashed orange.

solution. Since it has already been shown that the leading order model matches the full unimodal solution well close to the Rayleigh line, it is sufficient to compare the two models near the resonances only. This comparison is given by Fig 7.5.

These figures show a clear improvement between the leading order model and the second order model. Between the Rayleigh and shear wave lines in particular the second order model matches with the full unimodal solution remarkably well, with the two solutions almost indistinguishable. Even for larger values of K and around the asymptote where the model is predicted to not work as well, the level of matching remains highly accurate with a relative error in Ω of less than $\sim 2\%$ for these material parameters.

7.4 Concluding Remarks

In this work we have shown that by using the same method used to produce the leading order model for the Rayleigh wave field, it is possible to obtain a higher order correction term to the surface boundary condition while leaving the equations for the bulk unchanged. This correction term leaves the hyperbolic-elliptic nature of the system unchanged with the surface boundary condition still giving a hyperbolic equation. This correction term also converges with the second order Taylor expansion for a surface loading, demonstrating that in a general case the model obtained will converge to the exact solution.

This new higher order model has been applied to three different systems: a vertical harmonic forcing, a steady state point moving load, and an array of vertical resonators attached to the surface. Each of these problems has been treated by the leading order model previously to good effect. Applying the new higher order model to each has shown close matching to the full unimodal solutions and significant improvement over the existing leading order model, at the cost of a less succinct solution form.

The treatment of the harmonic forcing in particular shows how the second order model is an improvement over the leading order model. While the leading order model matches the exact solution only at the Rayleigh speed, the solution from second order model remains a good fit for the exact solution for a much greater range of speeds.

Furthermore, the moving load problem demonstrates how the added accuracy of the model does not necessarily come with an increased difficulty to solve. While the second order model is significantly more accurate than the leading order model, particularly for a wider range of load speeds, the process for solving the problem remains the same.

Finally, the resonator forcing demonstrates how well the second order model can

predict the resonances and band gaps caused by a structured surface. This is especially notable as the forcing is not applied, it is caused as a reaction to the existing motion of the half-space, and so the model must accurately represent both the initial motion and the effect of the reaction. These features are particularly sought after for their uses in controlling and suppressing wave propagation and have shown a recent increase in interest in such 'metasurfaces'.

From these results there is clear scope for further development of the model and application of this model in other situations. The leading order model has been extended to full 3D systems and both tangential and perpendicular applied stresses, and there is no reason why the same cannot be done for the higher order model. Similarly, the higher order model can be used to re-examine previously studied systems to gain further insight and extend those previous systems into more involved problems which the leading order model was not refined enough to accurately approximate.

CHAPTER 8

Conclusion

In the work presented within this thesis there has already been discussion and conclusions made for the individual problems. This chapter unifies the disparate problems and solutions into a broader body of work which taken together show scope for further research. First each of the preceding chapters will be discussed and then there will be a discussion both the immediate and distant future work which the content of this thesis has opened up for study.

8.1 Concluding Remarks

In the Literature Review in Chapter 1 it was mentioned that wave control by means of metamaterials and metasurfaces has had significant activity in recent years, with key developments in many different fields. The work presented aims to add to this active field with a focus on waves in linearly elastic structures, and also to introduce new models and methods to complement the research and assist in further work.

In Chapter 3 a novel 'bridging' scheme was introduced where a gap in a 2D membrane continuum was filled with a periodic array of 1D strings. Such a bridge was capable of perfectly replicating an incident wave pattern on the other side of the gap

with no reflections given that the wave had a wavelength much greater than the bridge spacing. Notably this bridging effect was dependent only on the materials parameters of the membrane and the strings, spacing of the periodic strings and the angle of incidence of the wave making this construction broadband. A similar effect was produced by inserting a periodic 'net' of strings, as well as introducing the possibility of a wave filtering effect.

In Chapter 4 the same bridging ideas were used to produce a similar system where waves on linear elastic structures are transferred over the gap. This includes two different bridging schemes, the first to bridge bulk waves and the second to bridge Rayleigh waves. Both of these exhibit some degree of success but the overall bridging requirements are predictably more complicated than the simpler membrane-string bridge.

For bulk waves it was demonstrated that there is no choice of bridge parameters for which an arbitrary incident wave is perfectly recreated on the other side of the gap. Instead, any incidence apart from normally incident waves will cause a wave conversion so the incident wave pattern cannot be perfectly replicated. For normally incident waves however, there is no wave conversion and there are broadband conditions for which both shear and longitudinal waves can both be bridged with no reflection.

The bridge for Rayleigh waves uses the same type of bridge as for bulk waves but imposes a strict condition on the bridge parameters. This condition is to prevent any wave conversion into bulk waves and accounts for how the Rayleigh wave decays with depth. However, since the decay has a dependence on wavelength, unlike the previous bridges this formulation cannot be broadband. Also unlike previous bridging attempts, waves are restricted to normal incidence and there is a strict requirement on the separation of bridge layers. It is however shown that it is possible to produce a Rayleigh bridging effect.

Each of the bridging schemes have multiple applications; in physical realisations of these systems an outside observer will be unable to tell whether or not a gap is present. This may conceal objects within the gap which would cause wave disturbances if the gap were attempted to be filled with a continuum. This gives a crude cloaking effect which can be easily reproduced with simple materials. The bridge also acts as a simple repair of the continuum while still being able to transfer wave energy.

In Chapter 5 an existing system of vertical rod-like resonators to alter wave propagation along the surface of a linearly elastic half plane was considered. Using the asymptotic model from Kaplunov and Prikazchikov [63] an explicit dispersion relation was produced which is both qualitatively and numerically nearly identical to the implicit dispersion relation from the original paper [25].

This work is followed with a similar but more involved system in Chapter 6; here the rod-like resonators are replaced by flexural resonators modelled as Euler-Bernoulli beams with a range of boundary conditions between the surface and the beams. Using the same asymptotic model explicit dispersion relations were produced for each. For completeness the full unimodal systems were also solved to produce implicit dispersion relations to verify the asymptotic results.

While the asymptotic model matches well graphically with the full unimodal solution, there are significant differences between the two solutions at key points. This is particularly visible for the fully matched boundary condition, which is also the most physically realistic of those treated. Since this is a mixed stress problem, which the existing model does not account for, two new models were developed to treat this problem. Neither, however, identify the key resonances of the system, although the second refined model does agree with the full unimodal solution at the Rayleigh line.

Chapter 7 proposes adding a second order term to the existing asymptotic model

which the preceding chapters have made extensive use of. This second order term has been shown to match with the Taylor expansion in the case of an arbitrary harmonic loading. Furthermore, the new model has shown significant improvement over the leading order model, at the cost of a less succinct solution form.

First it is useful to verify that the methods used in this work are valid in each instance. Chapters 3 and 5 demonstrate that the simple homogenisation used is valid for the periodic metamaterials in the long wave limit by comparing with non homogenised boundary conditions. Chapters 5 and 6 each verify the use of the asymptotic model from Kaplunov and Prikazchikov [63] to investigate how metasurfaces in linear elasticty control Rayleigh wave propagation. In each the results from the asymptotic model match well with the exact results. Testing both of these procedures indicates how the same homogenisation procedure and asymptotic model can be used in the production of more sophisticated bridging metamaterials and wave control metasurfaces. It is however noted that the asymptotic results from the beam resonator system are much less accurate than those from the rod resonator system. Hence while the asymptotic method is valid, the solutions demonstrate a potential need for a more refined model to more accurately detail all of the features of the system.

Some of the refinements developed for the asymptotic model are detailed in Chapters 5 and 6 with both showing the improvement of the new model. The first improvement to the model is the development of an asymptotic model for multiple stresses applied to the surface, where previous models have involved only either perpendicular or parallel stresses. While this new model is capable of producing a close approximation to the full unimodal dispersion relation it treats the applied stresses as independent. This leads to results from this model not necessarily converging with the full unimodal solution at the Rayleigh solution. A further refinement is then introduced which ac-

counts for stress interaction but requires the applied stresses to have a form which can be reduced to a linear function of the two displacement potentials. While more limited, this model does force convergence between the asymptotic and exact solutions in the region of the Rayleigh solution.

The second refinement to the model is proposed in Chapter 7. This development adds a second term to the existing leading order model, which has been shown to be an improvement over the existing leading order model in a variety of situations.

Finally Chapters 3,4 and 6 each introduce novel metamaterials or metasurfaces each designed to control wave propagation in different ways. These include the bridges aimed at reproducing wave behaviour on the other side of a gap, rendering the gap undetectable, and a resonator metasurface aimed at suppressing waves. Each of have multiple practical applications of controlling wave propagation.

Therefore it is clear that this work has introduced new materials with real world applications in wave suppression and control. This work has also made use of both new and existing methods for simple systems in order to verify that the same methods can be applied to more complicated problems to better analyse physical problems.

8.2 Future Work

The content in this thesis has several natural avenues of future work. The first of these is to develop the bridging metamaterials which are a simple route to controlling wave propagation and concealing voids and defects. However the materials used to construct the bridges are ideal mathematical objects and are not fully realisable in physical without further work. To see how functional these bridges are requires further work with more realistic mathematical models and possible experimental work.

The bridge metamaterials also each have many fundamental limitations. These include restrictions of incident angle, inability to ideally bridge multiple wave types, unintentional wave mode switching for the bulk wave bridge, and the single wavelength requirements of the Rayleigh bridge. Many of these limitations arise from the fundamental construction of the bridge, which is intentionally simplistic. It may be possible however to remove some of these restrictions with more sophisticated bridge designs, based around improved system design itself, or more sophisticated use of multiple materials. There are also numerous opportunities to extend the same bridging ideas to other systems. This may include other elastic media like flexural waves on plates and beams or possibly to other fields entirely.

There is also scope to use the new Rayleigh wave models developed to investigate more systems for linearly elastic half planes. This includes using the second order model developed in Chapter 6 and the leading order multi-stress models developed in Chapter 5. The second order model can more accurately investigate previous single stress problems than the leading order model, or can be used to predict and analyse more system characteristics than the leading order is capable of. Alternately the multi stress models can be used to investigate more sophisticated systems than the existing single stress model, particularly as most real physical systems will have both vertical and horizontal stress components. Therefore these two new developments to the model have made the asymptotic formulation much more applicable for physical systems and can more be reliably used for problems with difficult exact formulations.

In order to apply the new higher order model to the beam resonator system proposed in Chapter 5 would also require the higher order model to be able to treat both vertical and horizontal stresses. Therefore a further avenue to consider is to develop the higher order model to produce a multi-stress model using the methodology from

Chapter 5.

The final clear avenue for future work is to further develop the metasurfaces from Chapters 5 and 6. This development can take either of two possible routes; either further theoretical development with different resonators and boundary conditions which can more accurately model real world systems or experimental work to determine whether these metasurfaces are physically realisable.

While this experimental work could be conducted on a linearly elastic half plane, the use of the leading order asymptotic model also allows for half plane experiments to be conducted on membranes with appropriately constructed resonator analogues. This allows for complicated resonator arrangements to be experimentally tested on a much simpler and less expensive experimental setup.

Bibliography

[1] Y. Achaoui, T. Antonakakis, S. Brule, R. Craster, S. Enoch, and S. Guenneau. Clamped seismic metamaterials: ultra-low frequency stop bands. *New Journal of Physics*, 19(6):063022, 2017.

[2] J. D. Achenbach. *Wave propagation in elastic solids*. North-Holland, 1973.

[3] J. D. Achenbach. Explicit solutions for carrier waves supporting surface waves and plate waves. *Wave Motion*, 28(1):89–97, 1998.

[4] G. Athanasopoulos, P. Pelekis, and G. Anagnostopoulos. Effect of soil stiffness in the attenuation of Rayleigh-wave motions from field measurements. *Soil Dynamics and Earthquake Engineering*, 19(4):277–288, 2000.

[5] P. T. Bauman, H. B. Dhia, N. Elkhodja, J. T. Oden, and S. Prudhomme. On the application of the Arlequin method to the coupling of particle and continuum models. *Comput. Mech.*, 42(4):511–530, 2008.

[6] K. Bertoldi, D. Bigoni, and W. Drugan. Structural interfaces in linear elasticity. part i: Nonlocality and gradient approximations. *Journal of the Mechanics and Physics of Solids*, 55(1):1–34, 2007.

[7] K. Bertoldi, D. Bigoni, and W. Drugan. Structural interfaces in linear elasticity. part ii: Effective properties and neutrality. *Journal of the Mechanics and Physics of Solids*, 55(1):35–63, 2007.

[8] S. Brûlé, E. Javelaud, S. Enoch, and S. Guenneau. Experiments on seismic

metamaterials: Molding surface waves. *Physical Review Letters*, 112(13):133901, 2014.

[9] M. Brun, D. Colquitt, I. Jones, A. Movchan, and N. Movchan. Transformation cloaking and radial approximations for flexural waves in elastic plates. *New Journal of Physics*, 16(9):093020, 2014.

[10] M. Brun, S. Guenneau, and A. Movchan. Achieving control of in-plane elastic waves. *Applied Physics Letters*, 94:061903, 2009.

[11] M. Brun, S. Guenneau, A. B. Movchan, and D. Bigoni. Dynamics of structural interfaces: filtering and focussing effects for elastic waves. *Journal of the Mechanics and Physics of Solids*, 58(9):1212–1224, 2010.

[12] M. Brun, A. Movchan, and N. Movchan. Shear polarisation of elastic waves by a structured interface. *Continuum Mechanics and Thermodynamics*, 22(6-8):663–677, 2010.

[13] O. Casablanca, G. Ventura, F. Garescì, B. Azzerboni, B. Chiaia, M. Chiappini, and G. Finocchio. Seismic isolation of buildings using composite foundations based on metamaterials. *Journal of Applied Physics*, 123(17):174903, 2018.

[14] P. Chadwick. Surface and interfacial waves of arbitrary form in isotropic elastic media. *Journal of Elasticity*, 6(1):73–80, 1976.

[15] R. Chebakov, J. Kaplunov, and G. Rogerson. Refined boundary conditions on the free surface of an elastic half-space taking into account non-local effects. *Proceedings of the Royal Society A: Mathematical, Physical and Engineering Sciences*, 472(2186):20150800, 2016.

[16] H. Chen and C. Chan. Acoustic cloaking in three dimensions using acoustic metamaterials. *Applied Physics Letters*, 91(18):183518, 2007.

[17] H. Chen, C. Chan, and P. Sheng. Transformation optics and metamaterials. *Nature materials*, 9(5):387–396, 2010.

[18] Y. S. Cho. Non-destructive testing of high strength concrete using spectral analysis of surface waves. *NDT & E International*, 36(4):229–235, 2003.

[19] A. Colombi, V. Ageeva, R. J. Smith, A. Clare, R. Patel, M. Clark, D. Colquitt, P. Roux, S. Guenneau, and R. V. Craster. Enhanced sensing and conversion of ultrasonic Rayleigh waves by elastic metasurfaces. *Scientific Reports*, 7(1):6750, 2017.

[20] A. Colombi, D. Colquitt, P. Roux, S. Guenneau, and R. V. Craster. A seismic metamaterial: The resonant metawedge. *Scientific reports*, 6:27717, 2016.

[21] A. Colombi, S. Guenneau, P. Roux, and R. V. Craster. Transformation seismology: Composite soil lenses for steering surface elastic rayleigh waves. *Scientific reports*, 6:25320, 2016.

[22] A. Colombi, P. Roux, S. Guenneau, P. Gueguen, and R. V. Craster. Forests as a natural seismic metamaterial: Rayleigh wave bandgaps induced by local resonances. *Scientific reports*, 6:19238, 2016.

[23] A. Colombi, P. Roux, S. Guenneau, and M. Rupin. Directional cloaking of flexural waves in a plate with a locally resonant metamaterial. *The Journal of the Acoustical Society of America*, 137(4):1783–1789, 2015.

[24] A. Colombi, P. Roux, and M. Rupin. Sub-wavelength energy trapping of elastic waves in a metamaterial. *The Journal of the Acoustical Society of America*, 136(2):EL192–EL198, 2014.

[25] D. Colquitt, A. Colombi, R. Craster, P. Roux, and S. Guenneau. Seismic metasurfaces: Sub-wavelength resonators and Rayleigh wave interaction. *Journal of*

the Mechanics and Physics of Solids, 99:379–393, 2017.

[26] D. Colquitt, R. Craster, and M. Makwana. High frequency homogenisation for elastic lattices. *Quart. J. Mech. Appl. Math.*, 68(2):203–230, 2015.

[27] D. Colquitt, I. Jones, N. Movchan, and A. Movchan. Dispersion and localization of elastic waves in materials with microstructure. *Proceedings of the Royal Society of London A: Mathematical, Physical and Engineering Sciences*, 467:2874–2895, 2011.

[28] D. Colquitt, I. Jones, N. Movchan, A. Movchan, M. Brun, and R. McPhedran. Making waves round a structured cloak:Lattices, negative refraction and fringes. *Proceedings of the Royal Society of London A: Mathematical, Physical and Engineering Sciences*, 469:20130218, 2013.

[29] D. Colquitt, I. Jones, N. Movchan, A. Movchan, and R. McPhedran. Dynamic anisotropy and localization in elastic lattice systems. *Waves in Random and Complex Media*, 22(2):143–159, 2012.

[30] D. Colquitt, A. Movchan, I. Jones, and W. Daniels. Frequency related localisation of harmonic elastic waves in stratified welds. *Acta Mechanica Sinica*, 26(4):567–572, 2010.

[31] D. J. Colquitt, M. Brun, M. Gei, A. B. Movchan, N. V. Movchan, and I. S. Jones. Transformation elastodynamics and cloaking for flexural waves. *Journal of the Mechanics and Physics of Solids*, 72:131–143, 12/1 2014.

[32] S. A. Cummer, B.-I. Popa, D. Schurig, D. R. Smith, J. Pendry, M. Rahm, and A. Starr. Scattering theory derivation of a 3D acoustic cloaking shell. *Physical Review Letters*, 100(2):024301, 2008.

[33] S. A. Cummer and D. Schurig. One path to acoustic cloaking. *New Journal of*

Physics, 9(3):45, 2007.

[34] H.-H. Dai, J. Kaplunov, and D. Prikazchikov. A long-wave model for the surface elastic wave in a coated half-space. *Proceedings of the Royal Society of London A: Mathematical, Physical and Engineering Sciences*, 466(2122):3097–3116, 2010.

[35] J. M. De Ponti, A. Colombi, R. Ardito, F. Braghin, A. Corigliano, and R. V. Craster. Graded metasurface for enhanced sensing and energy harvesting. *arXiv preprint arXiv:1907.09297*, 2019.

[36] B. Djafari-Rouhani, S. El-Jallal, M. Oudich, and Y. Pennec. Optomechanic interactions in phoxonic cavities. *AIP Advances*, 4(12):124602, 2014.

[37] H. Draper. On diffraction spectrum photography, and the determination of the wave-lengths of the ultraviolet rays. *Nature*, 9:224–226, 1874.

[38] N. Ege, B. Erbaş, A. Chorozoglou, J. Kaplunov, and D. A. Prikazchikov. On surface wave fields arising in soil-structure interaction problems. *Procedia engineering*, 199:2366–2371, 2017.

[39] N. Ege, B. Erbaş, J. Kaplunov, and P. Wootton. Approximate analysis of surface wave-structure interaction. *Journal of Mechanics of Materials and Structures*, 13(3):297–309, 2018.

[40] N. Ege, B. Erbaş, and D. A. Prikazchikov. On the 3D Rayleigh wave field on an elastic halfspace subject to tangential surface loads. *ZAMMJournal of Applied Mathematics and Mechanics/Zeitschrift fr Angewandte Mathematik und Mechanik*, 95(12):1558–1565, 2015.

[41] B. Erbaş, J. Kaplunov, E. Nolde, and M. Palsü. Composite wave models for elastic plates. *Proceedings of the Royal Society A: Mathematical, Physical and Engineering Sciences*, 474(2214):20180103, 2018.

[42] B. Erbaş, J. Kaplunov, and D. A. Prikazchikov. The Rayleigh wave field in mixed problems for a half-plane. *The IMA Journal of Applied Mathematics*, 78(5):1078–1086, 2012.

[43] B. Erbaş, J. Kaplunov, D. A. Prikazchikov, and O. Şahin. The near-resonant regimes of a moving load in a three-dimensional problem for a coated elastic half-space. *Mathematics and Mechanics of Solids*, 22(1):89–100, 2017.

[44] T. Ergin, J. Fischer, and M. Wegener. Optical phase cloaking of 700 nm light waves in the far field by a three-dimensional carpet cloak. *Physical Review Letters*, 107(17):173901, 2011.

[45] T. Ergin, N. Stenger, P. Brenner, J. B. Pendry, and M. Wegener. Three-dimensional invisibility cloak at optical wavelengths. *Science (New York, N.Y.)*, 328(5976):337–339, Apr 16 2010.

[46] M. Farhat, S. Enoch, and S. Guenneau. Biharmonic split ring resonator metamaterial: Artificially dispersive effective density in thin periodically perforated plates. *EPL (Europhysics Letters)*, 107(4):44002, 2014.

[47] M. Farhat, S. Guenneau, and S. Enoch. Ultrabroadband elastic cloaking in thin plates. *Physical Review Letters*, 103(2):024301, 2009.

[48] J. Fischer, T. Ergin, and M. Wegener. Three-dimensional polarization-independent visible-frequency carpet invisibility cloak. *Optics Letters*, 36(11):2059–2061, 2011.

[49] F. Friedlander. On the total reflection of plane waves. *The Quarterly Journal of Mechanics and Applied Mathematics*, 1(1):376–384, 1948.

[50] L. H. Gabrielli, J. Cardenas, C. B. Poitras, and M. Lipson. Silicon nanostructure cloak operating at optical frequencies. *Nature Photonics*, 3(8):461–463, 2009.

[51] N. Glass and A. Maradudin. Shear surface elastic waves on large amplitude gratings. *Electronics Letters*, 17(21):773–774, 1981.

[52] S. Guenneau, A. Movchan, G. Pétursson, and S. A. Ramakrishna. Acoustic metamaterials for sound focusing and confinement. *New Journal of physics*, 9(11):399, 2007.

[53] D. Harutyunyan, G. W. Milton, and R. V. Craster. High-frequency homogenization for travelling waves in periodic media. *Proceedings of the Royal Society A: Mathematical, Physical and Engineering Sciences*, 472(2191):20160066, 2016.

[54] S. Haslinger, R. McPhedran, N. Movchan, and A. Movchan. Structured interfaces for flexural waves–trapped modes and transmission resonances. In *Journal of Physics: Conference Series*, volume 451, page 012024. IOP Publishing, 2013.

[55] S. Haslinger, N. Movchan, A. Movchan, and R. McPhedran. Transmission, trapping and filtering of waves in periodically constrained elastic plates. *Proceedings of the Royal Society A: Mathematical, Physical and Engineering Sciences*, 468(2137):76–93, 2011.

[56] C. L. Holloway, E. F. Kuester, J. Gordon, J. O. Hara, J. Booth, and D. R. Smith. An overview of the theory and applications of metasurfaces: The two-dimensional equivalents of metamaterials. *Antennas and Propagation Magazine, IEEE*, 54(2):10–35, 2012.

[57] A. A. Houck, J. B. Brock, and I. L. Chuang. Experimental observations of a left-handed material that obeys snells law. *Physical Review Letters*, 90(13):137401, 2003.

[58] M. Kadic, T. Bckmann, R. Schittny, and M. Wegener. Metamaterials beyond electromagnetism. *Reports on Progress in Physics*, 76(12):126501, 2013.

[59] J. Kaplunov, E. Nolde, and D. Prikazchikov. A revisit to the moving load problem using an asymptotic model for the rayleigh wave. *Wave motion*, 47(7):440–451, 2010.

[60] J. Kaplunov and D. Prikazchikov. *Explicit models for surface, interfacial and edge waves*, pages 73–114. Dynamic Localization Phenomena in Elasticity, Acoustics and Electromagnetism. Springer, 2013.

[61] J. Kaplunov, D. Prikazchikov, B. Erbaş, and O. Şahin. On a 3d moving load problem for an elastic half space. *Wave motion*, 50(8):1229–1238, 2013.

[62] J. Kaplunov, D. Prikazchikov, L. Sultanova, et al. Rayleigh-type waves on a coated elastic half-space with a clamped surface. *Philosophical Transactions A: Mathematical, Physical and Engineering Sciences*, 2019.

[63] J. Kaplunov and D. A. Prikazchikov. *Asymptotic theory for Rayleigh and Rayleigh-type waves*, volume 50 of *Advances in Applied Mechanics*, pages 1–106. Elsevier, 2017.

[64] J. Kaplunov, A. Zakharov, and D. Prikazchikov. Explicit models for elastic and piezoelastic surface waves. *IMA journal of applied mathematics*, 71(5):768–782, 2006.

[65] J. D. Kaplunov, L. Y. Kossovitch, and E. Nolde. *Dynamics of thin walled elastic bodies*. Academic Press, 1998.

[66] Y. D. Kaplunov and L. Y. Kossovich. Asymptotic model of Rayleigh waves in the far-field zone in an elastic half-plane. *Doklady Physics*, 49(4):234–236, 2004.

[67] A. Kiselev and D. Parker. Omni-directional Rayleigh, Stoneley and Schölte waves with general time dependence. *Proceedings of the Royal Society A: Mathematical, Physical and Engineering Sciences*, 466(2120):2241–2258, 2010.

[68] A. P. Kiselev and G. A. Rogerson. Laterally dependent surface waves in an elastic medium with a general depth dependence. *Wave Motion*, 46(8):539–547, 2009.

[69] A. G. Kolpakov, I. V. Andrianov, and D. A. Prikazchikov. Asymptotic strategy for matching homogenized structures. conductivity problem. *The Quarterly Journal of Mechanics and Applied Mathematics*, 71(4):519–535, 2018.

[70] U. Leonhardt. Optical conformal mapping. *Science (New York, N.Y.)*, 312(5781):1777–1780, Jun 23 2006.

[71] J. Li and C. T. Chan. Double-negative acoustic metamaterial. *Physical Review E*, 70(5):055602, 2004.

[72] J. Li and J. Pendry. Hiding under the carpet: A new strategy for cloaking. *Physical Review Letters*, 101(20):203901, 2008.

[73] R. Liu, C. Ji, J. J. Mock, J. Y. Chin, T. J. Cui, and D. R. Smith. Broadband ground-plane cloak. *Science (New York, N.Y.)*, 323(5912):366–369, Jan 16 2009.

[74] Z. Liu, X. Zhang, Y. Mao, Y. Zhu, Z. Yang, C. T. Chan, and P. Sheng. Locally resonant sonic materials. *science*, 289(5485):1734–1736, 2000.

[75] Lord Rayleigh. On waves propagated along the plane surface of an elastic solid. *Proceedings of the London Mathematical Society*, 17(1):4–11, 1885.

[76] A. Love. *A treatise on the mathematical theory of elasticity*. Cambridge University Press, 4th edition, 1944.

[77] A. A. Maradudin. *Structured surfaces as optical metamaterials*. Cambridge University Press, 2011.

[78] P. Martinsson and A. Movchan. Vibrations of lattice structures and phononic band gaps. *The Quarterly Journal of Mechanics and Applied Mathematics*, 56(1):45–64, 2003.

[79] G. W. Milton, M. Briane, and J. R. Willis. On cloaking for elasticity and physical equations with a transformation invariant form. *New Journal of Physics*, 8(10):248, 2006.

[80] G. W. Milton and A. V. Cherkaev. Which elasticity tensors are realizable? *Journal of Engineering Materials and Technology*, 117(4):483–493, 1995.

[81] G. W. Milton and J. R. Willis. On modifications of Newton's second law and linear continuum elastodynamics. *Proceedings of the Royal Society of London A: Mathematical, Physical and Engineering Sciences*, 463(2079):855–880, 2007.

[82] D. Morgan. *Rayleigh Wave Transducers*, pages 60–77. Rayleigh-Wave Theory and Application. Springer, 1985.

[83] A. Movchan and S. Guenneau. Split-ring resonators and localized modes. *Physical Review B*, 70(12):125116, 2004.

[84] New Zealand Government and B. English. 2016 budget: Budget policy statement. Technical report, New Zealand Government, 2015.

[85] X. Ni, Y. Wu, Z.-G. Chen, L.-Y. Zheng, Y.-L. Xu, P. Nayar, X.-P. Liu, M.-H. Lu, and Y.-F. Chen. Acoustic rainbow trapping by coiling up space. *Scientific reports*, 4:7038, 2014.

[86] M. Nieves, G. Carta, I. Jones, A. Movchan, and N. Movchan. Vibrations and elastic waves in chiral multi-structures. *Journal of the Mechanics and Physics of Solids*, 121:387 – 408, 2018.

[87] A. Nobili and D. A. Prikazchikov. Explicit formulation for the Rayleigh wave field induced by surface stresses in an orthorhombic half-plane. *European Journal of Mechanics-A/Solids*, 70:86–94, 2018.

[88] A. N. Norris. Acoustic cloaking theory. *Proceedings of the Royal Society of London*

A: Mathematical, Physical and Engineering Sciences, 464:2411–2434, 2008.

[89] A. N. Norris and A. L. Shuvalov. Elastic cloaking theory. *Wave Motion*, 48(6):525–538, 9 2011.

[90] M. Notomi, A. Shinya, S. Mitsugi, G. Kira, E. Kuramochi, and T. Tanabe. Optical bistable switching action of Si high-Q photonic-crystal nanocavities. *Optics Express*, 13(7):2678–2687, 2005.

[91] J. B. Pendry. Negative refraction makes a perfect lens. *Physical Review Letters*, 85(18):3966, 2000.

[92] J. B. Pendry, A. J. Holden, D. Robbins, and W. Stewart. Magnetism from conductors and enhanced nonlinear phenomena. *Microwave Theory and Techniques, IEEE Transactions on*, 47(11):2075–2084, 1999.

[93] J. B. Pendry, D. Schurig, and D. R. Smith. Controlling electromagnetic fields. *Science (New York, N.Y.)*, 312(5781):1780–1782, Jun 23 2006.

[94] R. Porter. Plate arrays as a water-wave metamaterial. In *Proc. 33rd Int. Workshop on Water Waves and Floating Bodies*, pages 165–169, 2018.

[95] J. F. Ramsay. Microwave antenna and waveguide techniques before 1900. *Proceedings of the IRE*, 46(2):405–415, 1958.

[96] V. Romero-García, A. Krynkin, L. Garcia-Raffi, O. Umnova, and J. V. Sánchez-Pérez. Multi-resonant scatterers in sonic crystals: Locally multi-resonant acoustic metamaterial. *Journal of Sound and Vibration*, 332(1):184–198, 2013.

[97] P. Roux, D. Bindi, T. Boxberger, A. Colombi, F. Cotton, I. Douste-Bacque, S. Garambois, P. Gueguen, G. Hillers, D. Hollis, et al. Toward seismic metamaterials: The metaforet project. *Seismological Research Letters*, 89(2A):582–593, 2018.

[98] D. Schurig, J. J. Mock, B. J. Justice, S. A. Cummer, J. B. Pendry, A. F. Starr, and D. R. Smith. Metamaterial electromagnetic cloak at microwave frequencies. *Science (New York, N.Y.)*, 314(5801):977–980, Nov 10 2006.

[99] V. M. Shalaev. Optical negative-index metamaterials. *Nature photonics*, 1(1):41–48, 2007.

[100] R. A. Shelby, D. R. Smith, and S. Schultz. Experimental verification of a negative index of refraction. *Science (New York, N.Y.)*, 292(5514):77–79, Apr 6 2001.

[101] Sina Corp. Online. *Sichuan Earthquake Casualties Summary.* `http://news.sina.com.cn/pc/2008-05-13/326/651.html`, 2008 (accessed Oct 06 2018).

[102] D. E. Siskind and United States Bureau of Mines. *Structure response and damage produced by ground vibration from surface mine blasting.* US Department of the Interior, Bureau of Mines, 1980.

[103] L. Slepyan. The strain wave in a bar with vibration-isolated masses. *Mechanics of Solids*, 2:57–64, 1967.

[104] E. Tuck. Transmission of water waves through small apertures. *Journal of Fluid Mechanics*, 49(1):65–74, 1971.

[105] B. Ungureanu, Y. Achaoui, S. Brule, S. Enoch, R. Craster, and S. Guenneau. Seismic wave shield using cubic arrays of split-ball resonators. *arXiv preprint arXiv:1904.10767*, 2019.

[106] A. Ward and J. Pendry. Refraction and geometry in Maxwell's equations. *Journal of modern optics*, 43(4):773–793, 1996.

[107] E. T. Whittaker and G. N. Watson. *A course of modern analysis.* Cambridge university press, 1996.

[108] E. G. Williams, P. Roux, M. Rupin, and W. Kuperman. Theory of multiresonant

metamaterials for A_0 Lamb waves. *Physical Review B*, 91(10):104307, 2015.

[109] R. C. Williamson and H. I. Smith. The use of surface-elastic-wave reflection gratings in large time-bandwidth pulse-compression filters. *IEEE Transactions on Microwave Theory and Techniques*, 21(4):195–205, 1973.

[110] J. P. Wolf and C. Song. Some cornerstones of dynamic soil–structure interaction. *Engineering Structures*, 24(1):13–28, 2002.

[111] P. Wootton, J. Kaplunov, and D. Colquitt. An asymptotic hyperbolic-elliptic model for flexural-seismic metasurfaces. *Proceedings of the Royal Society A: Mathematical, Physical and Engineering Sciences*, 475, 2019.

[112] Y. Xiao, J. Wen, and X. Wen. Flexural wave band gaps in locally resonant thin plates with periodically attached spring–mass resonators. *Journal of Physics D: Applied Physics*, 45(19):195401, 2012.

[113] C. Zhou, B. Yuan, Y. Cheng, and X. Liu. Precise rainbow trapping for low-frequency acoustic waves with micro Mie resonance-based structures. *Applied Physics Letters*, 108(6):063501, 2016.

[114] X. Zhou, X. Liu, and G. Hu. Elastic metamaterials with local resonances: an overview. *Theoretical and Applied Mechanics Letters*, 2(4), 2012.

APPENDIX

A.1 Beam Boundary Conditions

At the end of a beam there are four conserved quantities that will affect the beam motion: Out-of-plane displacement, bending angle, moment and out-of-plane force. Each of these corresponds to a derivative of the out-of-plane displacement. To determine the boundary conditions it is useful to introduce a 'dummy' beam in the coordinates (ζ, η) occupying the domain $0 < \zeta < -\zeta_1,\ \eta = \eta_1$. This beam will have out-of-plane displacement u_η and in-plane displacement u_ζ.

It is self evident that if the beam is fixed to another object that the displacements at the boundary between the two will match exactly. Similarly the flat end of the beam will be perpendicular to the central axis so if the end of the beam is pressed to a flat angled surface with in-plane displacement u_V then from fundamental geometry,

$$\frac{\partial u_\eta}{\partial \zeta} = \frac{\partial u_V}{\partial \eta}. \tag{A.1.1}$$

Next find the bending moment M caused by flexing of the beam. This is given by,

$$M = \int_0^{2\pi} \int_0^{h_b/2} r cos\theta\ \sigma_{\zeta\zeta}\ r\ dr d\theta. \tag{A.1.2}$$

where $\sigma_{\zeta\zeta}$ in the in-plane stress at the end of the beam. Using standard polar coordinates r and θ, where r is the centre axis of the beam, suppose that the stress can be

approximated around the centre of the beam by a Taylor series,

$$\sigma_{\zeta\zeta} = \sigma_{\zeta\zeta}|_{r=0} + r\cos\theta \ \frac{\partial \sigma_{\zeta\zeta}}{\partial \eta}|_{r=0} + \ldots \ . \tag{A.1.3}$$

From this expansion, a simple substitution shows that the first and third terms of the series tend to zero, which leaves the second term as the dominant term in the vicinity of the origin. Since the beams have a small cross section, this level of accuracy is sufficient. The bending moment along at the edge of the beam will therefore be given by,

$$M = \int_0^{2\pi} \int_0^{h_b/2} r^3 cos^2\theta \ \frac{\partial \sigma_{\zeta\zeta}}{\partial \eta} \ dr d\theta \tag{A.1.4}$$

$$= \frac{\pi h_b^4}{64} \frac{\partial \sigma_{\zeta\zeta}}{\partial \eta}. \tag{A.1.5}$$

To determine the sign of the moment and out-of-plane force at the end of the beam, impose a displacement and gradient at each end of the dummy beam so that at $\zeta = 0$, $u_\eta = 0$, $\frac{\partial u_\eta}{\partial \zeta} = 0$ and at $\zeta = -\zeta_1$, $u_\eta = \eta_1$, $u_{\eta,\zeta} = 0$. If the beam is infinitely stiff then the second and third displacements at $\zeta = 0$ will be,

$$\frac{\partial^2 u_\eta}{\partial \zeta^2} = \frac{6 \ \eta_1}{\zeta_1^2}, \qquad \frac{\partial^3 u_\eta}{\partial \zeta^3} = \frac{12 \ \eta_1}{\zeta_1^3}. \tag{A.1.6}$$

Physically a sudden positive displacement applied to the negative end of a stiff beam must cause a force in the positive direction and an anti-clockwise moment at the positive end. This leads to the boundary conditions at $\zeta = 0$,

$$B_b \frac{\partial u_\eta}{\partial \zeta} = -\frac{\partial \sigma_{\zeta\zeta}}{\partial \eta}, \qquad I_b B_b \frac{\partial^3 u_\eta}{\partial \zeta^3} = H, \tag{A.1.7}$$

where H is the out-of-plane force.

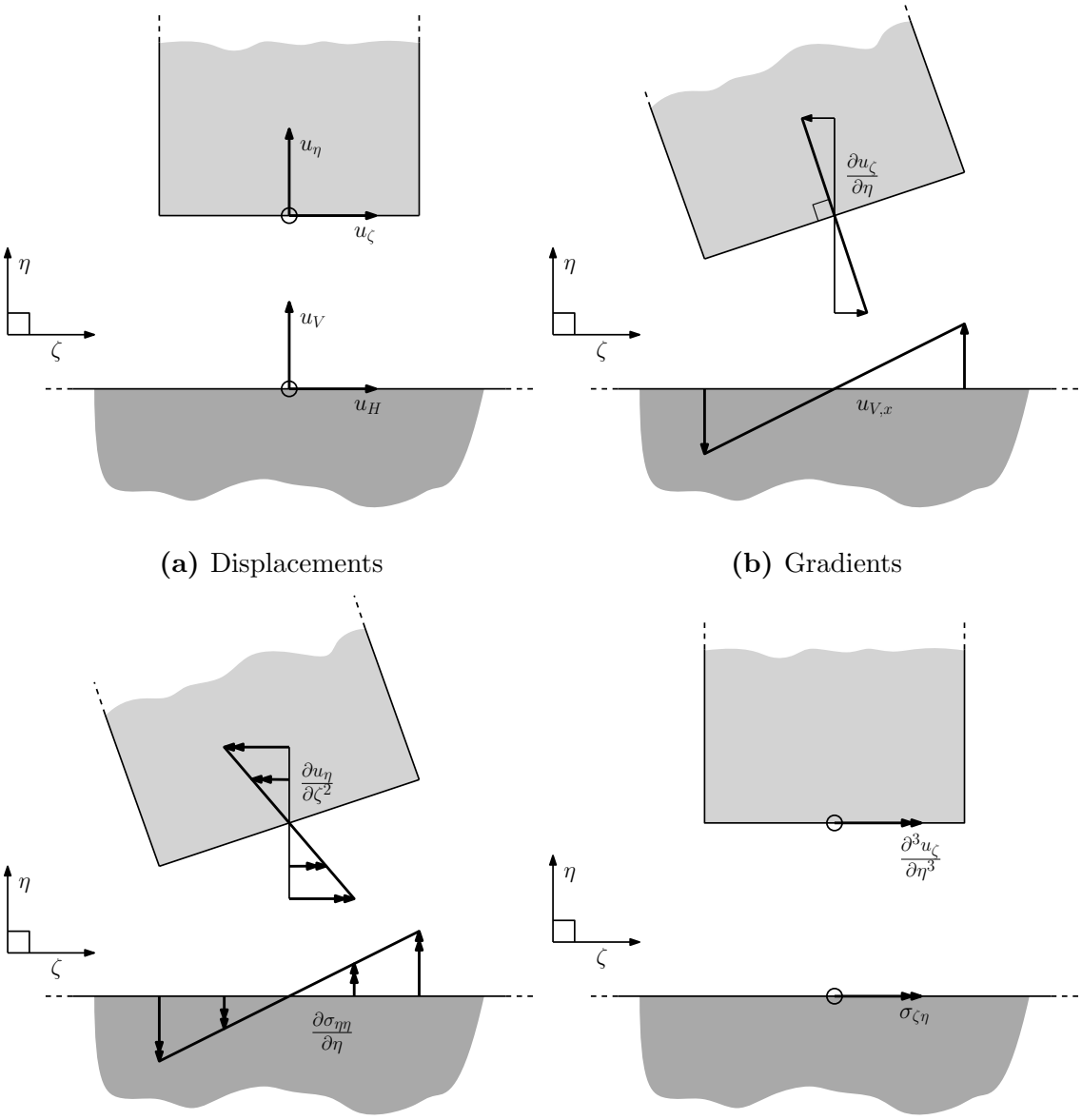

(a) Displacements **(b)** Gradients

(c) Bending moments **(d)** Horizontal stress

Figure A.1: A schematic representation of the system junction conditions, showing the end of the beam above the edge of the half-space. The relevant half-space quantities and corresponding beam quantities are indicated with a single arrow indicating a dimension of length and a double arrow indicating a dimension of stress.

A.2 Leading Order Asymptotic Model

In this section the method and results produced in Kaplunov and Prikazchikov [63] for the leading order model in §2.2.3 are summarised. This makes use of the governing equations for a linearly elastic half plane taken in the form (7.1.1), which are restated for ease of reference as

$$\begin{aligned} \phi_{,11} + \phi_{,33} - \frac{1}{c_1^2}\phi_{,tt} = 0, \\ \psi_{,11} + \psi_{,33} - \frac{1}{c_2^2}\psi_{,tt} = 0, \end{aligned} \tag{A.2.1}$$

and boundary conditions at $x_3 = 0$ (7.1.2),

$$\begin{aligned} 2\phi_{,13} + \psi_{,11} - \psi_{,33} = \frac{Q}{\mu}, \\ (\kappa^{-2} - 2)\phi_{,11} + \kappa^{-2}\phi_{,33} + 2\psi_{,13} = \frac{P}{\mu}, \end{aligned} \tag{A.2.2}$$

for a specified tangential stress Q and normal stress P and where

$$\kappa^{-2} = \frac{c_1^2}{c_2^2} = \frac{1 - \beta_R^2}{1 - \alpha_R^2}. \tag{A.2.3}$$

Suppose that ϕ and ψ have the two-term asymptotic expansions,

$$\phi = \epsilon^{-1}\phi_0 + \phi_1, \quad \psi = \epsilon^{-1}\psi_0 + \psi_1, \tag{A.2.4}$$

where, if the resulting perturbed wave solution has some speed c, the small parameter ϵ is given by the difference between the wave speed and the classical Rayleigh speed, c_R (7.1.4). Then on taking a usual multiple scales approach, introduce slow and fast time variables, τ_s and τ_f respectively, given by (7.1.5),

$$\tau_f = t, \qquad \tau_s = \epsilon t. \tag{A.2.5}$$

from which the time derivative can be expressed as (7.1.6),

$$\frac{\partial}{\partial t} = \frac{\partial}{\partial \tau_f} + \epsilon \frac{\partial}{\partial \tau_s}. \tag{A.2.6}$$

Substitution of this operator identity into the bulk equations (A.2.1) yields the perturbed bulk equations (7.1.7), again restated as,

$$\begin{aligned}\phi_{,33} + \alpha_R^2\phi_{,11} - 2\frac{\epsilon}{c_1^2}\phi_{,\tau_f\tau_s} - \frac{\epsilon^2}{c_1^2}\phi_{,\tau_s\tau_s} = 0,\\ \psi_{,33} + \beta_R^2\psi_{,11} - 2\frac{\epsilon}{c_2^2}\psi_{,\tau_f\tau_s} - \frac{\epsilon^2}{c_2^2}\psi_{,\tau_s\tau_s} = 0.\end{aligned} \tag{A.2.7}$$

Taking these at $O(1)$, the leading order terms of the displacement potentials are given by,

$$\phi_{0,33} + \alpha_R^2\phi_{0,11} = 0, \qquad \psi_{0,33} + \beta_R^2\psi_{0,11} = 0. \tag{A.2.8}$$

If a harmonic function $f(x_1, x_3)$ is defined by,

$$f_{,11} + a^2 f_{,33} = 0, \tag{A.2.9}$$

where a is a constant, then such a function obeys the Cauchy-Riemann identities,

$$f_{,3} = -af^*_{,1}, \qquad f_{,1} = \frac{1}{a}f^*_{,3}, \qquad f^{**} = -f \tag{A.2.10}$$

where f^* denotes the harmonic conjugate of f. Then, from this definition, it is clear that ϕ_0 and ψ_0 are harmonic functions. Furthermore, from Chadwick et al., [14] the displacement potentials along the surface can be expressed as a single plane harmonic function, with relations between ϕ and ψ,

$$\phi = -\frac{2\beta_R}{1+\beta_R^2}\psi^*, \qquad \psi = \frac{2\alpha_R}{1+\beta_R^2}\phi^*. \tag{A.2.11}$$

Similarly, at $O(\epsilon)$ the perturbed bulk equations (A.2.7) give,

$$\phi_{1,33} + \alpha_R^2\phi_{1,11} = \frac{2}{c_1^2}\phi_{0,\tau_f\tau_s}, \qquad \psi_{1,33} + \beta_R^2\psi_{1,11} = \frac{2}{c_2^2}\psi_{0,\tau_f\tau_s}. \tag{A.2.12}$$

Assume then that the second order terms of ψ and ϕ consist of a complementary solution and particular integral,

$$\phi_1 = \phi_{10} + x_3\phi_{11}, \qquad \psi_1 = \psi_{10} + x_3\psi_{11}, \tag{A.2.13}$$

where ϕ_{10} and ψ_{10} are again harmonic functions. Then substitution into the perturbed bulk equations (A.2.12) yields,

$$\phi_{11,13} = \frac{1}{c_1^2}\phi_{0,1\tau_f\tau_s}, \qquad \psi_{11,13} = \frac{1}{c_2^2}\psi_{0,1\tau_f\tau_s}. \tag{A.2.14}$$

Then using the leading order relations for ϕ_0 and ψ_0 yields,

$$\phi_{11,11} = -\frac{1}{\alpha_R^2 c_1^2}\phi_{0,3\tau_f\tau_s}, \qquad \psi_{11,11} = -\frac{1}{\beta_R^2 c_2^2}\psi_{0,3\tau_f\tau_s}. \tag{A.2.15}$$

Finally, substituting these into the surface conditions (A.2.2) at $O(1)$ gives, for a vertical stress (ie. $P = O(1)$, $Q = 0$),

$$2\phi_{10,113} - (1+\beta_R^2)\psi_{10,111} = \frac{2}{\alpha_R^2 c_1^2}\phi_{0,13\tau_f\tau_s} - \frac{2}{c_2^2}\psi_{0,11\tau_f\tau_s}, \tag{A.2.16}$$

$$(1+\beta_R^2)\phi_{10,111} - 2\psi_{10,113} = -\frac{4}{(1+\beta_R^2)c_2^2}\phi_{0,13\tau_f\tau_s} - \frac{1+\beta_R^2}{\beta_R^2 c_2^2}\psi_{0,11\tau_f\tau_s} - \frac{P_{,1}}{\mu}. \tag{A.2.17}$$

Then on taking advantage of the harmonic function relations (A.2.10) and relations between the potentials along the surface (A.2.11),

$$2\alpha_R\phi_{10,11} + (1+\beta_R^2)\psi^*_{10,11} = \left(\frac{2}{\alpha_R c_1^2} - \frac{1+\beta_R^2}{\beta_R c_2^2}\right)\phi_{0,1\tau_f\tau_s}, \tag{A.2.18}$$

$$(1+\beta_R^2)\phi_{10,11} + 2\beta_R\psi^*_{10,11} = \left(\frac{2}{c_2^2} - \frac{1+\beta_R^2}{\beta_R^2 c_2^2}\right)\psi_{0,1\tau_f\tau_s} - \frac{P}{\mu}. \tag{A.2.19}$$

Using the Rayleigh denominator (2.2.19), these solve simultaneously to give the leading order relation for ϕ_0 along the surface,

$$2\epsilon\phi_{0,\tau_f\tau_s} = -c_R^2\frac{1+\beta_R^2}{2\mu B}P. \tag{A.2.20}$$

Then from the time operator relation (A.2.6),

$$2\epsilon\frac{\partial^2}{\partial\tau_f\partial\tau_s} = \frac{\partial^2}{\partial t^2} - \frac{\partial^2}{\partial\tau_f^2} - \epsilon^2\frac{\partial^2}{\partial\tau_s\partial\tau_s}, \tag{A.2.21}$$

where, on assuming that the forcing produces a travelling surface wave, introduce the travelling wave ansatz,

$$\frac{\partial^2}{\partial\tau_f^2} = c_R^2\frac{\partial^2}{\partial x_1^2}. \tag{A.2.22}$$

Then on substitution the leading order term of the previous relation at $x_3 = 0$ is given in terms of the original variables by,

$$\phi_{,11} - \frac{1}{c_R^2}\phi_{,tt} = \frac{1+\beta_R^2}{2\mu B}P. \tag{A.2.23}$$

Following the same procedure for a horizontal stress (ie. $P = 0$, $Q = O(1)$) yields,

$$2\epsilon\psi_{0,\tau_f\tau_s} = c_R^2\frac{1+\beta_R^2}{2\mu B}Q, \tag{A.2.24}$$

yielding the leading order relation at $x_3 = 0$,

$$\psi_{,11} - \frac{1}{c_R^2}\psi_{,tt} = -\frac{1+\beta_R^2}{2\mu B}Q. \tag{A.2.25}$$